Characterization of SPECC1L Function in Palatogenesis

By
© 2019
Everett Gordon Hall
B.A. Biology, Westminster College, Missouri, 2013

Submitted to the graduate degree program in Anatomy and Cell Biology and the Graduate Faculty of the University of Kansas in partial fulfillment of the requirements for the degree of Doctor of Philosophy.

_____
Chair: Dr. Irfan Saadi

_____
Dr. András Czirók

_____
Dr. Brenda Rongish

_____
Dr. Paul Trainor

_____
Dr. Pamela Tran

_____
Dr. Jinxi Wang

Date Defended: April 26, 2019

The dissertation committee for Everett Gordon Hall
certifies that this is the approved version of the following dissertation:

Characterization of SPECC1L Function in Palatogenesis

_____
Chair: Dr. Irfan Saadi

Date Approved: May 16, 2019

Abstract

Orofacial clefts are among the most common congenital birth defects, occurring in as many as 1 in 800 births worldwide. Genetic and environmental factors contribute to the complex etiology of these anomalies. *SPECC1L* encodes a cytoskeletal protein with roles in adhesion, migration, and cytoskeletal organization. *SPECC1L* mutations have been identified in patients with atypical clefts, Opitz G/BBB syndrome, and Teebi hypertelorism syndrome. Our lab has previously shown that knockout of *Specc1l* in mice with gene trap alleles results in early embryonic lethality with defects in neural tube closure and neural crest cell delamination, as well as reduced PI3K-AKT signaling. However, the early lethality phenotype rendered these models incapable of recapitulating the human anomalies. To validate a role for SPECC1L in palatogenesis, we generated additional gene trap and truncation mutant *Specc1l* alleles. *Specc1l*$^{genetrap/truncation}$ compound heterozygote embryos survive to the perinatal period, allowing analysis at later developmental stages. Examination of compound mutant palates revealed a delay in palate elevation, abnormal oral adhesions, and ectopic expression of adherens junction protein β-catenin at the apical surface of oral epithelial periderm cells, as well as a global increase in actin filament staining. We also establish that transcription factor IRF6, which has a causative role in many cases of orofacial clefting, is required for SPECC1L expression in the palate. After establishing a role for SPECC1L in the palatal epithelium, we asked if it also acted in the migration of palatal mesenchyme. Indeed, time-lapse imaging analysis of primary mouse embryonic palatal mesenchyme (MEPM) cells from *Specc1l*$^{genetrap/truncation}$ mutant embryos show defects in migration. We also demonstrate that activation of the PI3K-AKT pathway with a small molecule activator improves mutant wound closure speed. Furthermore, random 2-D motility cultures revealed that MEPM cells have attributes of collective migration that are reduced in mutant cells.

Lastly, we generated a mouse allele with the T397P point mutation, located in the second coiled-coil domain (CCD2) of SPECC1L, that was previously identified in patients with Opitz G/BBB syndrome. Embryos with this allele displayed omphalocele and completely penetrant cleft palate defects that recapitulated the phenotype of patients with *SPECC1L* mutations. Together, these data identify roles for SPECC1L in palate epithelial integrity and mesenchymal remodeling, and thus firmly establish a requirement for SPECC1L in palatogenesis.

Table of Contents

CHAPTER ONE:

INTRODUCTION

1.1 Orofacial Clefting

1.1.1 Early craniofacial development

Craniofacial development of human embryos can be represented with morphologically distinct facial processes **(Fig. 1.1)** [Thomason, 2009; Dixon, 2011]. At four weeks post-conception, these include the frontonasal prominence (FNP), two maxillary processes, and two mandibular processes. Over the next few weeks these primitive structures grow, move, and fuse in a coordinated fashion to build the early head and face. Two nasal placodes invaginate from the FNP ectoderm to form the nasal pits. These pits are bordered by the medial and lateral nasal processes, which eventually fuse to form the alae of the nose. At the same time, the upper lip and primary palate are created through the fusion of the medial nasal process and maxillary processes, the upper jaw and cheeks by the maxillary processes, and the lower jaw by the fusion of the mandibular prominences.

Concurrent with the development of the other facial structures, the secondary palate is formed from the maxillary processes. Initial outgrowths from the maxillary processes, called the palatal shelves, grow vertically adjacent to the tongue. After this vertical outgrowth, the palatal shelves elevate to a horizontal position above the tongue and continue to grow medially until contact between the shelves is achieved. Lastly, the palatal shelves adhere and fuse along the midline to form the secondary palate, as well as anteriorly with the primary palate.

1.1.2 Orofacial clefting in humans

The complex organization of the facial processes allows the head and face to house some of the most intricate structures of the body. However, this complexity also renders craniofacial development particularly vulnerable to genetic and environmental insult [Dixon, 2011]. As a

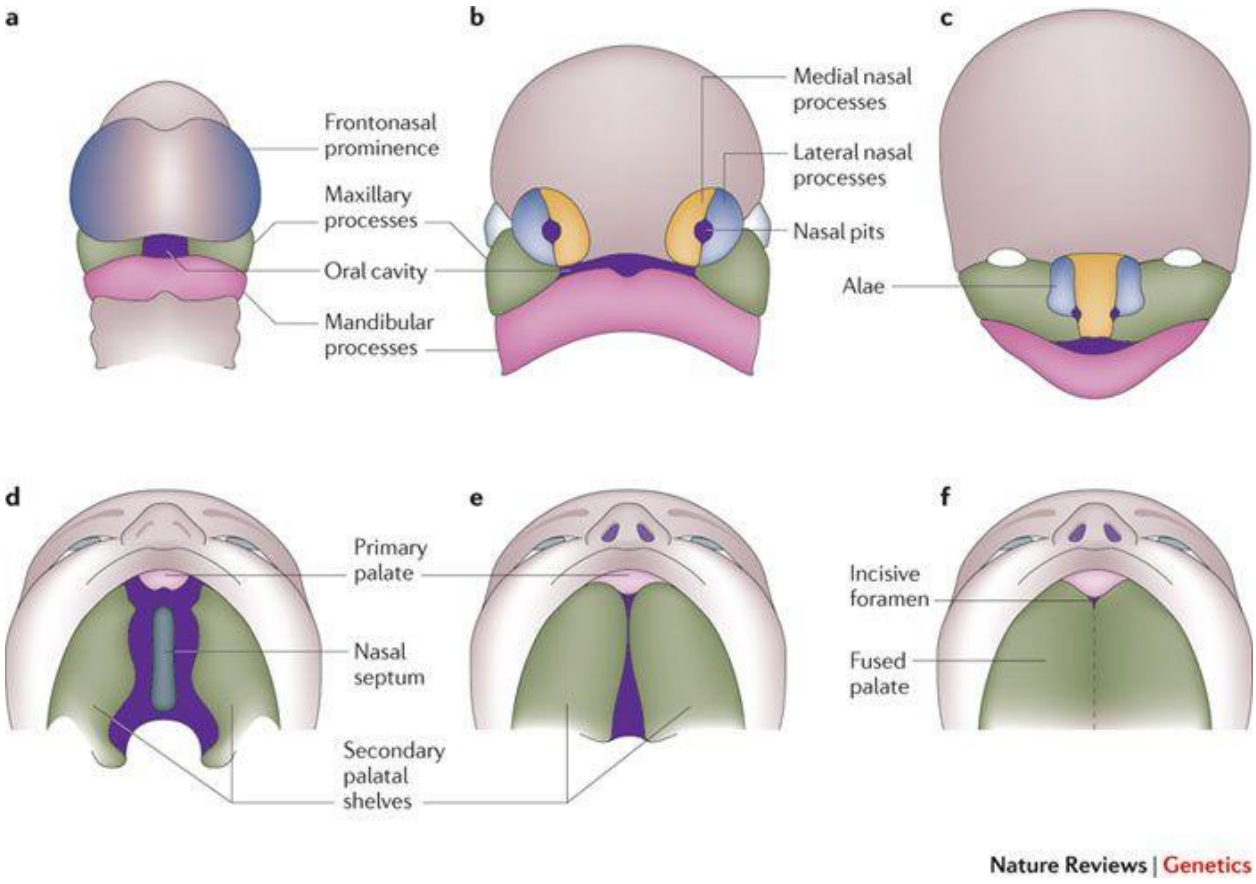

Figure 1.1: Human craniofacial development. A-C) Depiction of craniofacial processes during the fourth (A), fifth (B), and end of the sixth week (C) of human embryogenesis. **D-F)** Oral view of palate development during the sixth week of human embryogenesis before elevation (D), after elevation (E), and after fusion (F).

Dixon, M. J., Marazita, M. L., Beaty, T. H., & Murray, J. C. (2011). Cleft lip and palate: understanding genetic and environmental influences. *Nat Rev Genet, 12*(3), 167-178. doi:10.1038/nrg2933. Copyright 2011. Reprinted with permission from Springer Nature.

result, craniofacial anomalies are one of the most common types of birth defects, constituting over a third of congenital malformation cases. One of the most prominent craniofacial defects is an orofacial cleft (OFC), a defect resulting from the failed fusion between any of the various facial processes during embryogenesis. The severity of these defects is largely variable depending on the degree to which the development of the facial processes is disrupted. Some OFCs span large portions of the face and are often termed atypical clefts. These malformations were initially classified in a publication authored by Paul Tessier in 1976, where he grouped the clefts into 15 different types [Tessier, 1976]. Repair of these clefts generally require multiple surgeries over the early life of the patient. While these defects are extreme, they are relatively rare, making up only a small percentage of all OFCs.

Relatively milder OFCs such as cleft lip and cleft palate (CL/P) are much more common. These clefts can be found together or as isolated malformations [Dixon, 2011]. Many CL/P cases are associated with a syndrome that manifests with multiple malformations, of which more than 275 are described [Leslie, 2013]. However, syndromic CL/P only accounts for approximately 30% of cases, while 70% of orofacial clefting patients have no other clear malformations [Stanier, 2004]. Nonsyndromic CL/P (nsCL/P) can occur in as many as 1 in 800 live births [Rahimov, 2012; Mossey, 2012]. Surgical repair of CL/P is relatively simple compared to atypical clefts. However, any OFC can have a significant negative impact on the quality of life of the affected child, as well as a substantial financial burden on the patient's family [Wehby, 2010]. Therefore, it is imperative that the biomedical community continue to improve our understanding of how these defects occur, both to help patients and doctors understand these disorders, as well as to treat any complications that happen after repair.

1.1.3 Investigating the genetic etiology of orofacial clefts

OFC is a complex disorder with a multitude of genetic and environmental factors contributing to its etiology. One effective method of identifying genes implicated in CL/P is the genotyping and linkage analysis of affected families [Mangold, 2011; Dixon, 2011; Marazita, 2012]. This is particularly useful in families with syndromic CL/P, as most syndromic CL/P follows a Mendelian inheritance pattern. Through these efforts, the cause of many clefting syndromes have been narrowed down to a small number of genes. However, nsCL/P often presents in families with incomplete penetrance, even in those with no history of OFC. While sequencing of individual patients may reveal causative variants, the heterogeneous nature of OFC often limits the effectiveness of these analyses.

To account for the complex etiology of these disorders, scientists utilize genome-wide association studies (GWASs) to identify disease-associated variants that may not be discernable via linkage analysis. GWASs work by taking advantage of single nucleotide polymorphism (SNP) data and are largely possible because of recent advancements in microarray genotyping technologies [Witte, 2010, Mangold, 2011]. SNPs are natural variations in the human genome, and most have no impact on the health of individuals [W. Bush, 2012]. However, the collection of millions of SNPs from different populations allow large-scale statistical analyses that were previously impossible. By comparing the SNPs between healthy and affected populations, scientists can identify variations in genomic regions that correlate with an increased risk of many diseases [W. Bush, 2012]. This methodology has been used to great effect in the craniofacial field, resulting in the discovery of many genetic risk factors contributing to nsCL/P, including *MAFB* [Beaty, 2010], *PAX7* [Leslie, 2015], *IRF6* [Zucchero, 2004; Rahimov, 2008; Beaty; 2010; Leslie, 2016], *ARHGAP29* [Leslie, 2012], and many others [Reviewed in Dixon, 2011; Adeyemo, 2017].

GWASs along with other methodologies including copy number variation and exome sequencing have provided a wealth of information on the genetics of these disorders. However, disease-associated variations are not necessarily causal, so model systems must also be utilized to investigate the underlying mechanisms.

1.1.4 Mouse models of orofacial clefting

Alongside the various clinical discovery methods in human populations, animal model systems have been used to further our understanding of the mechanisms governing craniofacial development. The most common models include *Mus musculus* (mouse), *Gallus gallus* (chicken), *Danio rerio* (zebrafish), and *Xenopus laevis/tropicalis* (frog) [Van Otterloo, 2016]. The mouse is a particularly valuable model system. As mammals, mice are more closely related to humans than the other model organisms. Additionally, development of the murine palate is very similar to human palatogenesis, enhancing the clinical relevance of any data generated using this model **(Fig. 1.2)** [Bush, 2012]. Between embryonic day 12.5 (E12.5) and E13.5, the palatal shelves grow vertically on either side of the tongue. By E14.5, palatal shelf elevation occurs, and by E15.5, the elevated palatal shelves fuse at the midline.

This similarity in mammalian palatogenesis allows additional techniques to aid in the discovery of novel clefting genes. Genes important to craniofacial development can be identified through RNA expression profiling of the applicable tissues [Brunskill, 2014; Reviewed in Van Otterloo, 2016]. Novel genes can also be identified in an unbiased manner through mutagenesis screening with chemicals such as N-ethyl-N-nitrosourea (ENU) [Sandell, 2011; Caruana, 2013]. The embryos generated from these screens can be evaluated for relevant malformations and the isolated lines can be sequenced to find the mutated gene. However, perhaps the most important

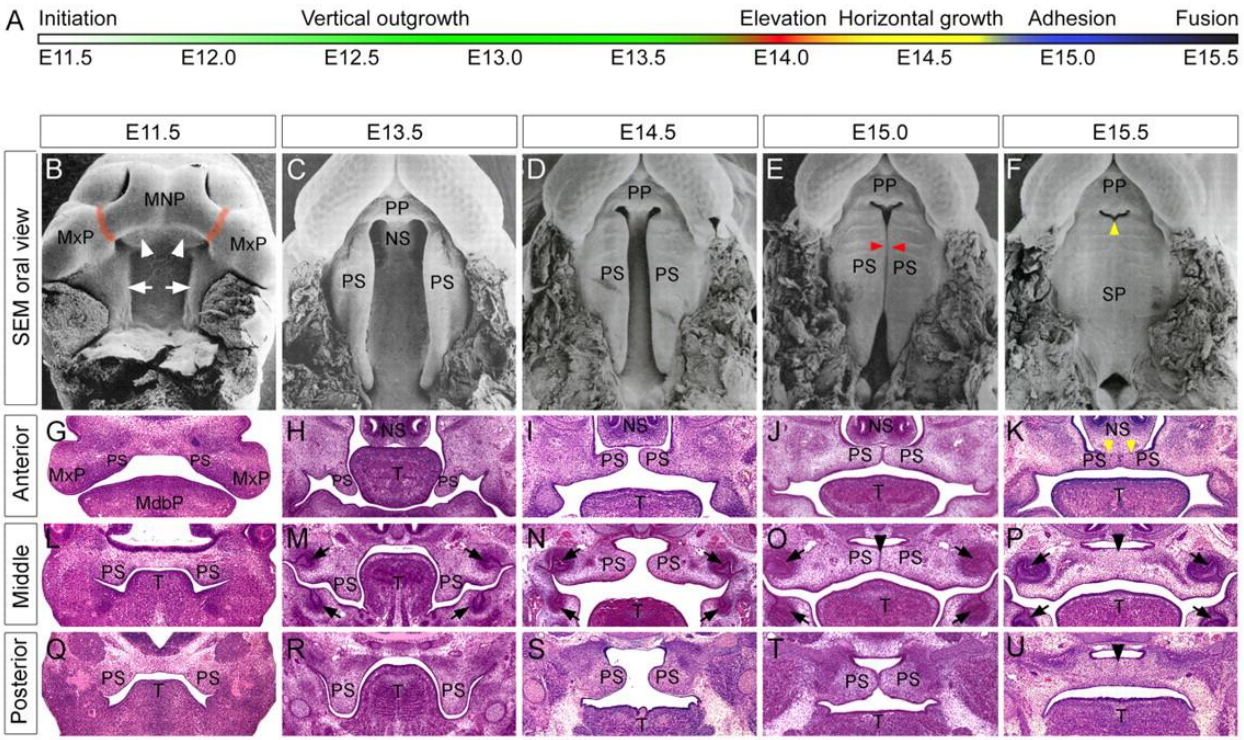

Figure 1.2: Stages of mouse palatogenesis. A) Bar showing the different stages of mouse palatogenesis from E11.5 to E15.5. **B-F**) Scanning electron micrographs of the developing mouse palate. **G-U)** Coronal H&E histology sections of the anterior, middle, and posterior palates. MdbP, mandibular process; MNP, medial nasal process; MxP, maxillary process; NS, nasal septum; PP, primary palate; PS, palatal shelf; SP, secondary palate; T, tongue.

Image (Palatogenesis in the mouse) from Bush, J. O., & Jiang, R. (2012). Palatogenesis: morphogenetic and molecular mechanisms of secondary palate development. *Development*, *139*(2), 231-243. doi:10.1242/dev.067082. Copyright 2012. Reprinted with permission from The Company of Biologists Ltd.

benefit of mouse models is that they allow examination of the underlying molecular and developmental mechanisms important for palatogenesis. For example, knockout (KO) mouse models were used to discover the integral role of *Osr2* in the proliferation of the medial palatal shelf [Lan, 2004] and of TGFβ3 in palate fusion [Yang, 2007]. Additionally, they also provide a biological system to investigate whether a CL/P-associated gene identified in humans is causative.

Despite the effectiveness of these models, interpreting these results for the context of the human system can be problematic. Many KO models result in early embryonic lethality, rendering the developmental role of a gene difficult to study [Papaioannou, 2012; Adams, 2013; Copp, 1995]. This limitation can be partially overcome by utilizing drug-inducible and tissue-specific conditional KO's [Friedel, 2011]. Additionally, knockout of a confirmed orofacial clefting gene in mice often does not result in clefting phenotypes [Gritli-Linde, 2008]. Cleft lip is also uncommon amongst OFC mouse models compared to cleft palate alone [Gritli-Linde, 2008]. These phenomena have several potential explanations, including the presence of genetic modifiers in different mouse strains, gene redundancy in the mouse genome, or simply morphological differences between human and mouse development [Dixon, 2004; Gritli-Linde, 2008; Doetschman, 2009]. Nonetheless, the value of mouse models to study the mechanisms of OFC is clear, and future studies will help delineate the relevant differences between the human and murine systems.

1.2 Palate Development

1.2.1 Neural crest cells

The development of the mammalian palate is highly dynamic and requires the coordinated integration of multiple tissue types from various embryonic origins. Neural crest cells (NCCs) are

a population of migratory cells that contribute to many tissues throughout the developing embryo. To achieve this, NCCs must leave their origin at the dorsal neural tube and migrate to the various regions to which they will contribute. Once they arrive, they proliferate and differentiate to contribute to numerous neural, connective, and bony tissues. NCCs are particularly important for craniofacial development, as they are responsible for giving rise to a relatively large portion of bone and cartilage of the head and face.

The exact timing of NCC specification in the early embryo is still under investigation. Two main hypotheses prevail in the current literature. The traditional model posits that specification occurs during neural tube closure as a result of integration of WNT, FGF, and BMP signaling at the junction between the neural plate and non-neural ectoderm [Reviewed in Trainor, 2005; Cordero, 2011]. Recent studies in avian embryos showed that induction of the NCC population requires PAX7 and begins at gastrulation [Basch, 2006]. PAX7 expression was also identified before neural plate formation in mouse embryos [Murdoch, 2012]. However, while PAX7 expression overlaps with the NCC lineage, it only contributes to a portion of the NCC-derived tissues [Murdoch, 2012]. *Pax7*-null mice exhibit only minor craniofacial malformities, suggesting a role for PAX7 in some, but not all NCCs [Mansouri, 1996].

As a result of signals at the neural plate border, NCCs gain a migratory phenotype through epithelial to mesenchymal transition (EMT). This process is characterized by dramatic changes in morphology stemming from the disassembly of cell-cell adhesions and loss of apico-basal polarity. Adherens junctions are disassembled through the downregulation or proteolysis of junction components, such as N-cadherin [Wheelock, 2003; Shoval, 2007; Taneyhill, 2008]. Tight junctions, another cell adhesion contributing to cell polarity, are also disassembled through the downregulation of claudin and occludin. Removal of these adhesions allows the detachment of

NCCs from the neural tube epithelium. This loss of epithelial adhesions is accompanied by changes to the cytoskeleton of NCCs stimulated by RHOB [Liu, 1998; Strobl-Mazzulla, 2012]. These changes in protein regulation are largely driven by transcription factors, such as SNAIL and FOXD3, which suppress the expression of epithelial markers while enhancing the transcription of mesenchymal markers [Dottori, 2001; Taneyhill, 2007; Theveneau, 2012; Strobl-Mazzulla, 2012].

After delamination, the NCCs migrate along specified pathways in order to reach the early craniofacial regions. The pathway taken depends on the axial level of origin and defines the structures to which each cohort of NCCs will contribute. [Reviewed in Minoux, 2010; Kulesa, 2010]. NCCs originating from the posterior mesencephalon and the first two rhombomeres will migrate to the first pharyngeal arch (PA1), a precursor to the maxillary and mandibular prominences [Lumsden, 1991; Serbedzija, 1992; Minoux, 2010]. These migrating populations rely on signals from the surrounding microenvironment to provide directional cues in order to arrive at the correct locations. NCCs migrating to PA1 express receptor Neuropilin 2, which stimulates a repulsive effect in the cells when bound to its Semaphorin 3f ligand, effectively creating a border that guides them down a particular route [Gammill, 2007; Schwarz, 2008]. These mechanisms along with others including Ephrin/Eph signaling shape the streams to prevent merging between them [Davy, 2004; Minoux, 2010]. The mechanisms responsible for NCC directionality have also been extensively studied [Reviewed in Shellard, 2016]. FGF8 and VEGF both have chemotactic effects on NCCs and are required for proper migration and survival of some NCC populations, but whether their endogenous role is chemotactic in nature has yet to be conclusively shown [Abu-Issa, 2002; McLennan, 2010; Sato, 2011]. NCC streams also have an intrinsic ability to migrate in a directional manner. Through a phenomenon called contact inhibition of locomotion, wherein contact with a neighboring cell results in the generation of extensions in the opposite direction, the

NCCs establish a leading edge of polarized cells that provide directionality to the stream [Carmona-Fontaine, 2008]. Cumulatively, these mechanisms result in focused and directional migration that lead the NCCs to their targets.

Patterning of the proliferation and differentiation of the NCCs upon arrival at the craniofacial primordia is dependent on a complex network of local growth factors, transcription factors, and signaling molecules. In PA1, the maxillary and mandibular processes are defined by different transcripts of distal-less homeobox (DLX) transcription factors. The maxillary process contains only DLX1/2, while endothelin signaling in the early mandibular process activates a signaling cascade that leads to the transcription of DLX5/6 and then DLX3/4 towards the end of the process [Qiu, 1997; Depew, 1999; Depew, 2002; Minoux, 2010]. These combinations of DLX proteins execute unique developmental programs that differentiate between the two processes as development proceeds. Other signaling molecules including Sonic hedgehog (SHH), bone morphogenic protein (BMP), and FGF also regulate the growth and patterning of the NCCs in a spatially and temporally controlled manner.

NCCs contribute to a wide variety of different tissues in the craniofacial region and throughout the body, so it follows that defects in the delamination, migration, survival, proliferation, or differentiation may have substantial negative impacts on the development of the embryo. Pathologies resulting from NCC deficiency are collectively termed neurocristopathies, many of which result in craniofacial malformations [Bolande, 1974; Etchevers, 2006]. A prominent example is mandibulofacial dysostosis, more commonly known as Treacher Collins syndrome (TCS), a disorder clinically characterized by hypoplasia of the maxilla and mandible, lower eyelid colobomas, and downward slanting eyes [Reviewed in Kadakia, 2014; Achilleos, 2015]. Many TCS patients also exhibit cleft palate. More cases of this disorder are associated with

mutations in *TCOF1*, *POLR1C*, and *POLR1D*, all of which are important in the transcription of ribosomal DNA [Reviewed in Achilleos, 2015; Noack Watt, 2016]. Experimental evidence in mouse models show that these defects stem from an increase in NCC apoptosis through p53 pathway activation, resulting in reduced NCC contribution to the craniofacial structures [Dixon, 2006]. CHARGE syndrome, another complex disorder, presents with a broad range of malformations including eye, ear, heart, and cranial nerve defects [Hsu, 2014]. Most diagnosed patients have mutations in the chromodomain helicase DNA-binding protein (*CHD7*) gene, which has been implicated in the regulation of migratory NCC genes Slug, Sox9, and Twist [Janssen, 2012; Bajpai, 2010]. Neurocristopathies impact the development of other tissues as well. For example, Hirschsprung's disease is due to incomplete trunk NCC contribution to the gut's enteric nervous system, resulting in improper bowel motility and subsequent obstructions [Kenny, 2010].

1.2.2 Mammalian palatogenesis: Mechanisms of palatal shelf outgrowth

Palatogenesis is a multistep process that requires the growth, elevation, and fusion of the palatal shelves (PS). These structures originate as a pair of outgrowths from the maxillary process and consist of two primary cell populations: the oral epithelium and NCC-derived mesenchyme. Proper palate development is directed through intersecting signaling pathways which dictate the growth and patterning of the PS. SHH signaling is a central pathway in initial PS outgrowth, with bone morphogenic protein (BMP) and Fibroblast growth factor (FGF) signaling also playing significant roles [Rice, 2006; Bush, 2012; Lan, 2015]. SHH signaling functions through binding to its receptor Patched 1 or 2 (PTCH). When not bound, the PTCH receptor inhibits the activation of the transmembrane signal transducer Smoothened (SMO). Upon SHH binding PTCH is internalized, allowing SMO to accumulate and initiate a signaling cascade through GLI

transcription factors [Carballo, 2018]. Activation of the SHH pathway in the developing palate upregulates several inducers of proliferation including Cyclin D1, Cyclin D2, FOXF1A, FOXF2, and OSR2 [Lan, 2009]. Indeed, conditional knockouts (cKO) of SHH signaling components in mice result in reduced PS growth, resulting in cleft palate [Rice, 2004; Lan, 2009].

Through these analyses, the dynamics of the epithelial-mesenchymal interactions driving PS outgrowth have been elucidated. For instance, cKO of SHH in the oral epithelium results in variable palate defects, but not knockout of SMO [Rice, 2004; Lan, 2009]. However, cKO of SMO in the palatal mesenchyme reduces proliferation in both tissues [Lan, 2009]. In addition, FGF and Bmp signaling were also shown to be required for the initiation and maintenance of SHH signaling during PS outgrowth [Zhang, 2002; Rice, 2004; Li, 2011]. Collectively, these studies reveal a reciprocal relationship between the mesenchyme and epithelium during PS outgrowth, wherein each population requires signaling from the other for proper palatogenesis.

It is important to note that growth within the PS is not uniform, with differences seen along the anteroposterior and mediolateral axes. Following outgrowth, the PS must elevate and fuse, after which the anterior palate undergoes ossification to form the hard palate, while the posterior becomes the soft palate [Bush, 2012]. The dynamic changes during elevation and specialization of the tissues require distinct patterns of growth and differentiation, explaining the need for variability between PS regions. These regions are primarily characterized through differential expression of growth and transcription factors. Anteriorly, MSX1 maintains SHH signaling through a positive feedback loop with BMP4, while BMP4 and OSR2 in the posterior palate are regulated by PAX9 [Zhang, 2002; Zhou, 2011; Zhou, 2013]. Similarly, DLX5 suppresses SHH signaling in the medial palate through FGF7 upregulation, while FGF10 and SHH drive each other's expression in the lateral palate [Han, 2009; Lan, 2009]. Other region-specific transcriptional regulators have been

identified, such as SHOX2 in the anterior palate [Yu, 2005; Li, 2007]. The dynamics of these proteins in the development of the palate are an area of active research.

1.2.3 Mammalian palatogenesis: Mechanisms of palatal shelf elevation

After outgrowth, the PS undergo a process of elevation, where the shelves reorient themselves from a vertical position adjacent to the tongue, to a horizontal position above the tongue. In mice, this takes place between E14.0 and E14.5. After elevation, the reoriented palatal shelves make contact at the midline and fuse by E15.5 [Bush, 2012]. This short timeframe has rendered the elevation process difficult to observe, and so the mechanisms driving the process have yet to be completely elucidated. Many potential models for elevation have been proposed, including a mechanical "flip" of the shelves to a horizontal position, remodeling of the shelf, and changes in directional growth toward the midline [Reviewed in Bush, 2012]. A comprehensive histomorphological analysis of murine palate elevation was performed to investigate the validity of these different models [Yu, 2011]. In the study, coronal sections of E14.5 embryos were separated into five different planes based on anatomical landmarks. This was followed by morphological classification of the palatal shelves into one of six different stages. Systematic examination of palate elevation in this manner has provided insights into differences along the anteroposterior axis **(Fig. 1.3)**. Elevation of the mid-palate resembled a "bulge" in the medial shelf wall, while the anterior palate exhibited a more rapid reorientation to the horizontal position. It was also noted that this remodeling of the mid-palate occurred before anterior elevation. This analysis corroborated previous findings that stated the mechanism of elevation differed along the anteroposterior axis, but contested conclusions that elevation began anteriorly and proceeded posteriorly or vice-versa [Walker, 1956; Coleman, 1965; Ferguson, 1978].

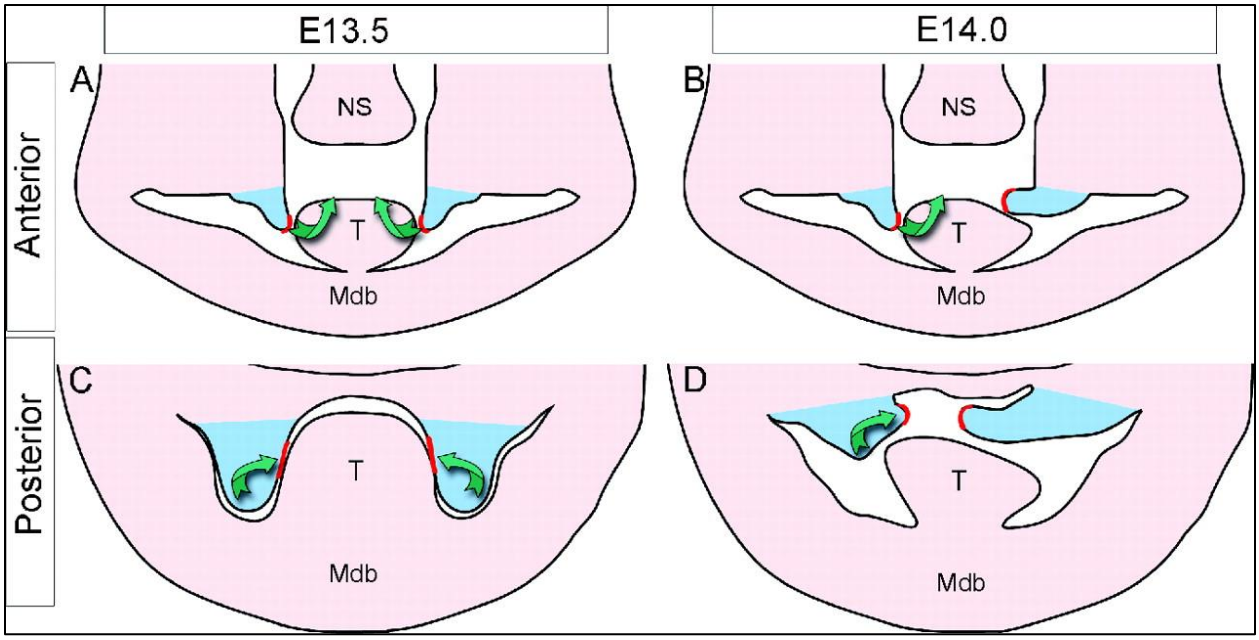

Figure 1.3: Differences in palate elevation along anteroposterior axis. A-D) Depictions of palatal shelf elevation in the anterior (A,B) and posterior palates (C,D). The anterior palate is thought to go through a "flip-up" mechanism (B). In contrast, the posterior palate undergoes a remodeling process with a medial bulge (D). Mdb, mandible; NS, nasal septum; T, tongue. Image (Distinct mechanisms for palatal shelf elevation) from Bush, J. O., & Jiang, R. (2012). Palatogenesis: morphogenetic and molecular mechanisms of secondary palate development. *Development*, *139*(2), 231-243. doi:10.1242/dev.067082. Copyright 2012. Reprinted with permission from The Company of Biologists Ltd.

Several mouse mutants exhibit defects or delays in palatal shelf elevation, allowing investigation into the causes for elevation failure as well as the molecular signals that govern the elevation process [Reviewed in Gritli-Linde, 2007; Gritli-Linde, 2008; Bush, 2012; Li, 2017]. Changes in shelf growth are a common reason for elevation failure. Mouse embryos null for transcription factor *Mn1* show decreased proliferation in the middle and posterior palatal shelves, leading to drastically reduced shelf size [Liu, 2008]. The palatal shelves fail to elevate in these regions and eventually recede into the maxilla. Conditional KO of *Foxf2* in the palatal mesenchyme also results in elevation failure due to reduced proliferation and hypoplastic shelves [Xu, 2016].

It is likely that some elevation defects in mutants with severe palatal shelf growth retardation are simply due to the significant decrease in palatal shelf size. However, smaller changes in region-specific proliferation can also result in elevation failure. KO of *Cyp26b1*, an enzyme responsible for degrading retinoic acid, causes elevation defects through decreased proliferation in the lateral half of the palatal shelves [Okano, 2012]. Further investigation revealed downregulation of *Tbx1*, *Fgf10*, and *Bmp2*, all of which are important in proliferation [Goudy, 2010; Rice, 2004; Zhang, 2002]. Similar elevation defects and decreases in medial shelf proliferation were also seen in embryos null for transcription factor *Osr2* [Lan, 2004]. Interestingly, proliferation in the medial half of the wildtype palate was greater than the lateral half [Lan, 2004]. This mediolateral asymmetry in proliferation toward the midline is likely a primary mechanism driving the "bulge" formation seen in the elevation of the middle palate, and alterations to this balance between medial and lateral proliferation could disrupt the process. Indeed, analysis of *Sprouty2* mutants shows increased mesenchymal proliferation in conjunction with elevation defects [Matsumura, 2011].

While changes in proliferation often result in palate defects, it is not the only requirement of elevation. The shelves must undergo extensive remodeling as they reorient and extend toward the midline. Therefore, it is reasonable to suggest that disruptions in the signals orchestrating this behavior could also result in palate defects. Evidence from several mouse models that exhibit cleft palate but do not exhibit changes in proliferation substantiate this claim. For example, KO mouse models of transcription factor *Zfhx1a* or growth factor BMP7 both show delays in elevation and subsequent cleft palate, but no detected differences in proliferation [Jin, 2008; Kouskoura, 2013]. While mediolateral proliferation ratios were not quantified in these studies, they indicate the likely requirement for instructive signals in palatal shelf remodeling during elevation.

Another possible mechanism for palate elevation includes the generation of force through regulation of the extracellular matrix (ECM) [Brinkley, 1986; Ferguson, 1988; Morris-Wiman, 1992; Meng, 2009]. The ECM is a dense network of structural molecules in which the cells of a tissue reside. Glycosaminoglycans (GAGs), a primary component of the ECM, are a group of polar polysaccharides that have been implicated in palatogenesis in several mouse models. Embryos homozygous for a targeted *Fgfr2* point mutation show altered GAG composition, but whether the changes contribute to the defects remains to be determined.

Lastly, elevation failure can occur due to factors extrinsic to the development of the palatal shelves [Reviewed in Bush, 2012; Okano, 2014]. cKO of TGFβ activated kinase 1 (Tak1) in the NCC lineage results in elevation defects, along with differences in tongue shape. [Song, 2013]. However, organ culture experiments with the lower jaw removed showed that mutant elevation occurred normally, indicating that obstruction by the tongue is a likely cause of cleft palate in these mutants. Deficits in mandibular growth can also result in micrognathia, a malformation strongly associated with cleft palate in many mouse mutants [Bjork, 2010; Lai, 2016]. These studies show

that coordinated growth of the surrounding craniofacial structures with the palatal shelves is required for proper palatogenesis.

1.2.4 Mammalian palatogenesis: Mechanisms of palatal shelf fusion

After elevation, the palatal shelves must make contact at the midline, adhere, and fuse to form the palate. The specialized section of the palate epithelium, called the medial edge epithelium (MEE), contacts the MEE of the opposing palatal shelf. Specification of the MEE is a temporally controlled process that does not require contact between the shelves, as evidenced by the presence of MEE markers in the unelevated palates of E14.5 *Zfhx1a* mutant embryos [Jin, 2008; Jin, 2010].

After adhesion, the MEE cells form a single layer called the medial epithelial seam (MES), which is selectively removed to allow proper fusion of the shelves [Bush, 2012]. Gene expression studies and mouse KO models have led to the identification of transforming growth factor beta 3 (TGFβ3) as a primary regulator of this process [Reviewed in Bush, 2012; Lan, 2015; Li, 2017]. TGFβ3 is expressed in the MEE during palatogenesis, and loss of TGFβ3 in mice results in cleft palate due to palatal shelf fusion failure [Fitzpatrick, 1990; Proetzel, 1995; Brunet, 1995]. Manual contact between the palatal shelves in organ culture experiments revealed that this defect is due to the persistence of the MES [Kaartinen, 1997].

Molecular studies utilizing *Tgfβ3*-null mice and other lines have elucidated the downstream effectors regulating palatal shelf fusion. Activation of TGFβ receptors 1 and 2 through TGFβ3 binding initiates a cascade of many transduction pathways within MEE cells to stimulate the fusion process [Reviewed in Li, 2017]. Canonical TGFβ signaling occurs through SMAD2 and/or SMAD3 which, upon phosphorylation, form a complex with SMAD4 that localizes to the nucleus to activate and suppress the transcription of target genes [Schmierer, 2007]. The requirement for

SMAD2 was demonstrated in palatal shelf culture experiments, where siRNA knockdown of SMAD2 prevented the dissolution of the MES [Shiomi, 2006]. However, cKO of *Smad4* in the palatal epithelium has only a mild impact on palatal fusion, indicating the presence of other contributing pathways [Xu, 2008; Lane, 2015]. Indeed, analysis of other cKO lines revealed that both SMAD-independent p38 MAPK signaling through TAK1 activation and a chromatin reader TRIM33/SMAD2 complex independently contribute to palate fusion [Lane, 2015].

The exact cellular drivers of MES removal have been under investigation for decades. Until recently, MES dissolution by apoptosis, migration, or EMT were the three most popular hypotheses [Reviewed in Dudas, 2007; Nawshad, 2008; Bush, 2012; Kim, 2015]. Cell death of MEE cells can be readily seen during palate fusion, and blocking apoptosis pharmacologically was shown to be sufficient to prevent fusion in organ culture experiments [Cuervo, 2004]. However, observation of normal palate fusion in mice lacking a component of the apoptotic caspase-3 pathway, *Apaf-1*, has led to the conclusion that apoptosis is not required for fusion to occur [Jin, 2006]. The same study also showed static evidence of cell migration of the palatal shelf epithelium, but this mechanism has yet to be examined further [Jin, 2006]. Whether or not MEE cells can enter the mesenchyme through EMT is likely the most controversial proposal of the three. Early studies into EMT utilized fluorescent dyes that could be incorporated into the palate epithelium during organ culture experiments. This method provided conflicting results, as some groups identified the presence of the dye in the palatal mesenchyme after fusion, while others did not [Nawshad, 2008]. The advent of the Cre/lox system and lineage tracing studies did little to resolve these conflicts. Utilizing LacZ expression driven by an epithelial-specific Cre, two studies found that LacZ staining was restricted to the epithelium of the palate. [Vaziri Sani, 2005; Xu, 2006]. However, a different group using the same method found evidence for LacZ staining within the palatal

mesenchyme [Jin, 2006]. One possibility for these conflicting findings is that some MEE cells may end up trapped within the palate during fusion and undergo cell death, rather than being truly incorporated into the mesenchyme.

Despite extensive investigation, these three proposals are still readily entertained as mechanisms of palate fusion in even recent reviews [Nakajima, 2018]. However, review of other recent studies has begun to form a clearer picture of MES dissolution, where the MEE cells take on some mesenchymal properties in order to be removed from the MES, rather than becoming incorporated into the mesenchyme through EMT [Reviewed in Li, 2017]. TGFβ3 signaling in the MEE cells activates SNAIL, thereby reducing E-cadherin expression and allowing the release of MEE cells from the underlying mesenchyme [Kitase, 2013; Li, 2017]. In addition, live-imaging studies of fusing palates have observed large actin cables formation of rosettes within the MES that actively extruded MEE cells. [Kim, 2015]. The regulation of E-cadherin and cell extrusion were shown to be dependent on the activity of the microtubule and actomyosin apparatuses, respectively, and their disruption through genetic or pharmacological means prevents proper palate fusion [Kitase, 2013; Kim, 2015]. Instead of intrinsic cell death or migration of MEE cells, these studies present a more comprehensive image of palate fusion that involves coordinated tissue morphology changes to drive MES dissolution.

1.2.5 Mammalian palatogenesis: Mechanisms of palatal shelf ossification and patterning

Although most investigations into palatogenesis concentrate on the outgrowth, elevation, or fusion of the palatal shelves, these alone do not result in a properly developed palate. After fusion is complete, the mesenchymal cells of the presumptive hard palate condense and differentiate into osteoblasts. This process, called intramembranous ossification, is controlled by

several molecular regulators, including those with roles in other steps of palatogenesis. For instance, BMP signaling is important for palatal shelf growth [Chapter 1.2.2; Zhang, 2002; Rice, 2004; Li, 2011], but also plays a central role in palate bone formation. This was demonstrated through the conditional knockout of BMP receptor gene *Bmpr1a* in the palatal mesenchyme of mice, which resulted in reduced palatal shelf growth, palatine bone defects, and submucosal cleft palate [Baek, 2011]. Upstream regulators of BMP signaling also contribute to bone formation in the palate, including transcription factors HOX2A [Rijli, 1993; Gendron-Maguire, 1993; Iyyanar, 2017] and PAX3 [Wu, 2008], as well as the Jagged1-Notch signaling pathway [Hill, 2014]. Given the broad functions of BMP signaling in palatogenesis, defects of palate ossification often coincide with other changes. This is seen in *Hoxa2*-null mice, which show increased osteogenesis and proliferation of the shelves, along with elevation failure [Iyyanar, 2017]. Conversely, conditional knockout of *Jagged1* in NCCs led to decreased osteogenesis in the palate, but increased proliferation [Hill, 2014]. Together, these studies show that the molecular control of palatal shelf growth and bone formation partially overlap and underline the complexity of these mechanisms.

The secondary palate consists of the bony hard palate at the front and the muscular soft palate at the rear. Though many regulators of palate ossification have been identified, how this bone formation is restricted to the hard palate is still under investigation. As mentioned in Chapter 1.2.2, the specific expression patterns of transcription and growth factors along the anteroposterior axis provide a basis for these differences. It has been hypothesized that thickened epithelial ridges on the palatal shelves, called rugae, may help define the two regions [Peterkova, 1987; Pantalacci, 2008; Welsh, 2009]. Rugae play a mechanical role in mastication, also contain many sensory structures that assist in eating [Peterkova, 1987; Nunzi, 2004; Ishizaki, 2006]. Detailed characterization of rugae development in mice revealed that the first three initially form around

E12.5 [Peterkova, 1987; Pantalacci, 2008]. Following this, additional rugae arise in a predictable manner until nine or ten have formed by E16.0 [Charles, 2007; Pantalacci, 2008]. *In situ* analysis revealed that the eighth ruga is located at the border between anterior *Shox2* and posterior *Meox2*, two transcription factors with a mutually exclusive expression pattern along the anteroposterior axis [Zhang, 2005; Jin, 2006]. Importantly, this ruga is also located at the transition point between the hard and soft palate. These data indicate that the eighth ruga may serve as a boundary between anterior and posterior signaling during mouse palatogenesis, thereby inducing different tissue fates [Pantalacci, 2008]. Additional studies on rugae signaling will be needed to determine if this is the case.

1.3 Broader roles of the epithelium: IRF6 network in periderm development and palatogenesis

The epithelium plays several roles during development, but none so critical as defining the border between different tissues. During embryogenesis, all surface epithelia consist of an inner layer of cuboidal basal cells and an outer layer of flattened periderm cells [Richardson, 2009]. The basal layer serves multiple roles, including proliferating to accommodate the growth of palatal shelf, and undergoing differentiation to give rise to the periderm layer [Richardson, 2014]. While the periderm may have other functions, the best characterized role is the prevention of improper adhesions between epithelial layers [Lan, 2015]. This was demonstrated by direct ablation of periderm cells through Cre-mediated expression of diphtheria toxin fragment A, which resulted in ectopic oral adhesions and cleft palate [Richardson, 2014]. To achieve this non-adhesive property, the apico-basal polarity of the periderm cells is tightly regulated [Richardson, 2014]. Expression of adhesion markers such as E-cadherin are restricted to the basal membrane, thereby preventing

adhesions from forming on the apical surface [Richardson, 2014]. Establishment of the periderm layer occurs during the first stratification event of the epithelium and persists until shortly before birth [Richardson, 2014]. To maintain this population during development, a balance must be struck between the highly proliferative basal cells and terminally differentiated periderm [Richardson, 2006]. This balance is controlled through a complex network of regulatory factors [Richardson, 2014; Reviewed in Kousa, 2016]. Of these, interferon regulatory factor 6 (IRF6) plays a central role [Kousa, 2016].

Unlike other members of the IRF family which are important in the regulation of the immune system and metabolism, IRF6 acts mainly in the development of the epidermis [Yanai, 2012; Zhao, 2015]. IRF6 is highly expressed in both epithelial layers during development and is responsible for mediating the switch that drives the basal cells towards differentiation [Richardson, 2006]. While IRF6 acts through transcriptional regulation, it also has posttranslational roles [Kousa, 2016]. For example, ΔNp63, an isoform of p63 expressed in the basal layer, drives *Irf6* expression [Moretti, 2010]. In turn, IRF6 targets ΔNp63 to be degraded by the proteasome, thereby creating a negative feedback loop to control differentiation [Moretti, 2010]. In addition to ΔNp63, NOTCH/JAGGED2 and TGFβ signaling have also been shown to drive *Irf6* expression [Jiang, 1998; Restivo, 2011; Iwata, 2013]. Consistent with this role in epithelial development, loss of function or deletion of *Irf6* in mice leads to a hyperproliferative basal layer that does not properly undergo differentiation [Ingraham, 2006; Richardson, 2006]. These epithelial abnormalities result in a broad range of defects including limb malformations and lack of a functional epidermal barrier [Ingraham, 2006; Richardson, 2006]. *Irf6* mutants also exhibit cleft palate due to permanent ectopic oral adhesions [Ingraham, 2006; Richardson, 2006].

Variants in *IRF6* are the major cause of two orofacial clefting syndromes: Van der Woude syndrome (VWS; OMIM #119300) and popliteal pterygium syndrome (PPS; OMIM #119500) [Kondo, 2002; Leslie, 2013; Reviewed in Kousa, 2016]. The two syndromes share many similarities, including characteristic lip pits and orofacial clefting [Schutte, 2003]. VWS is currently the most common OFC syndrome and causes around 2% of all OFC malformations [Kousa, 2016]. However, PPS is much rarer and can include additional defects such as syndactyly, adhesions between the upper and lower eyelids, and genital abnormalities [Schutte, 2003]. The presentation of these syndromes is extremely variable, even within family cohorts [Burdick, 1985; Schutte, 2003; Martelli-Junior, 2007; Busche, 2016]. Given the epithelial defects seen in *Irf6* null mice, disorders such as these are being given the relatively novel classification of "peridermopathies" [Richardson, 2014].

IRF6 mutations only account for approximately 68% of VWS cases [de Lima, 2009]. Therefore, there have been many efforts to identify new genes that contribute to the disorder. Sequencing of a Finnish VWS family revealed causative mutations in another transcription factor, Grainyhead-like 3 (*GRHL3*) [Peyrard-Janvid, 2014]. Mouse KO of *Grhl3* resulted in phenotypes similar to those in *Irf6* mutants, including loss of periderm cells, ectopic oral adhesions, and cleft palate [Peyrard-Janvid, 2014]. Surprisingly, cleft palate was only identified in a subset of the embryos, suggesting that the periderm was either abnormal or discontinuous, or that the loss of periderm is not solely responsible for the high penetrance of cleft palate in *Irf6*-null mice. In addition, analysis in zebrafish showed that *Irf6* directly regulates *Grhl3* expression [de la Garza, 2013]. Together, these results broaden the known genetic etiology of VWS, and further implicate the role of the periderm in OFC.

A small percentage of VWS patients present with only isolated CL/P as their primary clinical phenotype [Kousa, 2016]. Indeed, variants in IRF6 have also been associated with nsCL/P, indicating that common mechanisms may be responsible for VWS and some nsCL/P cases [Zucchero, 2004; Rahimov, 2008; Beaty; 2010; Leslie, 2016]. Consistent with this, genes downstream of *Irf6* have also been implicated in nsCL/P. A GWAS study searching for SNPs associated with nsCL/P identified statistically significant variants within *ABCA4* [Beaty, 2010]. While the expression of *ABCA4* was only identified in the retina, *ARHGAP29*, an adjacent gene coding for a Rho GTPase activating protein (GAP), was found to have broad craniofacial expression [Beaty, 2010; Leslie, 2012]. Consistent with these findings, multiple *ARHGAP29* coding variants, predicted to be detrimental to protein function, were identified in patients with nsCL/P [Leslie, 2012]. Furthermore, ChipSeq analysis identified an IRF6 binding site upstream of the region, and KO of *Irf6* resulted in a reduction of ARHGAP29 expression in mice [Botti, 2011; Leslie, 2012]. Two recent studies have identified additional *ARHGAP29* mutations in patients with isolated clefts, further solidifying *ARHGAP29* as an OFC gene [Liu, 2017; Savastano, 2017].

Guanine-nucleotide-exchange factors (GEFs) and GAPs, such as ARHGAP29, are important for regulating the actin cytoskeleton through the activation and deactivation of Rho proteins, respectively [Sit, 2011]. Through these mechanisms, these proteins are integral in many cellular processes that require changes in cytoskeletal dynamics, such as cell migration [Sit, 2011]. Given that ARHGAP29 is reduced in *Irf6* mutants, it follows that IRF6 may regulate this process. Consistent with this, live-imaging analysis of wound scratch assays showed that keratinocytes from *Irf6*-null mice failed to properly close the wound and had reduced speed and directionality compared to controls [Biggs, 2014]. The same study also identified increased actin stress fibers in *Irf6*-null keratinocytes, and found that pharmacological inhibition of ROCK, a downstream

effector of RHOA, was sufficient to rescue both the migration and stress fiber phenotypes [Biggs, 2014]. Importantly, the study showed impaired wound healing in *Irf6* mutant embryos and noted that this result was in agreement with previous reports of increased post-surgery complications in VWS patients [Jones, 2010; Biggs 2014]. ARHGAP29 has also been shown to regulate cell adhesion in the oral epithelium. Introduction of a point mutation in one copy of *Arhgap29* in mice resulted in a delay in palate elevation and ectopic oral adhesions [Paul, 2017]. These adhesions were accompanied by disorganized basal and periderm layers, along with changes in cytokeratin expression [Paul, 2017]. Together, these studies show that IRF6 can regulate both cell movement and adhesion and implicate ARHGAP29 as a primary mechanism.

Mouse models with disruptions in *Irf6* and *Irf6*-related genes are steadily revealing the importance of periderm differentiation and function in palatogenesis. Absence of periderm in *Irf6* mutant homozygotes or through direct genetic ablation results in permanent oral adhesions and cleft palate [Ingraham, 2006; Richardson, 2006; Richardson, 2014]. These drastic epithelial defects are also phenocopied in other mouse mutants including mice null for *Jagged2*, ΔNp63, IκB kinase-α (*Ikkα*), *Stratifin*, and receptor-interacting serine/threonine protein kinase 4 (*Ripk4*) [Jiang, 1998; Romano, 2012; Richardson, 2014; De Groote, 2015; Kousa, 2016]. While JAGGED2 and ΔNp63 have established connections to *Irf6*, the function of the other proteins in epithelial development and whether or not they interact with IRF6 is under investigation [Reviewed in Kousa, 2016]. In contrast, *Irf6* heterozygotes retain a stratified epithelium but still show transient oral adhesions [Richardson, 2006]. The periderm is still present in these embryos but is somehow abnormal, suggesting that *Irf6* is required for periderm function as well as differentiation. [Richardson, 2006]. Transgenic overexpression of *Irf6* in the basal layer of *Irf6*-null embryos resulted only in a partial rescue of the fusion defects, further reinforcing an autonomous role for IRF6 in the periderm

[Kousa, 2017]. Similar defects are seen in mice deficient for *Grhl3* and *Arhgap29*, as well as *Irf6*/*ΔNp63* and *Irf6*/*Jagged2* double heterozygotes [Richardson, 2009; Thomason, 2010; Peyrard-Janvid, 2014; Paul, 2017]. The ectopic oral adhesions in these mutants are not due to a total lack of epidermal differentiation, but rather a disorganized periderm layer or abnormalities in the function of the periderm itself [Richardson, 2006; Richardson, 2009; Thomason, 2010; Peyrard-Janvid, 2014; Paul, 2017]. One possible mechanism for these adhesions is the misexpression of cell adhesions markers, as seen in *Irf6*/*Jagged2* double heterozygotes [Richardson, 2009]. Furthermore, the delay in palate elevation identified in *Arhgap29* heterozygotes shows that transient adhesions may be able to slow down palate development without causing a permanent defect [Paul, 2017]. This represents a possible mechanism for nsCL/P in humans, wherein mutations that impact periderm function result in a predisposition to palate defects, even if not completely penetrant. Collectively, these models show that regulation of both periderm differentiation and function is important in palatogenesis and demonstrate the need to identify additional genes that contribute to nsCL/P through peridermal abnormalities.

1.4 Mesenchymal migration and remodeling in palatogenesis

Tissue patterning during embryonic development involves drastic morphological changes. These processes can be seen readily in craniofacial development, wherein proper palatogenesis requires the outgrowth, elevation, and fusion of the palatal shelves coordinated with the growth and movement of the other craniofacial processes [Bush, 2012]. As previously discussed in Chapter 1.2, analyses of mutant mouse models have shown that many clefts are due to insufficiencies in proliferation of the palatal mesenchyme, ectopic adhesions, failure to remove the MES, or obstruction due to structures [Bush, 2012]. In contrast, other mutants that exhibit none of

these changes can still present with palate defects, such as *Zfhx1a*-null mice, which show delayed palatal shelf elevation [Jin, 2008]. While force generation through hydration of hyaluronan-rich ECM has been suggested as a mechanism for the rapid flipping motion of the anterior palate, it does not explain the bulge formation in the middle palate during elevation [Brinkley, 1986; Ferguson, 1988; Yu, 2011]. Additionally, it has been suggested that the speed at which this elevation occurs precludes proliferation from being the sole cellular mechanism driving this medial extension [Walker, 1956]. Tissue rearrangement through collective cell migration is a well-studied phenomenon in other systems [Reviewed in Scarpa, 2016]. Thus, it is possible that directed migration is also occurring during palatal shelf morphogenesis.

The movement of the cranial neural crest cells (CNCC) is likely the most prominent example of collective migration in craniofacial development. Briefly, after delamination from the neural folds, CNCCs migrate through defined pathways toward the early craniofacial processes [Chapter 1.2.1; Minoux, 2010; Kindberg, 2018]. This migration pattern is characterized by an integration of contact inhibition of locomotion, co-attraction, and chemotaxis controlled through transient cell adhesions and cell polarity [Chapter 1.2.1; Scarpa, 2015; Barriga, 2015]. Despite extensive investigation into CNCC migration, relatively little is known about the behavior within the NCC-derived palatal mesenchyme. One of the first examples of mesenchymal migration was identified in a study of mice with deficiencies in WNT signaling, a pathway involved in a wide variety of developmental processes [Steinhart, 2018]. Mutants for ligand *Wnt5a* and/or its receptor *Ror2* exhibit cleft palate, and a detailed examination showed increased proliferation and *Sox9* expression in the presumptive nasal half of the anterior palate [He, 2008]. Interestingly, chimeric palatal shelf explants with EGFP-expressing and non-fluorescent halves revealed directional movement of palatal mesenchyme from the posterior to the anterolateral regions [He, 2008]. This

directional migration was absent in *Wnt5a* mutants but was rescued when WNT5A beads were placed in the culture [He, 2008]. This study found that FGF10 beads had a similarly chemotactic effect [He, 2008]. Together, these results depict a novel mechanism of heterogeneity in the palatal shelves wherein posterior mesenchyme can be driven anteriorly by various chemotactic factors to impact gene expression and ensuing proliferative or morphological changes in the anterior palate. Given the difference in *Sox9* distribution in *Wnt5a* mutants, mesenchymal movement may also serve to regulate the mediolateral asymmetry of gene expression in the palate. Additionally, these findings add a confounding factor to the interpretation of proliferation defects in mouse models with palate defects. If a deficit in mesenchymal migration results in proliferation changes, the proliferation may then be misconstrued as the primary cause of the malformations. Nevertheless, this study represents a novel perspective on the movement of palatal mesenchyme that had not been previously appreciated.

The various mechanisms underlying tissue morphogenesis and the forces driving them have been well-characterized [Reviewed in Heisenberg, 2013]. Through regulation of cell junctions, cytoskeletal contractility, and the ECM, collections of cells can rapidly reorganize to modify the shape of a tissue [Heisenberg, 2013]. The drastic changes seen during palate elevation indicate that similar rearrangements are occurring in palatogenesis. Consistent with this, early studies found changes in regional cell density and ECM distribution during elevation [Brinkley, 1986; Morris-Wiman, 1992]. These observations strongly suggested that remodeling plays a role, but it would be many years before follow-up experiments were performed. Recently, a computational analysis of serial sections has shed some light on the underlying dynamics of cleft palate in *Tbx1*-null embryos [Brock, 2016]. While some minor differences in palate dimensions, cell density, and proliferation were identified when compared to controls, the most striking change

was in the cell polarity [Brock, 2016]. Staining of Golgi bodies, serving as a proxy marker for the direction of cell movement, showed that orientation changes from ventral to medial immediately following elevation [Brock, 2016]. This change did not occur in *Tbx1*-null palates, suggesting that this change in cellular orientation may be important in palate elevation [Brock, 2016]. In a separate study, characterization of various palate-enriched ECM molecules found that *Tenascin-C* was expressed along the medial side of the middle palate before elevation but moved to the midline after elevation **(Fig. 1.4)** [Chiquet, 2016]. This shift in distribution is consistent with remodeling of the palatal shelf in the middle palate, as a static rotation of the shelf would result in a more dorsolateral distribution of Tenascin-C. Additionally, co-staining for F-actin with rhodamine-phalloidin and Tenascin-C showed an alignment of these markers with the vertical palatal shelves that became more randomized after elevation, indicating a presence of a potential tensile force [Chiquet, 2016]. A comparable change in the alignment of elongated nuclei was also observed, serving as a possible explanation for the difference in orientation found in Brock *et al.* 2016 [Brock, 2016; Chiquet, 2016]. Together, these studies highlight morphological changes in the palatal shelves during elevation and further implicate both ECM and cytoskeletal components in the remodeling of the mesenchyme.

To date the only functional study of ECM in palate remodeling examined the role of RAC1 [Tang, 2015]. As a member of the Rho GTPase family, RAC1 is integral for cytoskeletal organization but has also been shown to play a role in fibronectin ECM assembly [Dzamba, 2009; Sit, 2011; Payapilly, 2018]. Immunostaining of E13.5 shelves revealed fibrillar structure of fibronectin in the middle of the shelf with ring structures on either side, coinciding with lower and higher cell density, respectively. [Tang, 2015]. Electroporation of a constitutively active form of RAC1 resulted in an elevation failure and loss of this fibrillar arrangement [Tang, 2015]. Given

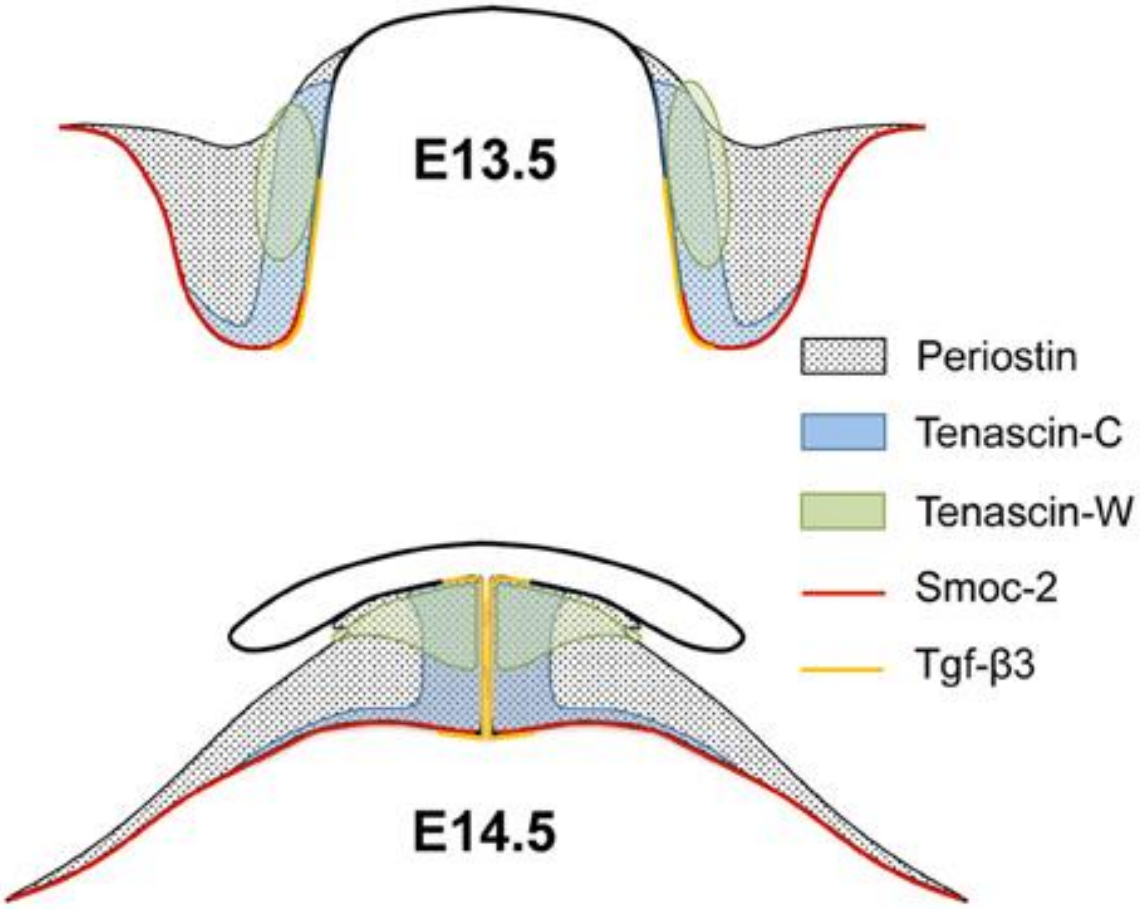

Figure 1.4: ECM protein distribution before and after palate elevation. Depictions of medial palatal shelves with superimposed gene expression patterns assessed by *in situ* hybridization and immunofluorescence experiments. Patterning before (top) and after (bottom) elevation is consistent with a remodeling process, rather than a "flip-up" mechanism.

Image (Scheme of the combined expression patterns of ECM genes in palatal shelves before and after elevation) from Chiquet, M., Blumer, S., Angelini, M., Mitsiadis, T. A., & Katsaros, C. (2016). Mesenchymal Remodeling during Palatal Shelf Elevation Revealed by Extracellular Matrix and F-Actin Expression Patterns. *Front Physiol, 7*, 392. doi:10.3389/fphys.2016.00392.

the similarities to the F-actin pattern identified by Chiquet *et al.* 2016, it is possible that the fibronectin fibers may also exert a tensile force during elevation [Chiquet, 2016]. Tang *et al.* 2015, on the other hand, hypothesized that the differences in fibronectin arrangement facilitated different migration speeds, thereby changing regional cell density and driving palate elevation [Tang, 2015]. It is also possible that the constitutively active RAC1 impacted mesenchymal migration directly through disruption of cytoskeletal dynamics. Further experiments will be required to determine the precise mechanism. Nevertheless, these results represent one of the first functional studies into the role of ECM in palate development and provide additional evidence to support the claim that remodeling and/or migration of the palatal mesenchyme is a driving force in palatogenesis.

1.5 SPECC1L in craniofacial development

1.5.1 SPECC1L mutations in human patients with orofacial clefts

The gene "Sperm Antigen With Calponin Homology And Coiled-Coil Domains 1-Like*"* (*SPECC1L*) encodes a cytoskeletal protein with roles in cytoskeletal organization, microtubule stability, cell migration, and cell adhesion [Saadi, 2011]. As the name suggests, SPECC1L contains eight coiled-coil domains (CCD) and a C-terminal calponin homology domain (CHD). Mutations in *SPECC1L* were originally detected in two patients with atypical facial clefts [Dasouki, 1988; Saadi, 2011]. The first patient exhibited severe bilateral oblique facial clefts, cleft palate, ocular hypoplasia, and calcaneovarus foot malformation, while the second had a unilateral oblique facial cleft, a lateral facial cleft, and cleft palate with no other defects [Dasouki, 1998; Saadi, 2011]. Genetic analysis of the first patient by karyotyping identified a balanced chromosomal translocation between chromosome 1 and 22 [Dasouki, 1988]. Further refinement through fluorescence in situ hybridization (FISH), southern blotting, and restriction digest experiments

pinpointed the breakpoint to intron 14 of *SPECC1L*, resulting in haploinsufficiency of the gene [Saadi, 2011]. Sequencing of the second patient identified the heterozygous point mutation p.Gln415Pro (Q415P; NM_015330.2) in the second CCD of the protein [Saadi, 2011]. These results were the first to associate *SPECC1L* with craniofacial development and OFC.

Additional sequencing led to the discovery of *SPECC1L* (NM_015330.3) mutations in Opitz G/BBB syndrome patients [Kruszka, 2015]. Opitz G/BBB syndrome can be either autosomal dominant or X-linked and most commonly presents with hypertelorism, abnormalities of the laryngotracheoesophageal region (larynx/trachea/esophagus), and cleft palate [Kruszka, 2015]. The Opitz G/BBB mutations p.Thr397Pro (Family A; T397P) and p.Gly1083Ser (Family B; G1083S) were identified in two multigenerational families [Kruszka, 2015]. Each family had multiple affected members, and each instance segregated with the respective mutation [Kruszka, 2015]. *SPECC1L* (NM_015330.3) mutations were also identified in two patients with Teebi hypertelorism syndrome [Bhoj, 2015]. As the name suggests, Teebi hypertelorism syndrome also presents with an abnormally large interocular distance, but also includes malformations such as interdigital webbing, shawl scrotum, and upslanting palpebral fissures [Bhoj, 2015]. The first Teebi mutation p.Glu420Asp (E420D) was identified in a family with both mother and child affected [Bhoj, 2015]. Lastly, a *de novo* deletion identified in the second Teebi patient resulted in an in-frame deletion of two amino acids (p.I400_H401del) [Bhoj, 2015]. Only Opitz G/BBB syndrome has a strong association with cleft palate. However, the phenotypes of both disorders partially overlap, and both show distinctive facial features such as a prominent forehead and broad nasal bridge, suggesting that they may have related etiologies [Kruszka, 2015; Bhoj, 2015].

Recently, a comprehensive report of the previous patients along with 16 additional individuals from 8 families with *SPECC1L* (NM_015330.4) variants has suggested the

classification of "*SPECC1L*-related syndrome" for the subset of patients originally identified with Opitz G/BBB or Teebi syndromes [Bhoj, 2018]. Compilation of the reported clinical anomalies in this group totaling 31 individuals revealed a wide variety of phenotypes [Bhoj, 2018]. These encompassed craniofacial defects such as CL/P and micrognathia, but also included malformations of the larynx, heart, diaphragm, reproductive organs, central nervous system, and ears [Bhoj, 2018]. A learning or intellectual disability was also present in a percentage of the patients [Bhoj, 2018]. Interestingly, all the mutations reside within or immediately adjacent to the second CCD or C-terminal CHD, suggesting that these domains are important in SPECC1L function. The study also compared these phenotypes to those seen in patients with mutations in *MID1*, the gene responsible for X-linked Opitz G/BBB syndrome [Taylor, 2010; Winter, 2016]. Like SPECC1L, the MID1 protein is involved in microtubule-stabilization [Winter, 2016; Bhoj, 2018]. The anomalies between both groups overlapped significantly, likely owing to the similar cellular function, but the study argued that the clinical presentation was distinct enough to separate the two [Bhoj, 2018]. Patients with *SPECC1L* mutations had an increased incidence of abdominal wall (omphalocele), diaphragm, and uterine anomalies, while patients with *MID1* mutations had a higher incidence of laryngeal clefts [Bhoj, 2018]. Interestingly, the urogenital defect hypospadias was exclusively identified in patients with *MID1* mutations, despite it being a common Opitz G/BBB syndrome phenotype [Bhoj, 2018]. Collectively, these results define these conditions resulting from *SPECC1L* and *MID1* mutations as two distinct syndromes, which further elucidates the etiology of patients with Opitz G/BBB and Teebi hypertelorism syndromes.

1.5.2 Diverse functions of coiled-coil and calponin homology domain-containing cytoskeletal proteins

The cytoskeleton is a complex network of filamentous proteins involved in virtually every cellular process including migration, vesicular trafficking, cell division, and adhesion [Tang, 2017; Bezanilla, 2015]. In mammalian cells, this network is composed of actin, microtubules, and intermediate filaments [Fletcher, 2010]. Integral to this system is a myriad of regulatory proteins that serve to control cytoskeletal dynamics [Fletcher, 2010]. Many cytoskeletal proteins act as molecular scaffolds that serve to mediate signal transduction or the assembly and stability of proteins complexes [Fletcher, 2010]. For example, microtubule and actin crosslinking factor 1 (MACF1) of the Spectraplakin family is required for the targeting of microtubules to focal adhesions [Wu, 2008; Reviewed in Zhang, 2017]. Another cytoskeletal crosslinker, IQGAP1, regulates the stability of endosome-associated networks, but also plays roles in cell adhesion and migration [Samson, 2017; Noritake, 2007].

Scaffold proteins often regulate cytoskeletal dynamics by directly binding to cytoskeletal components. Many of these proteins contain calponin homology domains (CHD), which allow binding to filamentous actin (F-actin) [Korenbaum, 2002]. Named after the muscle contraction protein calponin, CHDs are highly structurally conserved motifs consisting of four large, sandwiched α-helices connected by three smaller α-helices [Gimona, 2002]. CHD-containing proteins identified to date contain one, two, or four CHD repeats, and two CHDs in tandem form an actin binding domain (ABD) [Korenbaum, 2002; Gimona, 2002]. While ABDs have a high affinity for F-actin, proteins containing only a single CHD, such as IQGAP1, have also been shown to interact with the actin cytoskeleton [Gimona, 2002; Mateer, 2004].

Coiled-coil domains (CCD) are another motif common in cytoskeletal proteins [Burkhard, 2001; Truebestein, 2016]. Like CHDs, the structure of CCDs is highly conserved, comprising two supercoiled α-helices [Truebestein, 2016]. CCDs are found in proteins with a wide variety of functions [Truebestein, 2016]. For instance, the family of CCD-containing Golgin proteins act to tether vesicles to the Golgi body during vesicle transport [Witkos, 2015]. CCDs span most of the length of these proteins and serve as molecular spacers between each structure [Truebestein, 2016]. This function as a molecular spacer can also be seen in CCD-containing proteins involved in chromosome segregation and centriole architecture [Truebestein, 2016]. The highly standardized structure of CCDs allows them to be used as molecular rulers to measure distances in proteins with enzymatic or transcriptional roles, as well as maintain precise distances between components of a cytoskeletal complex [Truebestein, 2016]. Conformational changes of CCDs can also propagate down the length of the domain to other regions of the protein, allowing force to be propagated longer distances, such as in molecular motors [Truebestein, 2016]. In many cases, the length and structure of the coil is more critical than the amino acid sequence, leading to examples where the former, but not the latter, are conserved across species [Truebestein, 2016].

1.5.3 Cellular analysis of SPECC1L expression

SPECC1L contains eight CCDs along the length of the protein with a CHD at the C-terminal end. Endogenous SPECC1L has a punctate expression pattern distributed throughout the cell, with some nuclear expression [Saadi, 2011; Mattison, 2011]. Consistent with SPECC1L containing a CHD, much of SPECC1L expression aligns with F-actin, and reorganization of the actin cytoskeleton using ionomycin treatment results in concomitant reorganization of SPECC1L expression [Saadi, 2011]. SPECC1L also highly co-localizes with acetylated-α-tubulin in the

mitotic spindles and during mitosis [Saadi, 2011; Mattison, 2011]. Furthermore, SPECC1L also concentrates along cell adhesions and adherens junction markers, especially at high cell density [Wilson, 2016]. These expression studies indicate that SPECC1L is a cytoskeletal protein involved in the regulation of cell adhesions and division through association with F-actin and microtubules.

The function of SPECC1L domains has been analyzed using green fluorescent protein (GFP) tagged SPECC1L constructs [Saadi, 2011]. When a SPECC1L-GFP overexpression construct is transfected into cells, it results in a filamentous pattern very different from normal expression [Saadi, 2011]. This pattern associates largely with acetylated-α-tubulin [Saadi, 2011]. However, addition of syndromic human mutations in either CCD2 or the CHD disrupts this association [Saadi, 2011; Kruszka, 2015]. Likewise, truncation of the CHD ablates this expression pattern [Saadi, 2011]. In a different study, the authors evaluated the expression pattern of SPECC1L fragments (1-351, 351-851, and 851-1117) with respect to F-actin [Mattison, 2011]. They found that the C-terminal and middle fragments showed a strong and weak F-actin association, respectively [Mattison, 2011]. In contrast, the N-terminal fragment showed no co-localization with F-actin [Mattison, 2011]. These studies show that the C-terminal section of SPECC1L mediates F-actin association, while both the CCD2 and CHD are important for association with stabilized microtubules.

1.5.4 Cellular analysis of SPECC1L function

Knockdown of *SPECC1L* has been utilized to evaluate how loss of the protein impacts cell function [Saadi, 2011; Mattison, 2011; Wilson, 2016]. For example, when grown at low density, control and *SPECC1L*-kd U2OS cells exhibit similar morphology. However, at high density, *SPECC1L*-kd U2OS cells display an elongated phenotype compared to the cuboidal shape of

control cells [Wilson, 2016]. Similarly, *SPECC1L*-kd 293T cells cultured at high density lose adherence to the substrate and lift off in clumps [Saadi, 2011]. Although the consequence between cell types is different, both are examples of impaired regulation of cell-substrate and cell-cell contacts. In agreement with this, immunostaining of adherens junction markers β-catenin and E-cadherin in *SPECC1L*-kd U2OS cells reveals abnormally widened cell junctions compared to controls. These cells also have defects in cytoskeletal organization, as shown by staining for F-actin and non-muscle Myosin II-B (NM-IIB) [Saadi, 2011; Wilson, 2016]. This cytoskeletal defect is made even more apparent upon treatment with compounds that induce cytoskeletal reorganization, such as ionomycin or WNT5A [Saadi, 2011]. *SPECC1L*-kd U2OS cells also exhibit impaired migration during wound-repair assays [Saadi, 2011]. Lastly, knockdown of *SPECC1L* in HeLa using siRNA results in spindle rocking and defects in chromosomal distribution during mitosis [Mattison, 2011]. Collectively, these studies demonstrate a role for SPECC1L in a variety of cellular processes including adhesion, cytoskeletal organization, migration, and division.

Loss of SPECC1L has been linked with reduced PI3K-AKT signaling *in vivo* and *in vitro* [Wilson, 2016]. Canonical phosphatidylinositol 3-kinase (PI3K)-AKT signaling is mediated by receptor tyrosine kinases, such as Platelet-derived growth factor receptor α (PDGFRα) [Vasudevan, 2010]. After recruitment to the membrane by receptor tyrosine kinases, PI3K converts the phospholipid phosphatidylinositol 4,5-bisphosphate (PIP_2) into PIP_3 [Vasudevan, 2010; Manning, 2017]. In turn, PIP_3 recruits protein kinase B (AKT) to be phosphorylated, after which AKT proceeds to modulate downstream effectors to promote cellular survival, proliferation, migration, and a variety of other functions [Vasudevan, 2010; Xue, 2013; Manning, 2017]. Embryos containing a knock-in $Pdgfra^{PI3K}$ allele that prevents PI3K recruitment exhibit midline

blebbing and cleft palate, demonstrating the importance of PI3K-AKT signaling in craniofacial development [Fantauzzo, 2014].

Western blotting showed reduced pan-AKT levels in *SPECC1L*-kd U2OS cells [Wilson, 2016]. Upregulation of PI3K-AKT signaling with AKT activator SC79 partially rescued the cell shape and adherens junction defects in *SPECC1L*-kd U2OS cells [Jo, 2012; Wilson, 2016]. Likewise, PI3K inhibition by wortmannin was sufficient to induce *SPECC1L*-deficient phenotypes in control cells [Ui, 1995; Wilson, 2016]. These results suggest that SPECC1L regulates adherens junctions in part through the stabilization of AKT [Wilson, 2016].

1.5.5 Animal models of SPECC1L deficiency

The developmental consequences of SPECC1L-deficiency have been investigated in fruit fly, zebrafish, and murine model systems [Saadi, 2011; Gfrerer, 2014; Wilson, 2016]. In *Drosophila*, knockdown is achieved through conditional RNAi targeting of *SPECC1L*-orotholog *CG13366* [Saadi, 2011]. Ubiquitous knockdown using the *daughterless*-GAL4 driver results in crumbled or inflated wings, a cleft proboscis, and eventual death attributed to feeding difficulties [Saadi, 2011]. Crumpled or blistered wings, along with a dorsum fusion defect are also seen upon knockdown in the wing-imaginal-disc using the A9-GAL4 driver [Saadi, 2011]. The authors state that the wing phenotypes are reminiscent of those seen in knockdown models of integrins and integrin-associated proteins [Saadi, 2011; Narasimha, 2013]. Integrins are adhesive molecules with close ties to the actin cytoskeleton, and the similar phenotypes are consistent with a role for SPECC1L in cell adhesions [Delon, 2007].

The genetic utility combined with optically accessible development has allowed for the extensive study of craniofacial genetics in the zebrafish model [Van Otterloo, 2016; Machado,

2017; Duncan, 2017]. While the craniofacial skeleton may differ from mammals, parallels can be made for specific craniofacial structures, such as between the ethmoid plate and secondary palate in fish and mammals, respectively [Duncan, 2017]. Furthermore, the high degree of conservation between fish and mammalian genomes allows identification of functionally relevant homologs [Duncan, 2017; Machado, 2017]. The zebrafish genome contains two *SPECC1L* homologs on chromosomes 8 (*specc1la*) and 21 (*specc1lb*) [Saadi, 2011]. An initial study using morpholino (MO)-based knockdown of these homologs found no apparent phenotype [Saadi, 2011]. However, knockdown of a *SPECC1* homolog, a gene related to *SPECC1L*, did result in a dose-dependent "faceless" phenotype [Saadi, 2011]. In contrast to these previous findings, a second study described multiple defects after *specc1lb* knockdown, including clefts of the ethmoid plate and absent lower jaw [Gfrerer, 2014]. Why knockdown of *specc1lb* resulted in different consequences between the two studies is unclear, but may have been due to differences in morpholino design. These defects were partially rescued when embryos were treated with *specc1lb* mRNA, reinforcing the causal role of the initial knockdown [Gfrerer, 2014]. Furthermore, lineage tracing of NCC cells using a *sox10*-driven photoconvertible marker found that MO-treated embryos exhibited reduced NCC contribution to craniofacial structures, in addition to reduced proliferation in those regions [Gfrerer, 2014]. These studies showed the first example of craniofacial malformations in a vertebrate model of SPECC1L-deficiency, as well as established a role for SPECC1L in NCC function.

Murine palate development shares many similarities with the human process, making mice one of the most relevant model systems for studying orofacial clefting [Otterloo, 2016]. A relatively quick method of generating mouse knockout models is through the insertion of gene trap vectors into the genome, which disrupt a gene at the point of insertion [Friedel, 2010]. Recently,

our group generated two mouse models of SPECC1L deficiency using existing gene trap embryonic stem cell lines [Wilson, 2016]. These vectors, termed DTM096 and RRH048, reside within intron 1 and 15, respectively, and each consists of a splice acceptor, β-galactosidase reporter, and polyA tail [Wilson, 2016]. As DTM096 is inserted before the start of protein translation, only β-galactosidase is expressed, while the RRH048 allele results in a SPECC1L-βgal fusion protein [Wilson, 2016]. Embryos heterozygous for either allele displayed craniofacial phenotypes very rarely, along with a slightly reduced Mendelian ratio than expected [Wilson, 2016]. LacZ staining of these embryos revealed a pattern of SPECC1L expression that aligned closely with the NCC lineage, and immunofluorescence confirmed the overlap between SPECC1L and both SOX10 and AP2α, two widely-used NCC markers [Wilson, 2016].

In contrast to the relatively mild heterozygote phenotype, the homozygotes exhibited embryonic lethality between E9.5 and E10.5 with a cranial neural tube closure defect [Wilson, 2016]. Evaluation of the NCCs by immunostaining with SOX10 showed NCCs still present within the open neural folds of the homozygote, while NCCs within control embryos had already begun to enter the facial primordia [Wilson, 2016]. The delamination defect is consistent with the reduced NCC contribution to craniofacial structures in the *specc1lb* MO knockdown zebrafish model [Gfrerer, 2014].

Molecular analysis of *Specc1l* gene trap homozygotes recapitulated several of the *in vitro* findings from *SPECC1L*-kd U2OS cells [Wilson, 2016]. Staining for adherens junction and cytoskeletal markers showed increased intensity, and the levels of both phosphorylated and non-phosphorylated AKT were reduced [Wilson, 2016]. Consistent with the role of PI3K-AKT signaling in cell survival, a marked increase in apoptosis was also observed [Wilson, 2016]. Collectively, these results provide a possible mechanism for the NCC delamination defects in

homozygotes, wherein reduced AKT signaling leads to abnormal cell adhesions, which in turn prevent proper exit from the epithelial layer.

1.6 Study Significance

Orofacial clefts have a multitude of genetic and environmental causes. While the causes of these malformations have been identified in numerous patients, there remain many cases for which the basis is still unknown. This complex etiology necessitates continuous genetic screening of affected individuals to identify novel genes associated with these birth defects. Subsequent analyses into the molecular, cellular, and developmental function of these novel genes are essential for understanding how they contribute to orofacial clefts. Variants in *SPECC1L* have been identified in multiple patients with craniofacial anomalies, including cleft palate. This dissertation investigates the role of this cytoskeletal protein using both deficiency and gain-of-function models.

Chapter 2 describes the generation and characterization of a compound heterozygous mouse model containing one null and one truncation *Specc1l* allele. The data show that moderate *Specc1l* deficiency can cause a delay in palate elevation and establish a role for SPECC1L in the oral epithelium downstream of IRF6. In Chapter 3, we explore a role for SPECC1L in cell migration using both *SPECC1L*-kd U2OS cells and primary mouse embryonic palatal mesenchyme cells from compound heterozygotes. Thorough analyses of time-lapse imaging movies show that SPECC1L-deficiency in both cell types leads to reduced speed and poor collective movement during wound closure. We also show that activation of PI3K-AKT signaling can rescue the defects in wound closure speed. Lastly, Chapter 4 investigates the developmental impact of the p.Thr397Pro *SPECC1L* Opitz G/BBB syndrome mutation using a CRISPR Cas9-generated knock-in mouse model. This disruption to the second coiled-coil domain of SPECC1L

results in embryos with ventral body wall defects and fully penetrant cleft palate. Additionally, we show that SPECC1L localization is altered in mutant palates, consistent with a gain-of-function mutation. Taken together, these studies establish a direct role for SPECC1L in palatogenesis and connects it with a well-known orofacial clefting pathway. They also specify distinct functions for SPECC1L in the palatal mesenchyme and epithelium. Furthermore, the phenotypic differences between embryos with truncation and point mutation alleles demonstrate that each has a distinct impact on protein function. Future inquiries comparing the cellular and molecular consequences of different *Specc1l* alleles will be critical to understanding how mutations in this gene contribute to the anomalies in patients with *SPECC1L* mutations.

CHAPTER TWO:

SPECC1L REGULATES PALATE DEVELOPMENT DOWNSTREAM OF IRF6

Authors
Everett G. Hall, Luke W. Wenger, Nathan R. Wilson, Sraavya Undurty, Jennifer Standley, Eno A. Augustine-Akpan, Youssef A. Kousa, Diana S. Acevedo, Jeremy P. Goering, Lenore Pitstick, N. Natsume, Shahnawaz Yousaf, Tamara Busch, M. Ito, A. Mori, H. Imura, Wasiu L. Adeyemo, Mekonen A. Eshete, Bryan C. Bjork, Satoshi Suzuki, Jeffrey C. Murray, Brian C. Schutte, Azeez Butali, Irfan Saadi

Contributions
EGH, LWW and IS conceived and designed the experiments. EGH, LWW, NRW, SU, JS, EAA, YK, DSA, JPG, LP, SY, TB, and BCB performed the experiments. NN, MI, AM, HI, WLA, MAE, SS, JCM, and AB provided nsCL/P samples and SPECC1L sequencing data. EGH, LWW, NRW, SU, JS, YK, TB, BCB, BCS, AB and IS analyzed the data. EGH and IS wrote the paper. JK, BCB, BCS, and AB edited the manuscript. All authors reviewed the manuscript.

2.1 Abstract

SPECC1L mutations have been identified in patients with rare atypical orofacial clefts and with syndromic cleft lip and/or palate (CL/P). These mutations cluster in the second coiled-coil and calponin homology domains of SPECC1L and severely affect the ability of SPECC1L to associate with microtubules. We previously showed that gene trap knockout of *Specc1l* in mouse results in early embryonic lethality. We now present a truncation mutant mouse allele, *Specc1l*$^{\Delta C510}$, that results in perinatal lethality. *Specc1l*$^{\Delta C510/\Delta C510}$ homozygotes did not show cleft palate, however, when crossed with a gene trap allele, *Specc1l*$^{cGT/\Delta C510}$ compound heterozygotes showed a palate elevation delay with incompletely penetrant cleft palate. *Specc1l*$^{cGT/\Delta C510}$ embryos exhibit transient oral epithelial adhesions at E13.5, which may delay shelf elevation. Consistent with oral adhesions, we show periderm layer abnormalities, including ectopic apical expression of adherens junction markers, similar to *Irf6* hypomorphic mutants and *Arhgap29* heterozygotes. Indeed, SPECC1L expression is drastically reduced in *Irf6* mutant palatal shelves. Lastly, we wanted to determine if *SPECC1L* deficiency also contributed to non-syndromic (ns) CL/P. We sequenced 62 Caucasian, 89 Filipino, 90 Ethiopian, 90 Nigerian and 95 Japanese patients with nsCL/P and identified three rare coding variants (p.Ala86Thr, p.Met91Iso, p.Arg546Gln) in six

individuals. These variants reside outside of SPECC1L coiled-coil domains and result in milder functional defects than variants associated with syndromic clefting. Together, our data indicate that palate elevation is sensitive to deficiency of SPECC1L dosage and function, and that SPECC1L cytoskeletal protein functions downstream of IRF6 in palatogenesis.

2.2 Introduction

Orofacial clefting is the most common craniofacial congenital malformation, with an incidence of approximately 1 in 800 live-births [Rahimov, 2012; Mossey, 2012]. Among orofacial clefts, approximately 70% of cases manifest as isolated or non-syndromic cleft lip with or without cleft palate (nsCL/P) [Stanier, 2004], while the remaining 30% consists of more than 275 different syndromic forms of clefting [Leslie, 2013a].

The underlying pathology of many syndromic CL/P cases can be narrowed down to a single causative gene and shows a Mendelian inheritance pattern in affected families. In contrast, nsCL/P often presents in families with incomplete penetrance and represents a complex disorder with a heterogeneous genetic component [Murray, 1995; Jugessur, 2009; Rahimov, 2012; Pengelly, 2016]. Genome-wide association studies in conjunction with traditional candidate gene and linkage analyses have contributed to the identification of several nsCL/P-associated genes [Dixon, 2011; Marazita, 2012; Adeyemo, 2017]. One method of conceptualizing the effect of these many genes is by organizing them into regulatory networks. For instance, both *IRF6* and *GRHL3* mutations have been identified in patients with Van der Woude syndrome (VWS) [Kondo, 2002; Leslie, 2013b; Peyrard-Janvid, 2014; Kousa, 2016], as well as patients with isolated CL/P [Zucchero, 2004; Rahimov, 2008; Beaty, 2010; Leslie, 2016a; Leslie, 2016b; Gowans, 2017]. Previous studies have shown that IRF6 regulates GRHL3 expression [Botti, 2011; de la Garza,

2013], and mouse mutants for the two genes show similar phenotypes [Ingraham, 2006; Richardson, 2006; Peyrard-Janvid, 2014]. Together, these studies implicate functional deficiency of an IRF6-GRHL3 network in nsCL/P [Kousa, 2016; Leslie, 2016a; Leslie, 2016b]. This network has been expanded to include ARHGAP29 [Leslie, 2012; Letra, 2014; Savastano, 2017; Liu, 2017].

The IRF6-GRHL3 network is required for specification and proper differentiation of the periderm [Richardson, 2009; de la Garza, 2013; Peyrard-Janvid, 2014], a single layer of specialized epithelial cells that prevents abnormal epithelial adhesions during embryonic development [Richardson, 2014]. The periderm achieves this non-adhesive property by localizing adhesion molecules away from its apical surface, preventing cell-cell adhesion [Richardson, 2009; Richardson, 2014]. During palatogenesis, the periderm is selectively removed at the medial edge epithelium to allow palatal shelves to adhere at E14.5 [Reviewed in Lan, 2015]. Deficiencies in the IRF6-GRHL3 network result in an absent or abnormal periderm layer. *Irf6* mutants lack periderm and result in ectopic permanent adhesions all over the body, including the oral cavity, which causes cleft palate [Ingraham, 2006; Richardson, 2006]. Heterozygotes for $Irf6^{R84C}$ and $Irf6^{gt}$ alleles, as well as heterozygotes for an *Arhgap29* null allele, show transient oral adhesions [Richardson, 2006; Ingraham, 2006; Paul, 2017]. These transient oral adhesions frequently accompany a delay in palatal shelf elevation at E14.5 [Paul, 2017]. Considering that rare and common variants in *IRF6* have been associated with nsCL/P [Zucchero, 2004; Rahimov, 2008; Beaty, 2010], IRF6 regulation of the periderm represents a critical pathway in palatogenesis. Identification of additional members of this pathway is necessary to further elucidate nsCL/P etiology.

We first identified *SPECC1L* mutations in two patients with atypical clefts [Saadi, 2011]. At the time, we posited that atypical clefts are a severe manifestation of more common cleft lip and palate phenotype. Thus, we proposed that pathogenetic mechanisms underlying *SPECC1L* deficiency would also result in more common syndromic and nsCL/P. Consistent with our proposition, ten additional *SPECC1L* mutations were identified in a total of 31 patients originally diagnosed with clefting-associated autosomal dominant Opitz G/BBB (OMIM #145410) and Teebi Hypertelorism syndromes (OMIM #145420) [Kruszka, 2015; Bhoj, 2015; Bhoj, 2018]. Bhoj *et al.* 2018 compiled a relatively distinct phenotypic profile of patients with *SPECC1L* mutations that includes hypertelorism, orofacial clefting, wide short nose with large tip, and ventral body wall closure defects (omphalocele). This range of malformations led them to propose an independent autosomal dominant *SPECC1L* mutation syndrome. Interestingly, these syndromic mutations cluster in either the 2nd coiled coil or the calponin homology domains of SPECC1L.

To validate that a decrease in SPECC1L dosage or function can affect midface development, we generated gene trap and truncation *Specc1l* mutant mouse alleles. Indeed, compound heterozygotes with a gene trap and a truncation allele exhibit a delay in palate elevation. Furthermore, we identify defects in the periderm of *Specc1l* compound heterozygous embryos and show that SPECC1L expression in the palate requires IRF6. We also sequenced 426 individuals with nsCL/P from five different populations and identified three rare *SPECC1L* variants. A total of six individuals (1.4%) were heterozygous for one of these three variants. Functional analyses indicate that these variants result in partial loss of function. These studies show that deficiency of *SPECC1L* is sufficient to disrupt palate development and implicate *SPECC1L* in the expanding IRF6-GRHL3 orofacial clefting gene network.

2.3 Materials and Methods

2.3.1 Patient information

The study was approved by the ethical committee or by the Institutional Review Boards at all the participating sites in Ethiopia, Iowa, Nigeria and Philippines in accordance with the relevant guidelines and regulations. Study participants gave written informed consent for participation in this study in accordance with the Declaration of Helsinki and for the publication of this study. We also have adhered to standard biosecurity and institutional safety procedures in this study.

2.3.2 Generation of Specc1l$^{\Delta C510}$ truncation allele

A zinc-finger nuclease (ZFN) was targeted to exon 4 of *mSpecc1l* near the exon 4/intron 4 boundary. 0.25 ng of targeting primer **(Table 2.1)** was co-injected with the ZFN expression construct into FVB/C57BL6/J hybrid blastocysts at the University of Kansas Medical Center Transgenic Facility. The injected embryos were transplanted into pseudo-pregnant females. The resulting progeny were analyzed by PCR for genomic deletions. A founder animal carrying one or more deletions was outbred with wildtype C57BL6/J females to establish a line. Specc1lΔC510 was identified in such a manner. The deletion is 154bp in length and spans the *mSpecc1l* exon 4/intron 4 boundary (NM_153406.3:c.1825_1941+37del). RT-PCR and western blot analyses were performed to determine the functional consequences of this genomic deletion.

2.3.3 Generation of Specc1l^{cGT} gene trap allele

This strategy for generating a multifunctional gene trap targeting construct has been described previously **(Appendix A; Table 2.2)** [Nagy, 2003; Strassman, 2017]. In brief, 5' and 3' genomic homology regions (HR) from the second intron of *Specc1l* were PCR-amplified from

Table 2.1: *Specc1l*$^{\Delta C510}$ primer sequences.

Primer Name	Sequence
ZFN Targeting Forward	GTCTGAGCAGAAGGGCAAAG
ZFN Targeting Reverse	AAGAACGTGTTTACGTGGGC
Δ154 Genomic Forward	AGTGAGAACGAAAGGCTGGG
Δ154 Genomic Reverse	GAAGAGGAGCGGCTGACAAT
Δ154 RT-PCR Forward	AGAGCAGCGCTACATGGATT
Δ154 RT-PCR Reverse	CTTCTTGGCCTCTTCCTGGA

Table 2.2: *Specc1l*^{cGT} primer sequences.

Primer #	Primer Name	Sequence
965	Ad-SA-XhoI_R	TGAAGCCGCTCGAGACTGGAAAGACCGCGAAGA
1112	mPrdm16in2cGT-3'TargetPCR_F	GGGAGGATTGGGAAGACAAT
1115	mPrdm16in2cGT-5'TargetPCR_R	ACTGGAAAGACCGCGAAGAG
1125	bGeo_RT-R1	CGCCATGTCACAGATCATCAAG
1686	mSpecc1l-5'HomA-attB4f	GGGGACAACTTTGTATAGAAAAGTTGTTGTCCTCTGACACGCACTT
1687	mSpecc1l-5'HomA-attB1r	GGGGACTGCTTTTTTGTACAAACTTGACTGTTGCCATCTGCAAACTT
1688	mSpecc1l-3'HomB-attB2f	GGGGACAGCTTTCTTGTACAAAGTGGAAGTACTCTCATCTGCCGACTGT
1689	mSpecc1l-3'HomB-attB3r	GGGGACAACTTTGTATAATAAAGTTGCACATTGACTACGGGAAGCA
1712	Specc1l-HomA-5R	GGATGTCTTGATCCCTGGAA
1713	Specc1l-HomA-3F	AACTCTCAAGCCCTCCACAG
1717	Specc1l-HomB-3F	CACACAGCAGGCATCCATAA
1752	Specc1l-5'TargTest_F (w/ oBB1115)	TTCATGTCAAATGCCCAAGG
1753	Specc1l-3'TargTest_R (w/ oBB1112)	GGCAATGAGCACAGAACTGA
1754	Specc1lx2_F (w/ oBB1125)	ACCAAGAGGCAGCCCAGAAT
-	pUC_F	CTAGTCCACTGGCACAGCCTAC
-	Hsvtk_R	ACACTCCAGAGAGGGCAGAG

genomic DNA isolated from EDJ#22 (ATCC SCRC-1021) mouse 129S5/SvEvTac embryonic stem cells and cloned into pENTR-5'HR and pENTR-3'HR Entry clones. The three Entry clones, pENTR-5'HR, pENTR-3'HR, and prsFlipROSA*βgeo** TT0-ENTR11, and the pPNT-DEST-R4-R3 Destination vector described previously [Strassman, 2017] were combined to create the final ~20 kb targeted trapping vector, prsFlipROSA*βgeo**-*Specc1l*in2, via the *in vitro* Multisite GATEWAY recombination system using LR Recombinase II Plus enzyme following manufacturer's protocols (Thermo Fisher Scientific). Linearized plasmid DNA was electroporated into EDJ#22 ES cells. Positive ES colonies were selected first by Neomycin resistance using G418 (250 ug/ml) and then by RT-PCR for *Specc1l-βgeo** fusion gene trap transcript. Correctly targeted ES cells were microinjected into C57BL6/J blastocysts (KUMC Transgenic and Gene-Targeting Institutional Facility, Kansas City, KS). Chimeras were crossed to C57BL6/J mice for germline transmission. Heterozygous progeny was confirmed by PCR genotyping to identify the *Specc1l*^{cGT} allele. All animal studies were performed consistent with protocols approved by the KUMC Institutional Animal Care and Use Committees.

2.3.4 Histological analysis

Mating pairs were set up in timed matings and then checked for plugs on the following morning. Noon on the day the plug was identified is classified as embryonic day 0.5 (E0.5). At the given embryonic time-point, females were euthanized using a primary and a secondary method as approved by the institutional IACUC. Embryos were then harvested, washed in 1x PBS, and fixed overnight in 4% paraformaldehyde at 4°C. For paraffin sectioning, embryos were then gradually dehydrated in increasing concentrations of ethanol and processed for paraffin embedding using the Leica ASP300 tissue processor. For cryosectioning, embryos were submerged in 30% sucrose until

the tissue sank, embedded in OCT solution, and stored at -80°C until use. Sections were obtained between 8-10 µm.

2.3.5 Immunostaining analysis

For the U2OS transfection experiments, coverslips were fixed with ice cold 4% paraformaldehyde for 10 minutes, permeabilized with 0.5% Trixon X-100 in 1x PBS for 10 minutes, washed, and then blocked in 10% normal goat serum (Thermo Fisher Scientific, 50062Z) for one hour at room temperature. The primary antibody was incubated overnight at 4°C, washed in 1x PBS, then incubated in secondary antibody for one hour at room temperature covered from light. Lastly, the coverslips were washed again in 1x PBS and mounted on slides with Prolong Gold with DAPI (Invitrogen, P36930).

For immunostaining on embryo sections, conditions varied depending on the antibody used. Briefly, antigen retrieval was performed by heating the slides in sodium citrate buffer (10mM Sodium Citrate, 0.05% Tween 20, pH 6.0) at 96°C for 10 minutes. The slides were then washed in H_2O, permeabilized with 0.5% Triton X-100 in 1x PBS for 30 minutes, washed in PBS, then blocked in 10% normal goat serum. Primary and secondary antibodies were incubated as described above. For phalloidin staining, antigen retrieval was not used and the stain was included during secondary antibody incubation.

Primary antibodies: SPECC1L C-terminus [Saadi, 2011], SPECC1L N-terminus (Proteintech, 25390-1-AP), Acetylated-α-tubulin (Sigma, T6793), ΔNp63 (Biolegend, 619001), β-Catenin (Cell Signaling Technology; 2677), KI-67 (Cell Signaling Technology; 12202).

Secondary antibodies and stains: Goat anti-Rabbit IgG (H+L) Alexa 488 and 594 (Invitrogen; A-11008, A-11012), Goat anti-Mouse IgG1 Alexa 488 (Invitrogen, A-21121), Goat

anti-Mouse IgG2a Alexa 594 (Invitrogen, A-21135), Goat anti-Mouse IgG3 Alexa 594 (Invitrogen; A-21155), Acti-stain 555 phalloidin (Cytoskeleton, PHDH1-A).

2.3.6 Western blot analysis

Protein extraction was performed by sonicating flash-frozen embryonic tissue in radioimmunoprecipitation assay (RIPA) buffer with HALT protease inhibitor Cocktail (Thermo Scientific, 78440). Samples were then spun down for 10 minutes at 13,000 rcf and the supernatant collected. Lysates were then electrophoresed in 4-15% gradient Mini-Protean TGX Stain-Free precast gels (Bio-RAD, #4568084) and transferred onto Immobilon PVDF membranes (EMD Millipore, IPVH00010). PVDF membranes were then blocked in Odyssey Blocking Buffer (Li-Cor, 927-5000) either overnight at 4°C or at room temperature for 1 hour. Primary antibodies used were anti-N-SPECC1L (1:2000; Proteintech, 25390-1-AP) and anti-IRF6 (1:2000; Sigma, SAB2102995). The secondary antibody used was HRP-linked goat anti-rabbit IgG (1:10,000; Cell Signaling Technologies). Femto SuperSignal West ECL reagent (Thermo Scientific, 34095) was used to develop the signal. Image Lab software (Bio-Rad) was used for quantitative analysis of the western blots.

2.3.7 Cell culture and transfection analysis

Human U2OS osteosarcoma cells (ATCC, HTB-96) were cultured in DMEM media with high glucose and pyruvate, supplemented with 10% fetal bovine serum and penicillin/streptomycin. U2OS cells were transfected with either wildtype SPECC1L-expressing construct (33) or with constructs carrying the Q415P [Saadi, 2011], A86T, M91I, T299A and R546Q variants (present study). The GFP tag from previous studies [Saadi, 2011] was removed in

favor of visualizing the overexpressed protein by immunofluorescence. Transfected cells were analyzed for qualitative differences in the ability of SPECC1L to associate with microtubules and the extent of acetylation of associated microtubules [Saadi, 2011; Kruszka, 2015].

2.4 Results

2.4.1 Moderate reduction of Specc1l in mouse results in palate elevation defect

We previously reported that severe deficiency of *Specc1l* using gene trap constructs results in early embryonic lethality by embryonic day E9.5 [Wilson, 2016]. These mutants exhibited an open neural tube and defects in cranial neural crest cell delamination from the anterior neural folds. While a deficiency in neural crest cell function is a plausible cause of a craniofacial defect [Trainor, 2010; Snider, 2014], early embryonic lethality prevented confirmation of a direct role for SPECC1L in midface or palate development. Therefore, we sought to generate alternative *Specc1l*-deficient alleles that would allow embryos to survive longer in gestation to study these perinatal phenotypes. We utilized zinc-finger nuclease-based genomic deletions to target the 3' end of exon 4, which yielded a 154bp deletion **(Fig. 2.1A)**. RT-PCR sequencing analysis revealed that the deletion abolished the exon 4 splice donor site **(Fig. 2.1A)**, resulting in the use of a cryptic splice site within intron 4 and the subsequent introduction of a novel coding sequence **(Fig. 2.1B)**. This novel sequence coded for 9 amino acids followed by a stop codon, leading to premature truncation of the protein **(Fig. 2.1C)**. For clarity, we have termed this allele *Specc1l*$^{\Delta C510}$, as it results in the loss of the 510 amino acids at the C-terminal end of the protein **(Fig. 2.1C)**. To validate this truncation, we performed western blot analysis with an antibody targeting the N-terminal end of SPECC1L. Indeed, a band can be seen at ~100kDa in the mutant, compared to wildtype SPECC1L at ~150kDa **(Fig. 2.1D; right)**. Compared to the embryonic lethality seen in gene trap

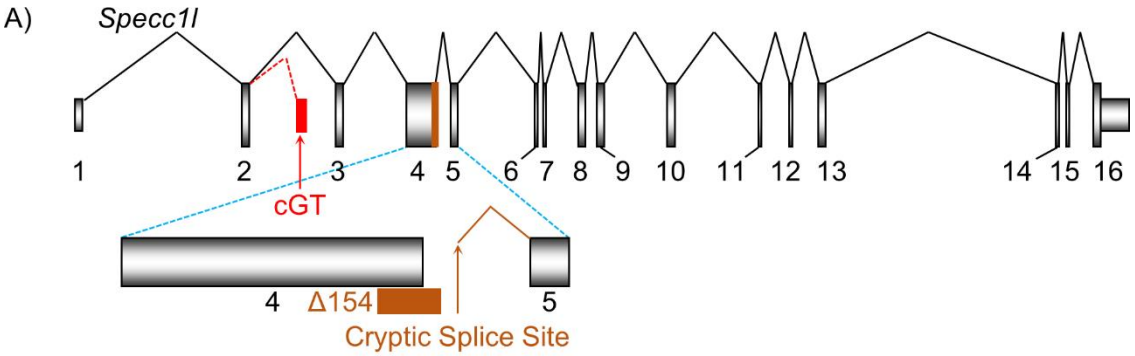
A)
Specc1l
1 2 3 4 5 6 7 8 9 10 11 12 13 14 15 16
cGT
4 Δ154 5
Cryptic Splice Site

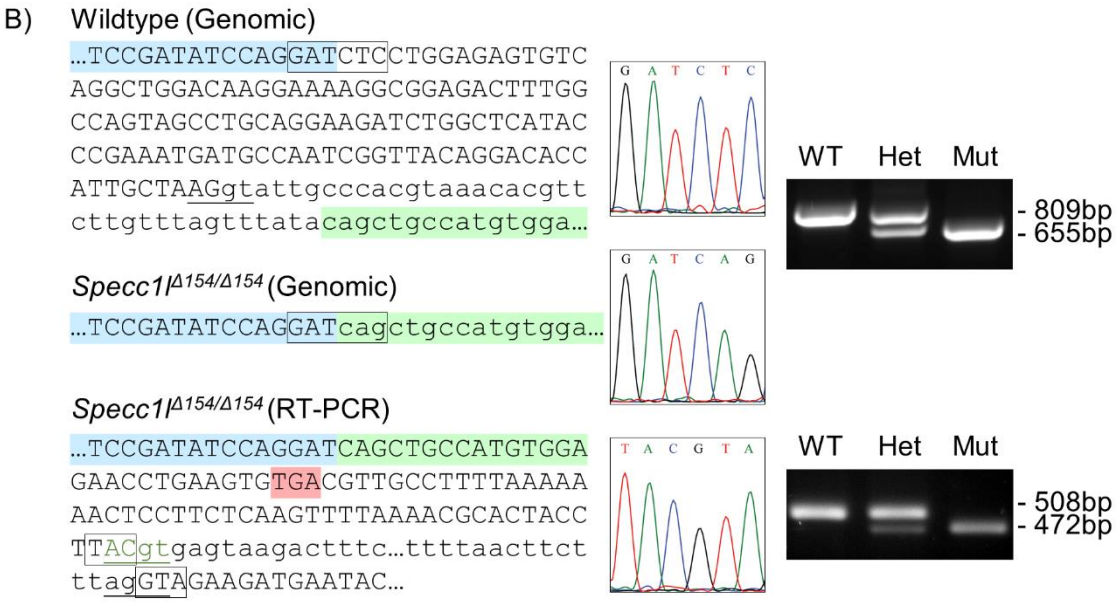
B)
Wildtype (Genomic)
…TCCGATATCCAGGATCTCCTGGAGAGTGTC
AGGCTGGACAAGGAAAAGGCGGAGACTTTGG
CCAGTAGCCTGCAGGAAGATCTGGCTCATAC
CCGAAATGATGCCAATCGGTTACAGGACACC
ATTGCTAAGgtattgcccacgtaaacacgtt
cttgtttagtttatacagctgccatgtgga…
WT Het Mut
- 809bp
- 655bp
Specc1l Δ154/Δ154 (Genomic)
…TCCGATATCCAGGATcagctgccatgtgga…
Specc1l Δ154/Δ154 (RT-PCR)
…TCCGATATCCAGGATCAGCTGCCATGTGGA
GAACCTGAAGTGTGACGTTGCCTTTTAAAAA
AACTCCTTCTCAAGTTTTAAAACGCACTACC
TTACgtgagtaagactttc…ttttaacttct
ttagGTAGAAGATGAATAC…
WT Het Mut
- 508bp
- 472bp

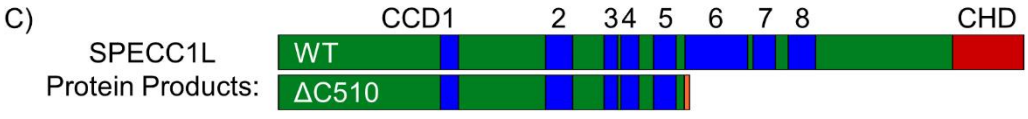
C)
SPECC1L
Protein Products:
CCD1 2 34 5 6 7 8 CHD
WT
ΔC510

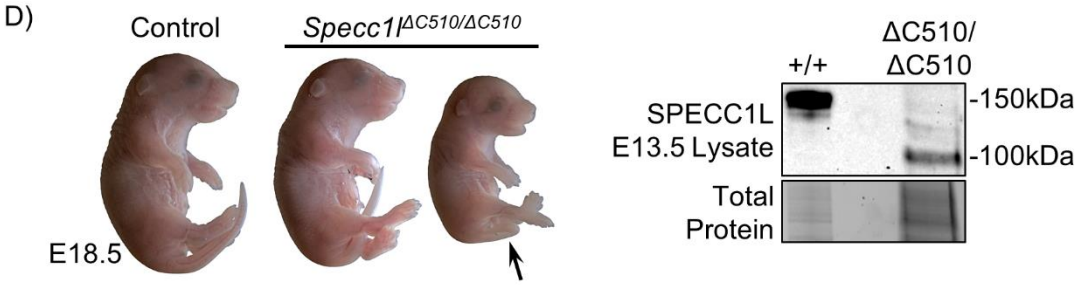
D)
Control
Specc1l ΔC510/ΔC510
E18.5
ΔC510/
ΔC510
+/+
SPECC1L
E13.5 Lysate
-150kDa
-100kDa
Total
Protein

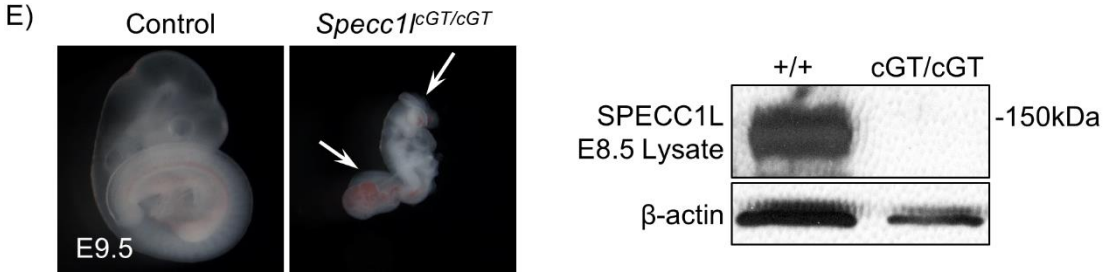
E)
Control
Specc1l cGT/cGT
E9.5
+/+
cGT/cGT
SPECC1L
E8.5 Lysate
-150kDa
β-actin

Figure 2.1: Generation of truncation *Specc1l* allele. A) Schematic of *Specc1l* introns and exons depicting the locations of the cGT construct (red) and zinc-finger nuclease deletion Δ154 (orange). **B)** Δ154 ZFN deletion removes the canonical splice donor of exon 4, resulting in the usage of cryptic splice donor within intron 4 (RT-PCR; underlined green sequence) and subsequent truncation of the protein due to the introduction of a stop codon (RT-PCR; red highlighting). Genotyping by PCR amplification of genomic DNA and RT-PCR reveals a size difference between WT and Δ154 bands. **C)** Diagram of WT and ΔC510 SPECC1L protein. Orange section represents the 9 novel amino acids. **D)** *Specc1l*$^{\Delta C510/\Delta C510}$ embryos are smaller compared to littermate control and die shortly after birth. Western blotting shows a ~50kDa size decrease in ΔC510 homozygotes compared to WT control lysates. **E)** *Specc1l*$^{cGT/cGT}$ embryos exhibit embryonic lethality with open neural folds (arrows) at E9.5, compared to littermate control. Western blotting shows a loss of SPECC1L protein in cGT homozygotes compared to WT control lysates.

homozygotes, *Specc1l*$^{\Delta C510/\Delta C510}$ mutants showed perinatal lethality **(Fig. 2.1D)**. *Specc1l*$^{\Delta C510/\Delta C510}$ homozygotes showed no gross malformations, apart from occasional size differences and curly tail phenotypes **(Fig. 2.1D; arrow)**. Additionally, we did not detect instances of cleft palate on the C57BL6/J background (N=6).

We hypothesized that a further reduction in *Specc1l* dosage by crossing gene trap and truncation alleles would result in palate defects. To achieve this, we utilized a newly generated gene trap allele, termed *Specc1l*$^{cGT\text{-}ko}$ (abbreviated *Specc1l*^{cGT} from here on) using a multifunctional gene trap cassette adapted for targeted trapping **(Fig. 2.1A)** [Schnutgen, 2005; Strassman, 2017]. Homozygous *Specc1l*$^{cGT/cGT}$ mutants undergo embryonic lethality at E9.5 **(Fig. 2.1E)**, consistent with our previous gene trap alleles, *Specc1l*^{RRH048} and *Specc1l*^{DTM096} [Wilson, 2016]. Interestingly, *Specc1l*$^{cGT/cGT}$ homozygotes often show complete neural tube closure failure **(Fig. 2.1E; arrows)**, while *Specc1l*^{RRH048} and *Specc1l*^{DTM096} mutants only show closure defects in the cranial neural tube [Wilson, 2016]. This is indicative of an increased trapping efficiency of the *Specc1l*^{cGT} allele.

To evaluate the impact of *Specc1l*$^{cGT/\Delta C510}$ compound heterozygosity on palate development, we harvested embryos at E13.5-E15.5. Compared to control embryos **(Fig. 2.2A,C,E)**, *Specc1l*$^{cGT/\Delta C510}$ mutants **(Fig. 2.2B,D,F,G)** appeared smaller and manifested subepidermal blebbing at E13.5 **(Fig. 2.2B; arrowheads)**, and at E14.5 **(Fig. 2.2D; arrowheads)**. This blebbing resolved by E15.5, except in occasional cases of hemorrhaging **(Fig. 2.2F,G; arrowheads)**. Importantly, approximately 66% (n=9) of *Specc1l*$^{cGT/\Delta C510}$ mutants showed vertically oriented (unelevated) palatal shelves when compared to littermate controls at E14.5 **(Fig. 2.2D; arrows)**. The palate elevation defect persists in approximately 8% of mutants at E15.5 and

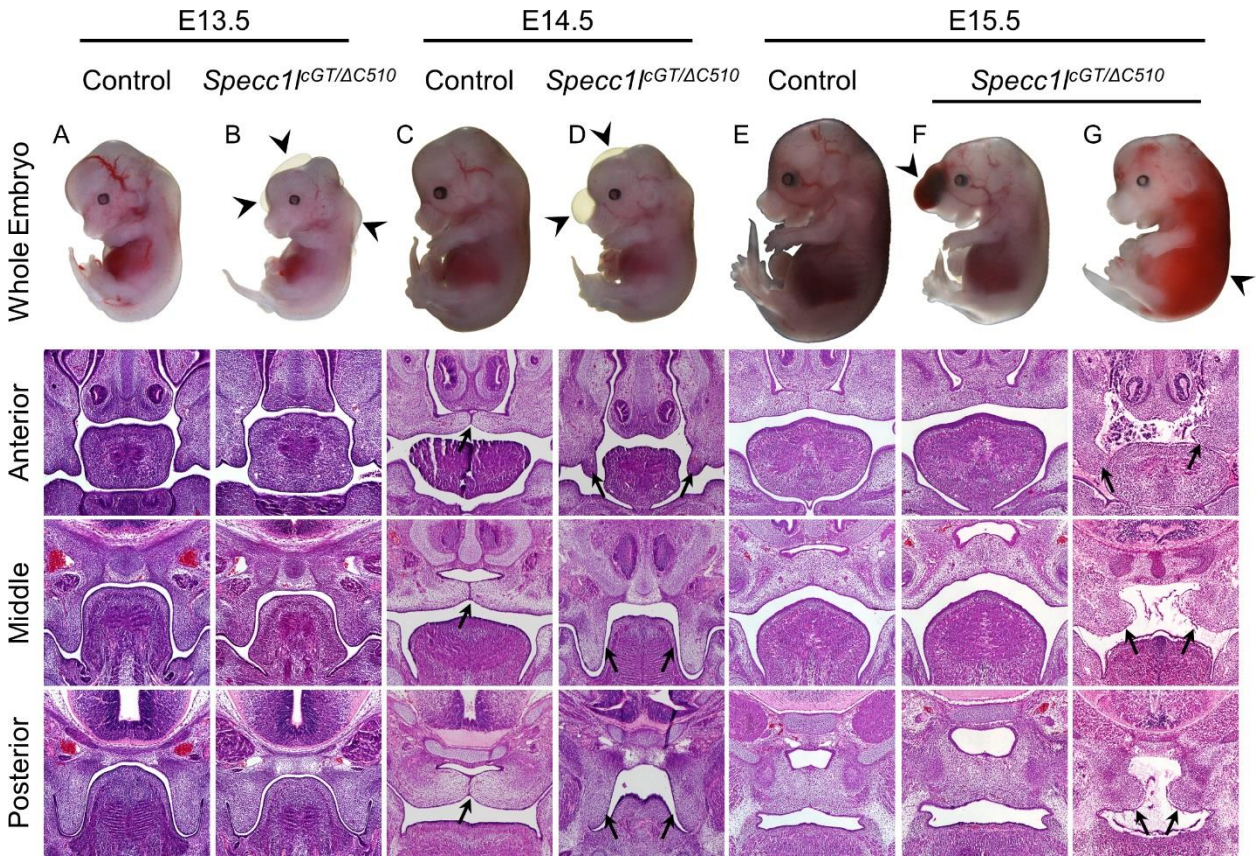

Figure 2.2: *Specc1l*$^{cGT/\Delta C510}$ compound mutants exhibit palatal shelf elevation delay. A-G) Representative whole mount images (top row) and coronal H&E palate sections (bottom three rows) of control and *Specc1l*$^{cGT/\Delta C510}$ embryos from E13.5-E15.5. Compound mutants show edema, midline subepidermal blebbing (B,D; arrowheads), and occasional hemorrhaging (F,G; arrowheads) compared to control embryos. At E14.5, approximately 66% of mutant embryos had palatal shelves that had not elevated (D; arrows) compared to littermate controls (C; arrows). By E15.5, most mutants had closed palates (F), indicating that these mutants experience a delay in palatal shelf elevation. However, cleft palate can occur in mutant embryos with severe phenotypes (G; arrows).

later (n=12), resulting in cleft palate **(Fig. 2.2G; arrows)**. These results confirmed our assertion that palate development is sensitive to functional *Specc1l* dosage.

2.4.2 Specc1l$^{cGT/\Delta C510}$ mutants show ectopic oral adhesions and abnormal periderm

A delay in palatal shelf elevation is also found in other mouse models [Reviewed in Gritli-Linde, 2007; Gritli-Linde, 2008; Bush, 2012]. Most notably, *Arhgap29* heterozygotes showed a palate elevation delay accompanied by ectopic transient oral adhesions [Paul, 2017]. Therefore, we histologically scanned the oral cavity of our mutants. Indeed, our *Specc1l* compound mutants showed several occurrences of ectopic adhesions **(Fig. 2.3)**. Evidence of oral adhesions was found in the anterior nasal cavity **(Fig. 2.3, A vs. B)**, the palate hinge region **(Fig. 2.3, C vs. D)**, and between palatal shelf and buccal or lingual epithelia **(Fig. 2.3, E vs. F)**. These oral adhesions almost always accompanied a dissociation of epithelia from the underlying mesenchyme in paraffin sections **(Fig. 2.3, A' vs. B', C' vs. D', E' vs. F')**.

2.4.3 Specc1l$^{cGT/\Delta C510}$ mutants show abnormal adherens junction staining in the periderm

To investigate how SPECC1L deficiency in our compound mutants could cause both a delay in palatal shelf elevation and transient oral adhesions, we first evaluated SPECC1L expression in the palate by co-staining cranial E13.5 and E14.5 sections for SPECC1L and ΔNp63, a marker for the basal epithelium **(Fig. 2.4A-C, A'-C')**. Indeed, we found that SPECC1L is expressed in the CNCC-derived palatal mesenchyme **(Fig. 2.4A-C, A'-C')**, as well as both the ΔNp63-positive basal cells **(Fig. 2.4A')** and ΔNp63-negative periderm cells of the palatal shelf **(Fig. 2.4A'; arrow)**.

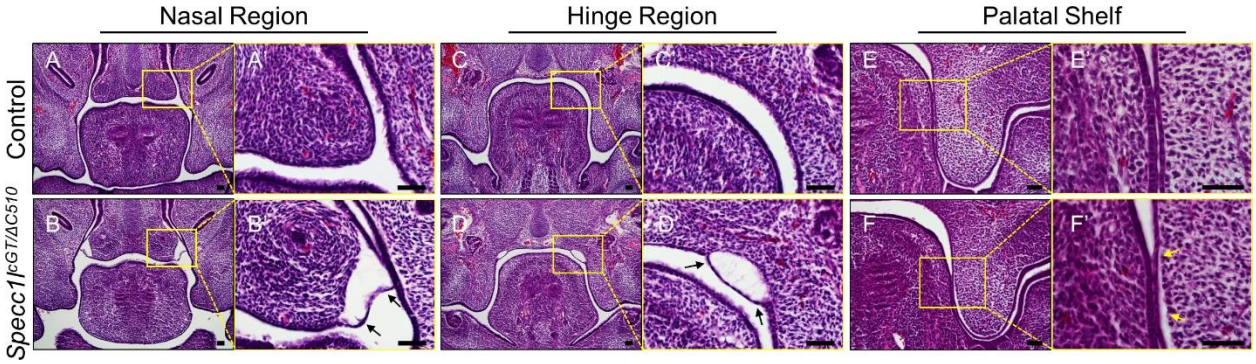

Figure 2.3: *Specc1l*$^{cGT/\Delta C510}$ compound mutants show transient oral adhesions. A-F) Coronal H&E palate sections of WT and *Specc1l*$^{cGT/\Delta C510}$ mutant embryos at E13.5. Compound mutants show evidence of adhesions between the oral and nasal cavity epithelia (A vs. B; arrows) and between the oral and tongue epithelia (C vs. D; arrows). Adhesions were also identified at the junction between the tongue and palatal shelf (E vs. F; arrows), which resulted in separation of the palatal shelf epithelium from the mesenchyme (F'; arrows). Scale bars are 50μm.

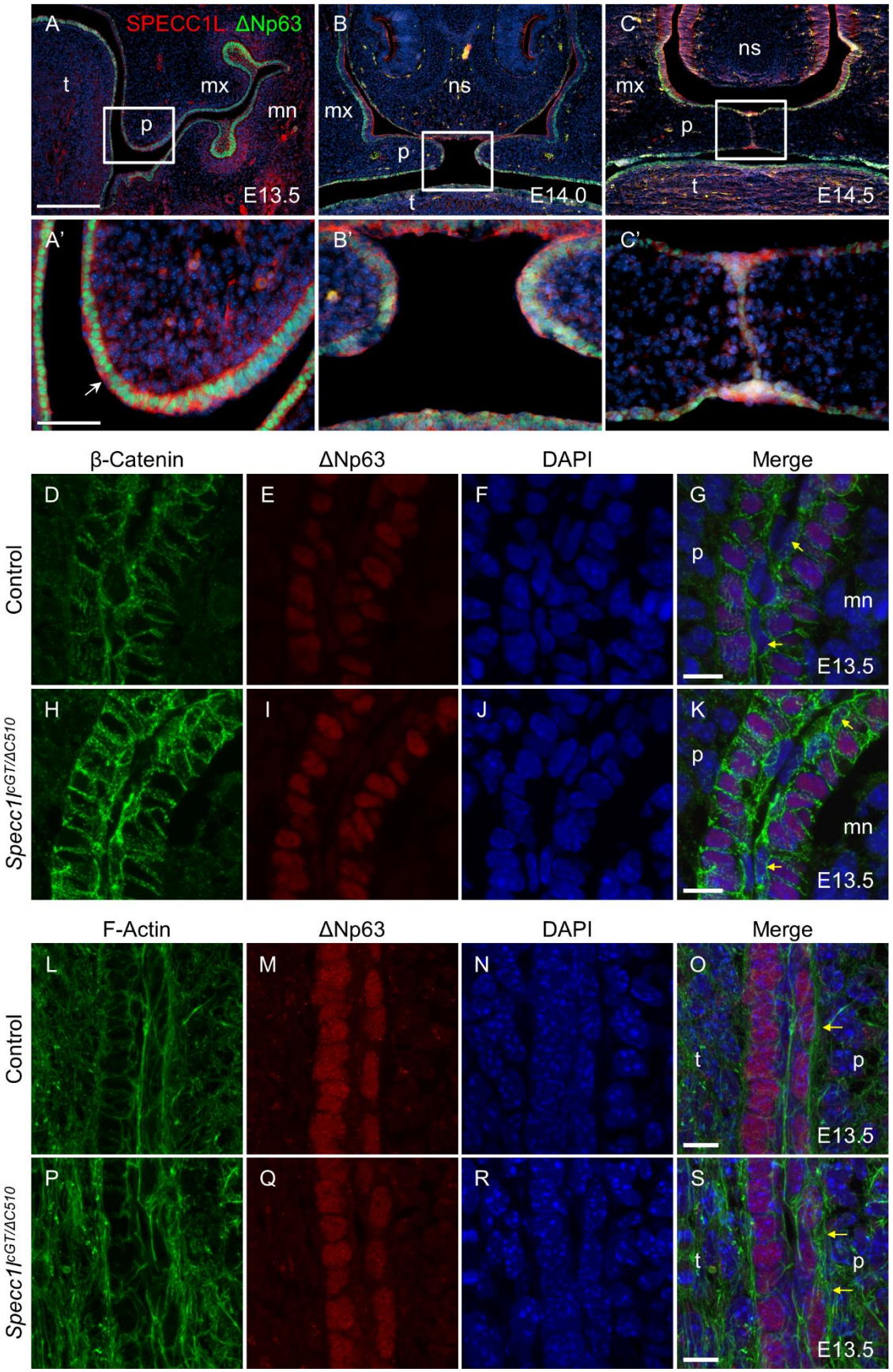
A
SPECC1L ΔNp63
t
mx
mn
p
E13.5
B
ns
mx
p
t
E14.0
C
ns
mx
p
t
E14.5
A'
B'
C'
β-Catenin
ΔNp63
DAPI
Merge
Control
D
E
F
G
p
mn
E13.5
Specc1cGT/ΔC510
H
I
J
K
p
mn
E13.5
F-Actin
ΔNp63
DAPI
Merge
Control
L
M
N
O
t
p
E13.5
Specc1cGT/ΔC510
P
Q
R
S
t
p
E13.5

Figure 2.4. Periderm of *Specc1l*$^{cGT/\Delta C510}$ embryos show changes in F-actin and adherens junction markers consistent with abnormal adhesion. A-C) Immunostaining for SPECC1L (red) and ΔNp63 (green; basal epithelial marker) on coronal sections between E13.5 and E14.5. SPECC1L expression is present in the periderm and basal layers of the epithelium (A'; arrow), as well as the underlying mesenchyme. **D-K)** Coronal sections of E13.5 WT and *Specc1l*$^{cGT/\Delta C510}$ palatal shelve epithelia co-immunostained for cell junction marker β-catenin (D,H) and basal epithelium marker ΔNp63 (E,I). Both wildtype and mutant sections contain flattened, ΔNp63-negative periderm cells (G,K; arrows). However, the mutant sections have abnormal apical β-catenin staining on some periderm cells (G vs. K; arrows). **L-S)** Sections stained with phalloidin (L,P) show increased F-actin staining in the mutants compared to controls (O vs. S). Scale bars are 2mm for A-C, 50μm for A'-C', and 10μm for D-S. p=palatal shelf; mx=maxillary process; mn=mandibular process; t=tongue; ns=nasal septum.

Previous studies have shown that ectopic oral adhesions involve abnormalities of the periderm [Casey, 2006]. *Irf6* mouse mutants exhibit a complete absence of periderm cells [Richardson, 2009], resulting in severe oral adhesions and permanent cleft palate [Richardson, 2006; Ingraham, 2006].However, partial loss of IRF6 function has been shown to result in the mislocalization of adherens junction markers to the apical surface of the periderm, which is normally devoid of cell adhesion molecules [Richardson, 2009; Richardson 2014]. IRF6 deficiency also results in increased actin stress fiber formation [Biggs, 2014]. Similarly, we previously showed increased actin filament and adherens junction marker staining upon SPECC1L deficiency [Saadi, 2011; Wilson, 2016]. Therefore, we examined these markers in the oral periderm of our compound mutants. Co-staining for ΔNp63 and β-catenin **(Fig. 2.4D-K)** revealed abnormal apical expression of membrane-associated β-catenin in mutant periderm **(Fig. 2.4, G vs. K; arrows)**. These instances of apical expression were present at the buccal and lingual palatal shelf interfaces, consistent with the occurrence of ectopic adhesions. We also stained for filamentous actin (F-actin) using phalloidin and found a generally increased staining in mutant palate epithelium and mesenchyme with regions of disorganized filaments **(Fig. 2.4L-S; arrows)**. Together, these results indicate that the transient oral adhesions seen in our *Specc1l* mutants may be due to ectopic apical expression of cell adhesion markers.

2.4.4 SPECC1L expression in the palate is dependent upon IRF6 transcription factor

The similar adhesions and molecular changes in *Irf6* and *Arhgap29* heterozygotes and our *Specc1l* mutants suggest that SPECC1L regulation of the periderm may functionally overlap with the IRF6 pathway. To test if SPECC1L could be connected to the IRF6 regulatory pathway, we looked at SPECC1L expression in the palate of *Irf6* knockout embryos (*Irf6*$^{-/-}$) [Ingraham, 2006].

Indeed, SPECC1L expression was reduced in the epithelium of the *Irf6*$^{-/-}$ palatal shelves **(Fig. 2.5, A vs. B)**. It was previously shown that *K14* promoter-based transgenic expression of *Irf6* in the oral epithelia (*Tg*$^{K14\text{-}Irf6/+}$) partially rescued the oral adhesion phenotype in *Irf6* knockout mice [Kousa, 2017]. Consistent with this rescue, SPECC1L expression was restored in the oral epithelium of *Irf6*$^{-/-}$; *Tg*$^{K14\text{-}Irf6/+}$ embryos **(Fig. 2.5, B vs. C)**. Furthermore, IRF6 expression was not altered in our *Specc1l*$^{cGT/\Delta C510}$ mutants **(Fig. 2.5D,E)**. Together, these results show that SPECC1L expression in the palatal shelves requires IRF6 function.

2.4.5 Identification of nonsynonymous SPECC1L coding variants in nsCL/P patients

Given that *SPECC1L* mutations were identified in patients with atypical and syndromic CL/P [Saadi, 2011; Kruszka, 2015; Bhoj, 2015; Bhoj, 2018], we posited that variants would also contribute to nsCL/P. To test this, we sequenced the coding region of *SPECC1L* (NM_015330.5; NP_056145.4) in 426 nsCL/P patient samples. These included 62 samples from Iowa Caucasians, 89 from the Philippines, 90 from Ethiopia, 90 from Nigeria, and 95 samples from Japan **(Fig. 2.6)**. One novel (c.273G>A, p.Met91Iso), two rare (c.256G>A, p.Ala86Thr; c.1637G>A, p.Arg546Gln), and one population specific (895A>G, p.Thr299Ala) variant were identified. The variants p.Met91Iso, p.Arg546Gln and p.Thr299Ala were identified once each in the Filipino, Iowa Caucasian, and Japanese samples, respectively. The p.Met91Iso variant was not present in either ExAC or gnomAD databases (n=372576) [Lek, 2016]. The p.Ala86Thr novel variant was identified in four different Japanese individuals with nsCL/P (n=95; Allele Frequency = 0.042) compared to 0/8654 and 1/18394 occurrence in East Asian samples in ExAC and gnomAD databases (n=27048; Allele Frequency = 0.000037), indicating a strong enrichment. The p.Arg546Gln variant was not present in the ExAC database (n=121096), but was present in six

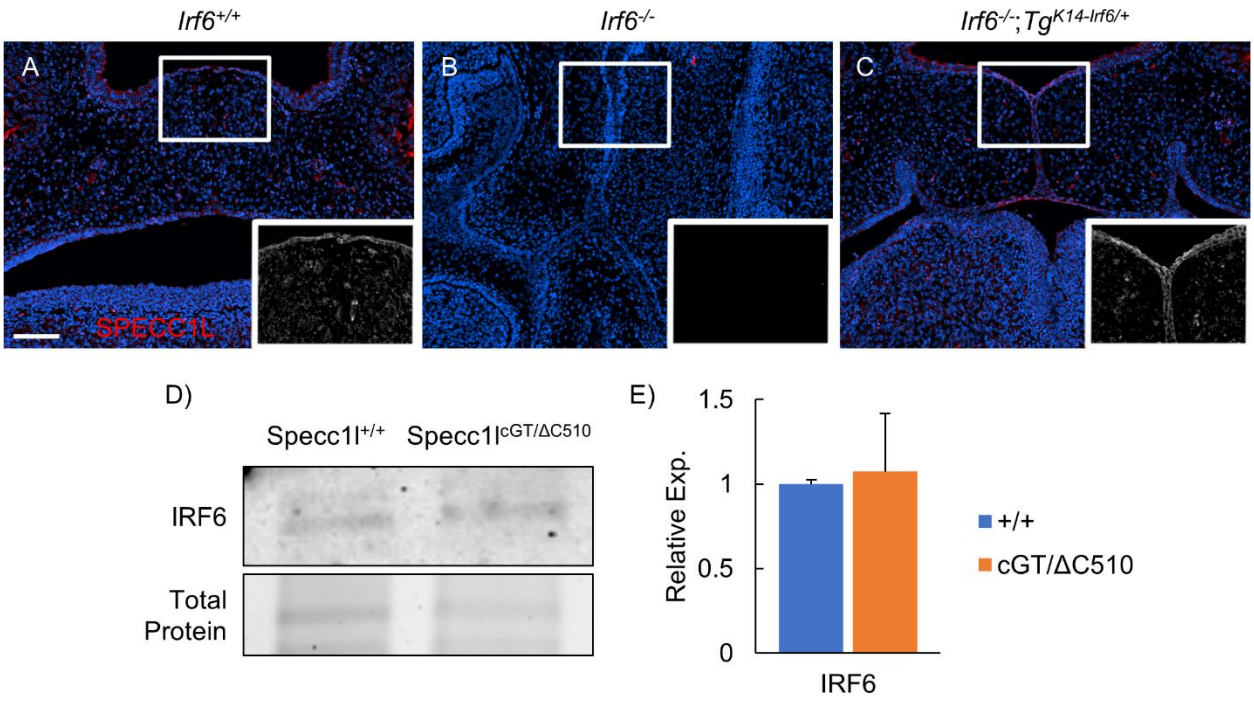

Figure 2.5: IRF6 is required for SPECC1L expression in the palate. Immunostaining of coronal embryonic palate sections at E15.5. **A)** SPECC1L is expressed widely (red) in the palate in wildtype mice. **B)** *Irf6*-null mice exhibit abnormal oral adhesions throughout the oral cavity and loss of SPECC1L expression. **C)** These phenotypes are rescued with transgenic expression of *Irf6* in the oral ectoderm using a Keratin 14 promoter. Grayscale insets are of red channel. Scale bar is 100μm. **D)** Representative images from IRF6 western blots of wildtype and *Specc1l*$^{cGT/\Delta C510}$ mutant craniofacial lysate. **E)** Bar graph showing relative expression normalized by total protein. There is no significant difference in IRF6 protein levels between the wildtype and mutant samples. n=3. Error bars show SEM.

A)

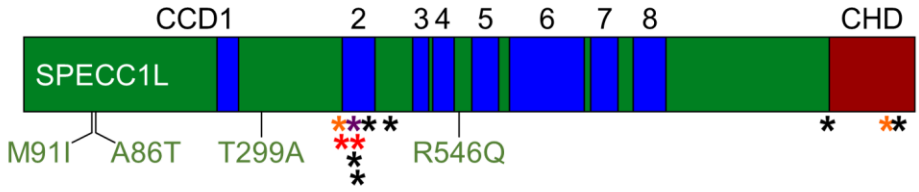

B)

Patient Population	Identified Mutations	Polyphen2	SIFT	ExAC db Occurrence	gnomAD db Occurrence
Caucasian (62)	R546Q (1)	Probably Damaging	Tolerated	0 / 121096	6 / 282708
Filipino (89)	M91I (1)	Benign	Tolerated	0 / 121096	0 / 251480
Japanese (95)	A86T (4)	Benign	Affects Protein Function	0 / 121096	1 / 251480 (1 / 18394 East Asians)
	T299A (1)	Benign	Tolerated	31 / 8654 (East Asians)	57 / 19952 (East Asians)
Ethiopian (90)	-				
Nigerian (90)	-				
Total: 426 patients analyzed					

Figure 2.6: *SPECC1L* variants in patients with non-syndromic orofacial clefting. A) Schematic representation of SPECC1L protein showing positions of the eight coiled-coil domains (CCD; blue), calponin homology domain (CHD; red), as well as the heterozygous mutations identified in patients with non-syndromic cleft lip/palate (A86T, M91I, T299A, R546Q; green text). Also shown are the previously identified mutations found in a patient with Oblique Facial Clefts (Q415P; purple asterisk), two multigenerational families with autosomal dominant Opitz G/BBB syndrome (T397P, G1083S; orange asterisks), patients with Teebi Hypertelorism Syndrome (400-401del, E420D; red asterisks), and the additional syndromic patients identified in Bhoj *et al.* 2018 (black asterisks). **B)** Chart describing the source of the patient samples that were sequenced in this analysis including the patient population, the incidence of each variant within that population, Polyphen2 and SIFT substitution predictions, and occurrence in ExAC and gnomAD databases [Adzhubei, 2010; Sim, 2012; Lek, 2016].

individuals in the gnomAD samples (n=282708; Allele Frequency = 0.0000025). The p.Thr299Ala variant (rs146907080) was encountered a combined 88 times only in East Asian samples of the ExAC and gnomAD databases (n=28606; Allele Frequency = 0.00308), indicating that it is an East Asian population specific variant.

The identification of one novel, one enriched and one very rare variant suggested that they may affect SPECC1L function. None of these variants lie in any of the coiled-coil domains of SPECC1L protein, in contrast with previously identified *SPECC1L* mutations in patients with atypical facial clefts [Saadi, 2011], autosomal-dominant Opitz G/BBB syndrome [Kruszka, 2015], and Teebi Hypertelorism syndrome [Bhoj, 2015; Bhoj, 2018]. Thus, we hypothesized that these variants from nsCL/P patients will affect SPECC1L function to a different or lesser degree than those identified in syndromic patients.

2.4.6 Expression analysis of SPECC1L variants shows reduced acetylation of SPECC1L-associated microtubules

We previously analyzed pathogenic *SPECC1L* variants identified in syndromic patients in a qualitative assay using a SPECC1L-GFP fusion construct [Saadi, 2011; Kruszka, 2015], where wildtype (WT) SPECC1L-GFP expression in U2OS osteosarcoma cells, 24-hours post-transfection, resulted in strong association with a subset of microtubules. We further showed that this subset of microtubules is heavily acetylated [Saadi, 2011]. Compared to WT SPECC1L-GFP, none of the four variants showed any demonstrable differences in the ability to associate with microtubules after 24-hours of transfection (not shown). To sensitize the assay, we first removed the C-terminal GFP tag to prevent any ectopic microtubule association or aggregation that may be mediated by the tag itself, and used anti-SPECC1L antibody to detect transfected cells **(Fig. 2.7)**. We also added an 8-hour timepoint following transfection and co-stained for acetylated

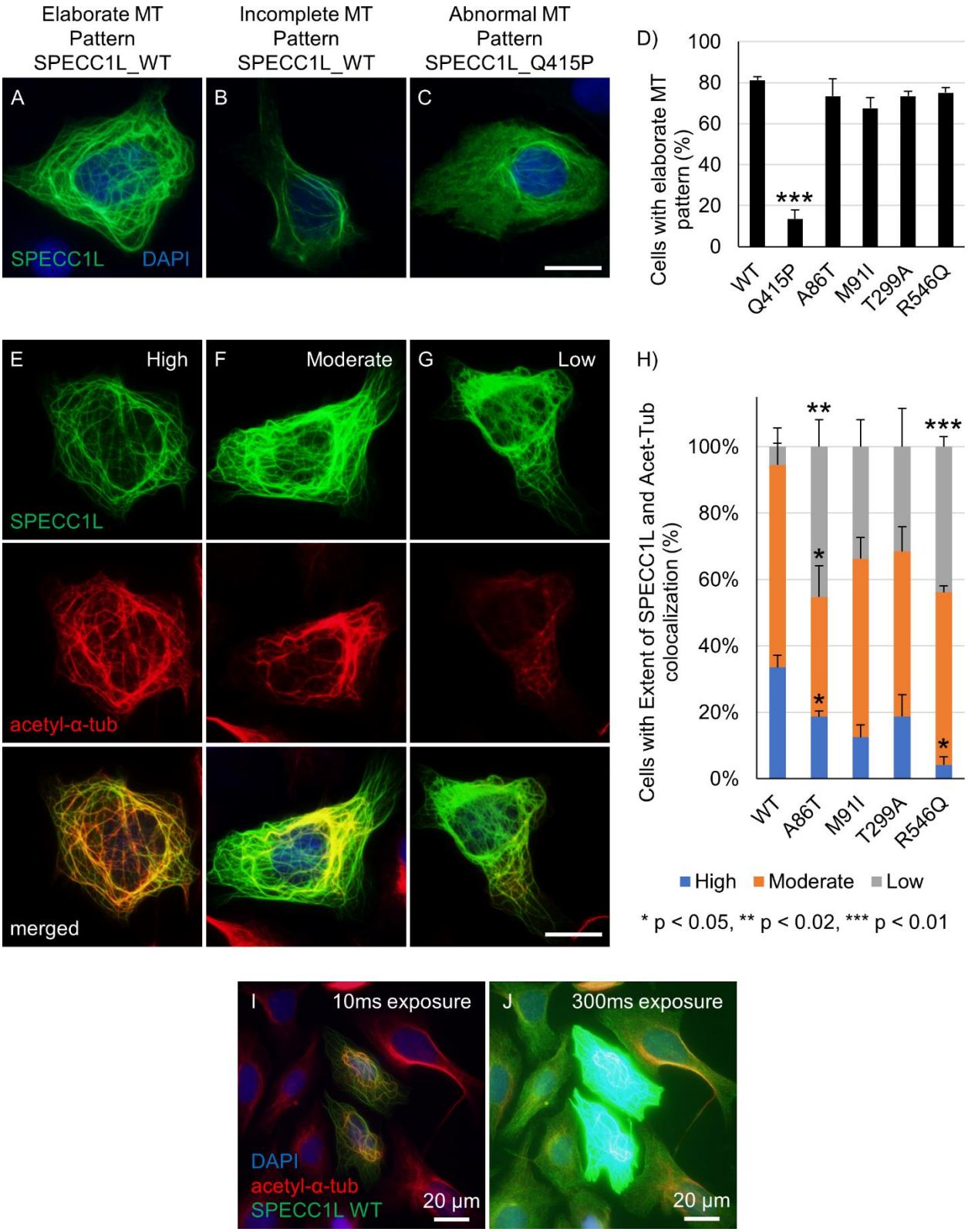
Elaborate MT Pattern SPECC1L_WT
Incomplete MT Pattern SPECC1L_WT
Abnormal MT Pattern SPECC1L_Q415P
A
B
C
SPECC1L
DAPI
D)
Cells with elaborate MT pattern (%)
100
80
60
40
20
0
***
WT
Q415P
A86T
M91I
T299A
R546Q
E
High
F
Moderate
G
Low
SPECC1L
acetyl-α-tub
merged
H)
Cells with Extent of SPECC1L and Acet-Tub colocalization (%)
100%
80%
60%
40%
20%
0%
**
***
*
WT
A86T
M91I
T299A
R546Q
High
Moderate
Low
* p < 0.05, ** p < 0.02, *** p < 0.01
I
10ms exposure
DAPI
acetyl-α-tub
SPECC1L WT
20 μm
J
300ms exposure
20 μm

Figure 2.7: *SPECC1L* variants from non-syndromic patients result in reduced association with acetylated microtubules. A-C) Representative images of U2OS cells transfected with wildtype (A,B) and Q415P (C) SPECC1L in U2OS cells. SPECC1L (green) was visualized by immunofluorescence and counterstained with DAPI (blue). **D)** Transfected cells were scored for elaborate (A) or incomplete/abnormal microtubule patterning (B,C). The four variants identified in syndromic patients showed no changes, while the Q415P syndromic mutation resulted in a markedly reduced proportion of elaborate patterning. **E-G)** Transfected cells were co-stained with SPECC1L (green) and acetylated-α-tubulin (red) and binned into high (E), moderate (F), or low (G) groups based on the extent of SPECC1L-associated acetylated tubulin staining. **H)** Compared to wildtype, cells transfected with the A86T- and R546Q-SPECC1L constructs exhibited a significantly increased proportion of cells in the low group, and a significantly decreased proportion in the high (A86T, R546Q) and moderate (A86T) correlation groups. **I-J)** Representative images of transfected cells taken at 10ms and 300ms exposure to demonstrate the difference in the level of overexpressed SPECC1L compared to endogenous (J). Scale bars are 20μm.

microtubules. We found that even without the GFP tag, wildtype SPECC1L associated with a subset of microtubules that formed an elaborate cytoplasmic pattern within almost 80 percent of transfected cells **(Fig. 2.7A,D)**. Only a small fraction of cells showed an incomplete microtubule pattern, which may represent cells where the elaborate pattern is not yet developed. As expected, a syndromic mutation (Q415P) failed to generate this elaborate pattern in ~90% of the transfected cells **(Fig. 2.7C,D)**. Instead, cells transfected with the Q415P construct transfected cells showed fine, punctate, incongruent pattern, which we described previously for pathogenic syndromic variants [Saadi, 2011; Kruszka, 2015]. However, all four nsCL/P variants were able to form this elaborate pattern to near-WT levels, between 70-80% of transfected cells **(Fig. 2.7D)**. Thus, we concluded that the kinetics of microtubule association is not affected by these nsCL/P variants. Next, we evaluated the levels of acetylation among these SPECC1L-associated microtubules **(Fig. 2.7E-G)**. To minimize variability, we only assayed cells with elaborate microtubule pattern in WT and all four variants. Interestingly, we found that ~95% of WT transfected cells showed strong or moderate microtubule acetylation just 8 hours after transfection, while ~5% showed low acetylation **(Fig. 2.7H)**. These results suggest that this phenomenon is a two-step process, wherein SPECC1L first associates with a subset of microtubules, and then facilitates microtubule acetylation. We next analyzed acetylation of microtubules in cells expressing the nsCL/P variants 8 hours after transfection. We found a statistically significant reduction in the number of highly acetylated microtubules, and a statistically significant increase in microtubules with low acetylation for the A86T and R546Q variants **(Fig. 2.7H)**. The M91I and T299A variants did not show statistically significant differences from WT **(Fig. 2.7H)**. It is possible that no significant change was identified in M91I samples because either the functional consequence on SPECC1L was too mild to be detected in our assay, or it impacted SPECC1L function in a manner that did

not alter microtubule acetylation. Compared to syndromic variants (Q415P) [Saadi, 2011; Kruszka, 2015], which fail to form the elaborate pattern, the two nsCL/P variants (A86T and R546Q) show a moderate reduction in SPECC1L function where they are able to associate with microtubules and form an elaborate pattern, but are delayed in subsequent acetylation of these microtubules.

2.5 Discussion

Pathogenic *SPECC1L* variants were found in patients with atypical [Saadi, 2011], syndromic [Kruszka, 2015; Bhoj, 2015], and now non-syndromic orofacial clefting. Interestingly, even with a small number of mutations identified, *SPECC1L* variants from atypical and syndromic orofacial clefting patients cluster in the second coiled coil and calponin homology domains. In contrast, the present variants from nsCL/P patients reside outside of these SPECC1L domains **(Fig. 2.6)**. Functional analysis also indicates that the nsCL/P mutations are less severe than their syndromic counterparts **(Fig. 2.7)**. As we better understand SPECC1L function at the molecular level, especially of the second coiled coil domain, the functional differences between variants will become clearer.

We utilized a mouse model with a novel *Specc1l* truncation allele to confirm a role for SPECC1L in the regulation of palate development, consistent with the cleft palate phenotype observed in some patients with *SPECC1L* mutations [Saadi, 2011; Kruszka, 2015; Bhoj, 2018]. Our results show that palatal shelf elevation is particularly sensitive to *Specc1l* deficiency. While most *Specc1l*$^{cGT/\Delta C510}$ mutants eventually completed palatal shelf fusion, they frequently showed mild abnormalities in shape and rugae pattern (not shown). Considering that we did not observe any differences in the extent of vertical growth **(Fig. 2.2)** or cell proliferation of palatal shelves at

E13.5 **(Fig. 2.8)**, it is unlikely that the delay in palatal shelf elevation in *Specc1l*$^{cGT/\Delta C510}$ mutants is due to an overall underdevelopment of the embryos. It is important to note that a delay in palatal shelf elevation presents a potential model both for incomplete cleft palate penetrance that is frequently observed in syndromic CL/P [Jugessur, 2009; Dixon, 2011], and for the complex etiology of nsCL/P where this delay may predispose the developing embryo to cleft palate pending additional genetic or environmental insult.

We have shown previously that SPECC1L affects cell adhesion [Saadi, 2011; Wilson, 2016] and cell migration [Saadi, 2011]. Adherens junction markers E-cadherin and β-catenin, as well as F-actin, show increased expression upon SPECC1L deficiency *in vitro* and *in vivo* [Wilson, 2016]. Consistently, E-cadherin expression is decreased upon ectopic IRF6 expression [Ke, 2015]. In the *Specc1l*$^{cGT/\Delta C510}$ mutants, we again see a general increase in F-actin staining. Importantly, β-catenin is mislocalized to the apical surface of the periderm cells in regions where the palatal shelf epithelium interfaces with both the tongue and buccal region. Such ectopic localization of adherens junction molecules has previously been shown in the periderm of *Irf6* mutants [Richardson, 2009], suggesting that transient oral adhesions can slow palatal shelf elevation due to increased "friction".

IRF6 mutations result in Van der Woude (1/35,000) and Popliteal Pterygium (1/300,000) syndromes. Importantly, approximately 10-15% of *IRF6* mutations manifest as nsCL/P. Several studies have also associated common *IRF6* variants with nsCL/P at large [Zucchero, 2004; Rahimov, 2008; Beaty, 2010]. One of these variants is located in an upstream enhancer element of *IRF6* [Rahimov, 2008] and affects *IRF6* expression levels [Fakhouri, 2012], and it is also associated with the severity of nsCL/P [Kerameddin, 2015]. We now show that SPECC1L expression in the palate epithelium and mesenchyme is dependent upon IRF6, thereby expanding the IRF6 network. In the future, it would be interesting to explore expression levels of SPECC1L

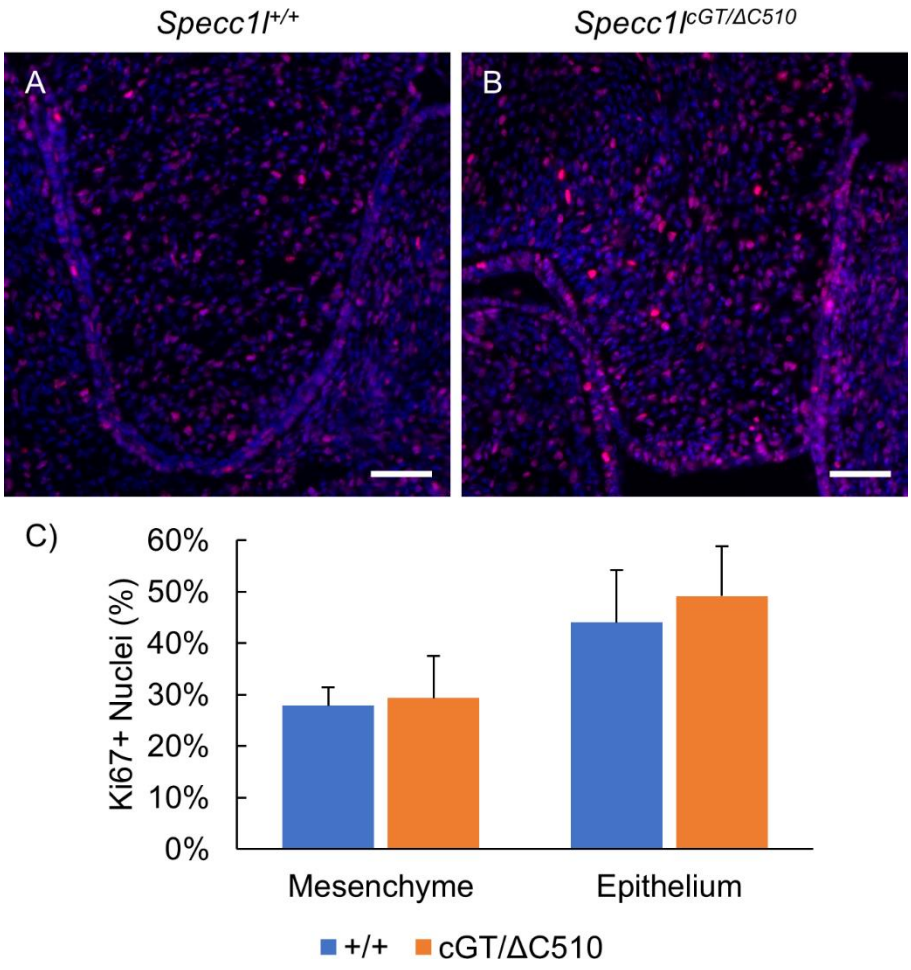

Figure 2.8: Palates of *Specc1l*$^{cGT/\Delta C510}$ E13.5 embryos show no changes in cell proliferation. **A-B)** Representative images of palatal shelves from E13.5 wildtype and *Specc1l*$^{cGT/\Delta C510}$ mutant coronal sections immunostained for Ki67 (red) and counterstained with DAPI (blue). Scale bars are 50μm. **C)** The proliferation index was determined by measuring the proportion of Ki67+ nuclei in the mesenchyme and epithelium of the palatal shelves of three embryo pairs. The index is not significantly different between wildtype and mutant samples. Error bars show SEM.

in mouse mutants for other genes known to interact with *Irf6*, including *Grhl3* [Peyrard-Janvid, 2014], *Tfap2a* [Kousa, 2017; Kousa, 2019] and *Spry4* [Kousa, 2017]. In conclusion, our data suggest SPECC1L is a downstream cytoskeletal effector molecule in the palate, regulated by IRF6 transcription factor.

CHAPTER THREE:

MIGRATION DEFECTS IN SPECC1L-DEFICIENT PALATAL MESENCHYME CELLS CAN BE RESCUED BY ACTIVATION OF THE PI3K-AKT PATHWAY

Authors
Everett G. Hall, Jeremy P. Goering, Dona Greta Isai, Nathan R. Wilson, Edina Kosa, Luke W. Wenger, Zaid Umar, Abdul Yousaf, Andras Czirok, Irfan Saadi

Contributions
EGH, JPG, NRW, AC, and IS conceived and designed the experiments. JPG, EGH, NRW, EK, and LWW performed the experiments. DGI and AC performed the time-lapse imaging analysis. JPG, ZU, and AY performed the manual cell tracking. EGH, and JPG wrote the paper. EGH, JPG and IS edited the manuscript. All authors reviewed the manuscript.

3.1 Abstract

Clefts of the lip and/or palate (CL/P) are common anomalies that occur in 1/800 live births. Pathogenic *SPECC1L* variants identified in patients with rare atypical clefts and syndromic CL/P suggest the gene plays a primary role in face and palate development. Palatogenesis requires extensive mesenchymal remodeling, especially during palatal shelf elevation. We posit that this remodeling involves collective migration of neural crest-derived palatal mesenchyme cells. Live time-lapse microscopy was performed to visualize *in vitro* wound-repair assays with SPECC1L-deficient U2OS osteosarcoma and primary mouse embryonic palatal mesenchyme (MEPM) cells. SPECC1L-deficient cells consistently showed delayed closure in wound-repair assays. To evaluate which features of cellular movement were responsible, we performed automated particle image velocimetry (PIV) and manual cell tracking. The analyses revealed that both cell speed and directionality are disrupted in SPECC1L-deficient cells compared to controls. Stream formation is a hallmark of collective migration. Indeed, MEPM cultures displayed correlated movement of neighboring cells. Consistent with a role in collective migration, correlation length was reduced in SPECC1L-deficient cultures. Furthermore, we previously demonstrated SPECC1L to be a novel regulator of PI3K-AKT signaling, with SPECC1L-deficiency leading to reduced pan-AKT levels. We show that activation of this pathway with the 740 Y-P small molecule can rescue the wound closure delay in both SPECC1L-deficient U2OS and MEPM cells. Cell tracking analyses show

that this rescue is in part due to increased speed and improved directionality. Altogether, our data show a novel role for SPECC1L in collective cell migration through modulation of P13K-AKT signaling.

3.2 Introduction

The development of the secondary palate involves the coordinated growth and movement of the palatal shelves in conjunction with surrounding craniofacial structures [Reviewed in Bush, 2012; Lan, 2015; Li, 2017]. In mice, the palatal shelves originate as a pair of vertical outgrowths from the maxillary processes at embryonic day 11.5 (E11.5) and extend downward adjacent to the tongue until E13.5 [Bush, 2012]. Over the next 24-hour period, the palatal shelves elevate to position themselves horizontally above the tongue and extend toward the midline by E14.5. By E15.5 the shelves have adhered and fused at the midline to form the secondary palate. Defects in palatal shelf outgrowth, elevation, or fusion can lead to cleft palate, one of the most common human birth defects [Mossey, 2009; Bush, 2012]. Of these steps, elevation is the most poorly understood. During this process, the palatal shelves display drastic morphological changes. Histological studies of palate elevation have shown that the mechanism differs along the anteroposterior axis [Jin, 2010; Yu, 2011; Reviewed in Bush, 2012]. The anterior palate exhibits a “flipping up” motion where the distal ends of the shelves turn up toward the midline. In contrast, the middle and posterior sections of the palate undergo more extensive remodeling, wherein the medial wall of the shelves extends medially as the distal ends of the shelves retract [Walker, 1956; Jin, 2010; Yu, 2011]. This latter process can be referred to as mesenchymal remodeling [Jin, 2010]. Interestingly, the “bulging” appears to occur first, indicating it may be the driving event during elevation [Yu, 2011].

Several cellular mechanisms for mesenchymal remodeling during palate elevation have been proposed [Reviewed in Gritli-Linde, 2007; Bush, 2012; Lan, 2015; Li, 2017]. The concurrence of elevation defects with changes in proliferation in numerous mouse mutants has led to proliferation as a commonly discussed model [Lan, 2004; Okano, 2012; Matsumura, 2011]. Previous studies have shown increased proliferation in the medial half of palatal shelves at E13.5, suggesting that a mediolateral asymmetry of growth could promote formation of the bulge at the medial edge [Lan, 2004]. Nevertheless, elevation defects in other mutants without apparent changes in proliferation show that proliferation is required, but not sufficient, for elevation to occur [Jin, 2008; Kouskoura, 2013; Lan, 2016]. Regional accumulation of glycosaminoglycans (GAG), such as hyaluronic acid (HA), are also hypothesized to drive elevation [Brinkley, 1986; Brinkley, 1987; Ferguson, 1988]. The high affinity for water of GAGs is proposed to result in osmotic swelling of specific regions of the palate. Identification of altered GAG composition in mouse mutants with elevation defects lends credibility to this idea [Snyder-Warwick, 2010; Lan, 2016]. However, whether these differences contribute to the failed elevation in these models is still unclear.

Mesenchymal remodeling and migration represent a third possibility for palate elevation. Tissue reorganization through collective cell movement has been described in several model systems [Scarpa, 2016]. This phenomenon has been extensively studied in cranial neural crest cells (CNCC), a migratory cell population that contributes to many craniofacial tissues, including the mesenchyme of the palatal shelves. Organ culture of chimeric palatal shelf explants have shown that palatal mesenchyme also has migratory properties [He, 2008]. Additionally, WNT5A and FGF10 have both been found to have chemotactic effects on palatal mesenchyme cells [He, 2008]. A different study showed that regional differences in fibronectin organization within the palatal

shelf were partially regulated by RAC1 and demonstrated that introduction of a constitutively active RAC1 construct could induce elevation [Tang, 2015]. Since fibronectin organization was shown to impact migration speed *in vitro*, it was suggested that changes in regional fibronectin organization may facilitate different migration speeds during palate remodeling [Tang, 2015]. Together, these studies show evidence that migration may contribute to palatal remodeling, but whether palate mesenchymal cells can migrate collectively has not been shown.

SPECC1L is a cytoskeletal protein that associates with both filamentous actin and microtubules [Saadi, 2011; Mattison, 2011]. Mutations in *SPECC1L* have been identified in multiple patients with craniofacial malformations, including cleft palate [Saadi, 2011; Bhoj, 2015; Kruszka, 2015; Bhoj, 2018]. Mouse embryos homozygous for a null *Specc1l* gene trap allele die between E9.5-E10.5 with open neural folds and defects in CNCC delamination [Wilson, 2016]. Loss of SPECC1L also results in increased staining of adherens junction markers β-catenin and E-cadherin, as well as defects in actin cytoskeleton organization [Saadi, 2011; Wilson, 2016]. In Chapter 2, we reported the generation of a truncation *Specc1l* allele ($Specc1l^{\Delta C510}$) that causes perinatal lethality. Crossing this allele with a gene trap ($Specc1l^{cGT}$) resulted in $Specc1l^{cGT/\Delta C510}$ compound mutant embryos that exhibit a delay in palate elevation [Chapter 2]. These mutants also show transient oral adhesions and improper localization of adherens junction markers to the apical surface of periderm cells [Chapter 2]. We proposed that these adhesions were contributing to the delay in palate elevation by inhibiting the movement of the shelves [Chapter 2]. However, *Specc1l* is broadly expressed in both the palatal mesenchyme and epithelium, suggesting that it may also play a role during mesenchymal remodeling. Consistent with SPECC1L playing a role in cell migration, *SPECC1L*-kd U2OS cells close the wound more slowly than controls in wound-repair assays [Saadi, 2011; Wilson, 2016].

In this study we report a quantitative analysis of wound closure in *SPECC1L*-kd U2OS cells to determine which aspect of cell behavior is responsible for these migration defects. We also perform random motility and wound-repair experiments using primary mouse embryonic palatal mesenchyme (MEPM) cells from wildtype and *Specc1l*$^{cGT/\Delta C510}$ mutant embryos, as they represent a more relevant model of palate development. Importantly, we find that MEPM cells exhibit stream formation, an attribute of collective migration, and show that this behavior is reduced in mutant MEPM cells. Lastly, we investigate whether pharmacological activation of the PI3K-AKT pathway, which is reduced in *Specc1l* mutants, is sufficient to rescue migration defects in these cells. Together, these data show a novel role for SPECC1L in cell migration through regulation of the PI3K-AKT signaling pathway, as well as establish MEPM cells as a proxy model for migration during palatogenesis.

3.3 Materials and Methods

3.3.1 U2OS and MEPM cell culture

Control and *SPECC1L*-kd U2OS cells (ATCC HTB-96) were cultured in 10% DMEM as previously shown [Saadi, 2011; Wilson, 2016]. For MEPM isolation and culture, *Specc1l*$^{\Delta C510/+}$ x *Specc1l*$^{cGT/+}$ mouse mating pairs were placed together overnight, and the female was checked for plugs each morning. Upon identification of a plug, females were removed from the male into a separate cage until the desired stage. Gestational stage was defined as embryonic day 0.5 (E0.5) at noon of that day. Females were euthanized at E13.5 or E14.5 using a primary and a secondary method as approved by the institutional IACUC. Embryos were then harvested from euthanized dams under aseptic conditions and washed in sterile 1x PBS. Palatal shelf isolation was performed by first decapitating the embryos and removing the jaw. Next, a transverse slide was made above

the eyes to create a flat surface and the head was flipped to expose the palatal shelves. Using fine forceps and microdissection scissors, palatal shelves were cut away from the rest of the oral cavity, placed in a 1.5mL tube with 0.5mL of 0.25% Trypsin (ThermoFisher, 25200056), and incubated at 37°C for 10 minutes. Occasional pipetting up and down was performed to accelerate dissociation of the shelves by mechanically breaking apart the tissue. The resulting MEPM cells in the Trypsin solution were then mixed with 5mL of DMEM (HyClone, SH30243.01) containing 10% FBS (Corning, 35-010-CV) in a conical tube. The tube was then centrifuged at 200rcf for 10 minutes to pellet the cells. After removing the supernatant, the MEPM cells were resuspended in standard high glucose DMEM containing 10% FBS, plated on tissue culture treated plastic dishes, and incubated at 37°C for propagation of the cells. Cells were cryopreserved upon isolation, and only passaged up to 3 times for use in experiments.

3.3.2 Time-lapse imaging assays

For wound assays, control and *SPECC1L*-kd U2OS cells were seeded in silicone inserts (Ibidi, 81176) on tissue culture treated plastic dishes at a density of 2.3 x 10^3 cells/mm^2. *Specc1l*$^{+/+}$ and *Specc1l*$^{cGT/\Delta C510}$ MEPM cells were seeded at a density of 1.4 x 10^3 cells/mm^2. All cells were allowed to continue growth for 48 hours post-confluence before the silicone insert was removed, leaving a cell-free gap of 500μm. For MEPM drug experiments, 100μg/mL 740 Y-P (ApexBio, B5246) was added 24 hours prior to imaging. The drug was added again at the start of imaging, and it remained throughout the duration of imaging. An equal proportion of water was added to vehicle control wells. For U2OS drug experiments, 100μg/mL 740 Y-P and 10-30μM wortmannin (ApexBio, A8544) were instead dissolved in DMSO. For stream formation analysis of *Specc1l*$^{+/+}$ and *Specc1l*$^{cGT/\Delta C510}$, MEPM cells were seeded at low, medium, and high densities; 36 cells/mm^2,

10^7 cells/mm^2, and 321 cells/mm^2 respectively. For these three density analyses, MEPM cultures were seeded onto tissue culture plastic dishes that contained 3D-printed rings with the same dimensions as one well of a standard 96 well plate. All live-imaging experiments were performed in normal culture conditions with phase contrast images collected every 10 minutes over a period of 48-72 hours at 10x magnification. Imaging was performed using the EVOS FL Auto Imaging System (ThermoFisher, AMAFD1000) with the EVOS Onstage Incubator (ThermoFisher, AMC1000). Cell cultures were kept in a humidified, 5% CO2 environment at 37°C during imaging.

3.3.3 Time-lapse imaging analysis

Analysis of the live imaging was performed using software developed at the University of Kansas Medical Center by Dr. András Czirók, Ph.D. Three primary types of analyses were performed. First, percentage coverage was performed by automated imaging analysis to generate confluence and front propagation graphs. Secondly, displacement, flow plots, co-movement, and correlation lengths were all quantified from particle image velocimetry (PIV) analysis [Czirok, 2013]. In brief, the image field was divided into small grid segments and the pixel values were analyzed over time to generate a velocity vector field. For displacement, the average velocity of the field was calculated over time. For flow analysis, each vector was compared to their "neighbors" both parallel and perpendicular to their direction of movement and averaged across all vectors. The generated plots were then fitted to a curve from which the co-movement (average constant across larger distances) and correlation length (lower rate of drop-off proceeding from center results in larger values) were calculated. Co-movement speed is analogous to propagation speed of wound, while correlation length is an approximate measure of collective migration.

3.4 Results

3.4.1 SPECC1L-kd U2OS cells show migration defects during wound closure

To evaluate the effect of *SPECC1L* deficiency on migration, we performed wound-repair assays with control and *SPECC1L*-kd U2OS cells **(Fig. 3.1A-F)**. Similar to previous findings [Saadi, 2011; Wilson, 2016], control cells closed the wound before *SPECC1L*-kd cells, signifying a defect in migration **(Fig. 3.1C vs F)**. To quantify the wound closure, we measured the occupied wound area and calculated the percentage of confluency at each 10-minute interval **(Fig. 3.1G)**. The rate of the control cell closure is much faster than the *SPECC1L*-kd cells, as shown by the higher slope of the control closure line, and reaches confluency at an earlier frame **(Fig. 3.1G, green vs. red lines)**. Averaging of the slopes into a single value similarly shows a front propagation speed in the controls **(Fig. 3.1H)**. We also performed automated PIV analysis to approximate the behavior of cells within the monolayers. To determine if the impaired wound closure was due to the decreased motility, we calculated the average PIV displacement within the fields over time **(Fig. 3.1I)**. Indeed, the control fields show a spike in displacement during wound closure that is much less pronounced in the *SPECC1L*-kd **(Fig. 3.1I)**.

SPECC1L has been implicated in the regulation of the actin cytoskeleton and cell junctions, both of which are essential for the collective migration of cells. Therefore, we hypothesized that coordinated movement may also be affected in *SPECC1L*-kd cells. To do this, we first performed manual tracking on the cells during wound closure. Migration plots show that *SPECC1L*-kd cells exhibited an increased dispersion pattern during initial phase of wound closure **(Fig. 3.1J).** We also measured the flow by comparing each vector to their neighbors both perpendicular and parallel to the direction of movement **(Fig. 3.1K-L)**. Compared to controls, *SPECC1L*-kd cells showed a decrease in flow. Similarly, the co-movement speeds and correlation lengths both showed a

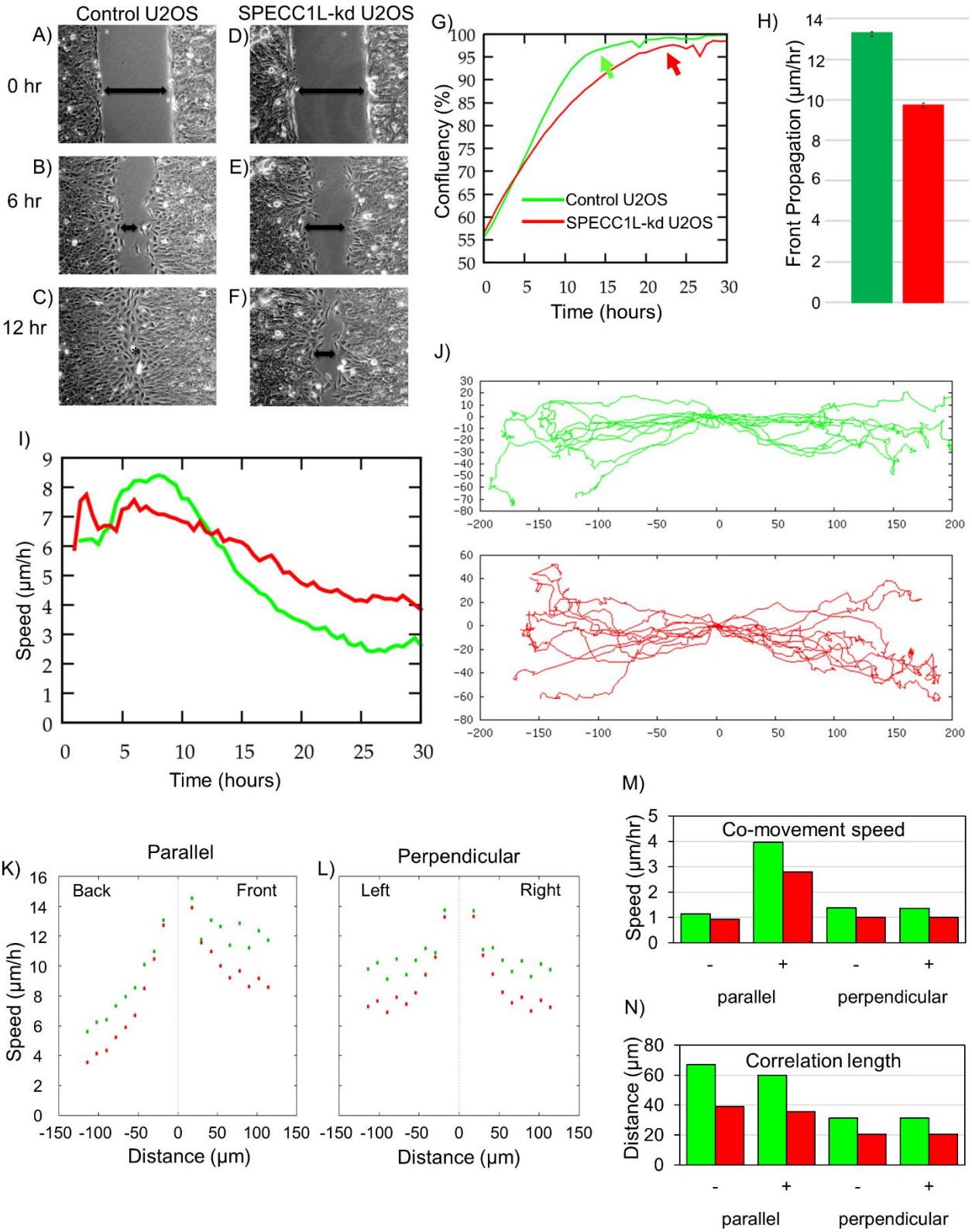
Control U2OS
SPECC1L-kd U2OS
A)
D)
0 hr
B)
E)
6 hr
C)
F)
12 hr
G)
Confluency (%)
Time (hours)
Control U2OS
SPECC1L-kd U2OS
H)
Front Propagation (µm/hr)
J)
I)
Speed (µm/h)
Time (hours)
M)
Co-movement speed
Speed (µm/hr)
parallel
perpendicular
N)
Correlation length
Distance (µm)
parallel
perpendicular
K)
Parallel
Back
Front
Speed (µm/h)
Distance (µm)
L)
Perpendicular
Left
Right
Distance (µm)

Figure 3.1: *SPECC1L*-kd U2OS cells have migration defects. A-F) Images from wound-repair assays using control (A-C) and *SPECC1L*-kd (D-F) U2OS cells. At the onset of wound closure (A, D; 0 hr) neither wound contains cells. A delay in knockdown cell wound closure can be appreciated by mid-closure at 6 hr (B,E) and upon control wound closure (C,F). **G-H)** Automated confluence analysis of wound-repair experiments showing the average percentage of wound closure over time (G) and the average speed of front propagation (H) is decreased in knockdown cultures (red) compared to control (green). **I)** Average displacement calculated from automated PIV analysis shows an initial spike in knockdown speed. Wildtype displacement overtakes mutant displacement during wound closure, but decreases after wound is closed at ~12.5hr. **J)** Manual cell tracking data show increased spread of *SPECC1L*-kd cells compared to wildtype. **K-L)** PIV flow plot shows average speed of movement surrounding a given point in both the parallel (K) and perpendicular (L) directions. Movement in the positive parallel direction (K; front) is higher compared to the negative direction (K; back). Knockdown cultures show decreased speed at all points (K,L red dots). **M)** Calculating the constant of the fitted curve shows reduced knockdown co-movement speed, analogous to front propagation. **N)** Slower drop-off of the fitted curves converted to correlation length showed an increase in correlation length in control cultures compared to knockdown.

decrease in knockdown cells, indicating that neighboring cells were migrating in a less coordinated fashion **(Fig. 3.1M-N)** Collectively, these results show that both decreased individual cell speed and poor directed motility may contribute to the wound closure delay seen in *SPECC1L*-kd U2OS cultures.

3.4.2 Mouse embryonic palatal mesenchyme (MEPM) cells display attributes of collective movement

To study SPECC1L deficiency in a model that was more relevant to the palate defects seen in human patients and our mouse models, we isolated mouse embryonic palatal mesenchyme cells (MEPM) from wildtype and *Specc1l*$^{cGT/\Delta C510}$ compound mutant embryos. We initially characterized the dynamics of MEPM growth and movement with time-lapse videos of cultures plated at different densities **(Fig. 3.2 A-C)**. Confluency analysis showed that each plating density resembled different ranges within a typical S-shaped logistic growth curve, with lower densities just entering the rapid growth phase and higher densities reaching a plateau by the end of imaging **(Fig. 3.2D)**. The slopes of *Specc1l*$^{cGT/\Delta C510}$ MEPM cells showed a slower rate of growth at the low and medium plating densities compared to wildtype **(Fig. 3.2D)**. PIV analysis of the cultures showed that increasing cell density coincided with lower displacement likely due to a reduced freedom of movement **(Fig. 3.2E)**. Mutant MEPM cells show reduced PIV displacement at the low and medium plating densities **(Fig. 3.2E)**.

Next, we asked if MEPM cells had any attributes of collective movement. Interestingly, cell tracking videos showed adjacent cells moving in similar directions (data not shown). This behavior appeared to be more robust at high density, suggesting that the proximity to neighboring cells played a role in their direction of movement. To quantify this, 2-D random motility was

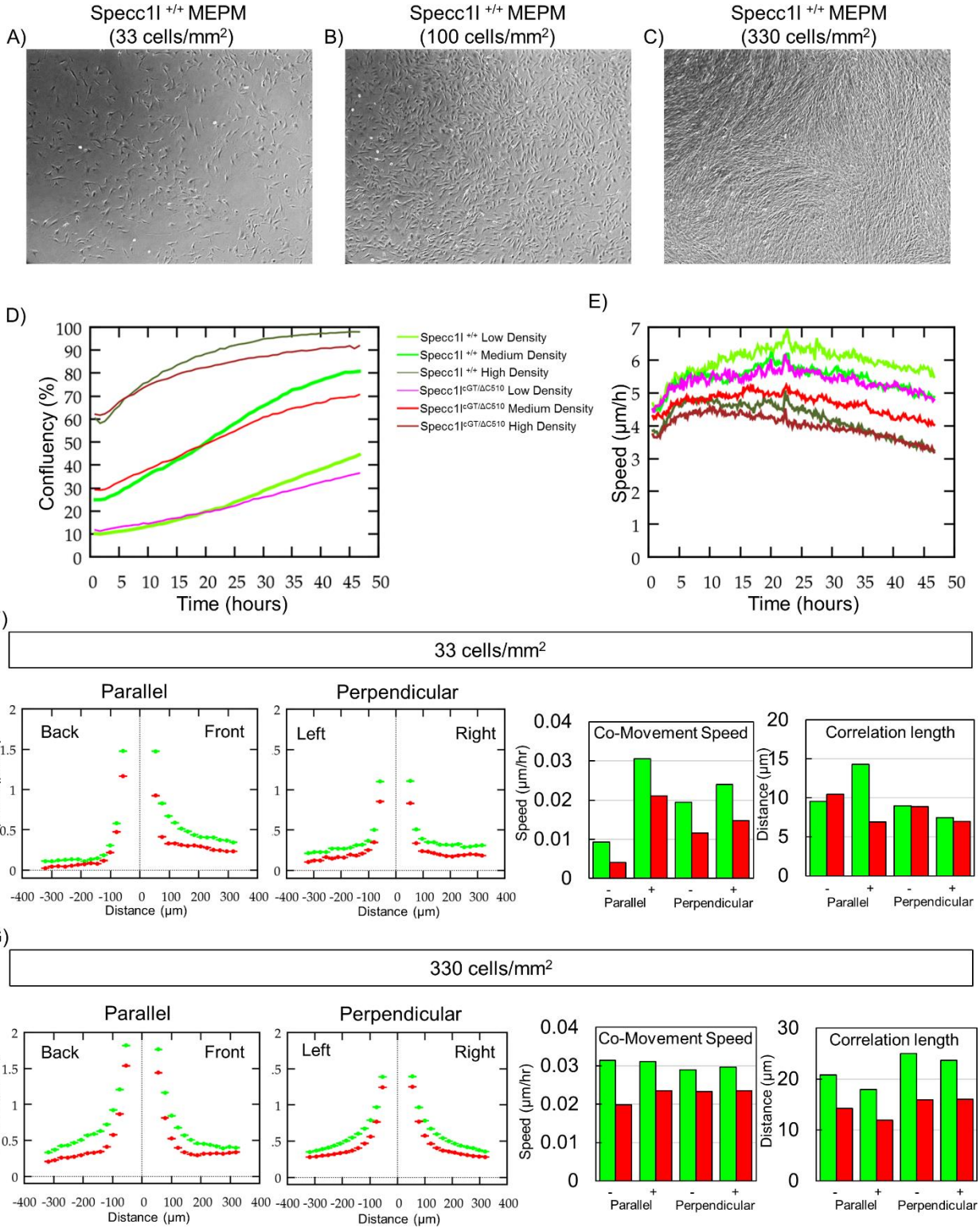
A)
Specc1l +/+ MEPM
(33 cells/mm2)
B)
Specc1l +/+ MEPM
(100 cells/mm2)
C)
Specc1l +/+ MEPM
(330 cells/mm2)
D)
Confluency (%)
Time (hours)
Specc1l +/+ Low Density
Specc1l +/+ Medium Density
Specc1l +/+ High Density
Specc1lcGT/ΔC510 Low Density
Specc1lcGT/ΔC510 Medium Density
Specc1lcGT/ΔC510 High Density
E)
Speed (µm/h)
Time (hours)
F)
33 cells/mm2
Parallel
Perpendicular
Back
Front
Left
Right
Speed (µm/h)
Distance (µm)
Speed (µm/hr)
Co-Movement Speed
Distance (µm)
Correlation length
Parallel
Perpendicular
G)
330 cells/mm2
Parallel
Perpendicular
Back
Front
Left
Right
Speed (µm/h)
Distance (µm)
Speed (µm/hr)
Co-Movement Speed
Distance (µm)
Correlation length
Parallel
Perpendicular

Figure 3.2: *Specc1l*$^{cGT/\Delta C510}$ MEPM cells exhibit decreased correlation length in 2-D random motility assays. A-C) Representative images of wildtype MEPM random motility cultures at low, medium, and high plating densities. **D)** Confluency curves show an increased rate of growth in wildtype MEPM cultures (green shades) compared to mutant cultures (red shades). **E)** PIV displacement plots show higher speeds in wildtype cultures compared to mutant cultures at a given density. Displacement speed decreases at higher densities. **F)** Analysis of low density MEPMs (33 cells/mm^2) PIV flow plots show decreased co-movement speed in mutant cultures compared to wildtype with less difference in correlation length. G) Analysis of high density MEPMs (330 cells/mm^2) PIV flow plots show decreased co-movement speed and correlation length in the mutant cultures.

assessed by PIV flow analysis **(Fig. 3.2F,G)**. Correlation between neighboring vectors was higher at close proximities and tapered off as distance increased across all conditions, but the low density showed a more immediate drop-off **(Fig. 3.2F,G)**. At high density, mutant MEPM cells showed a lower co movement speed and correlation length than wildtype cells, suggesting that their ability to form streams is impaired **(Fig. 3.2F,G)**.

Lastly, we performed wound-repair assays to determine if these defects could impact the ability for mutant MEPM cells to close the gap. Mutant MEPM cells took longer to close the wound than wildtype cells **(Fig. 3.3A-F)**, confirmed by the averaged confluency and front propagation **(Fig. 3.3G-H)**. Importantly, this result validated our findings of poor cell migration with SPECC1L-deficient U2OS cells. Average displacement was also reduced in mutant wounds **(Fig. 2.3I)**. However, contrary to the results from 2-D random motility assays, PIV analysis showed only minor reduction in co-movement speed and no significant changes in correlation length in mutant cultures **(Fig. 3.3J-M)**. These results demonstrate that *Specc1l* deficiency can perturb MEPM cell growth and speed, as well as their ability to move collectively. However, the collective movement defect was only identified in the context of the random motility assay.

3.4.3 Upregulation of PI3K-AKT signaling rescues SPECC1L-deficient migration defects

We previously reported that loss of SPECC1L results in decreased PI3K-AKT signaling along with defects in cell adhesion and cell shape [Wilson, 2016]. Pharmacological activation and inhibition of the pathway was sufficient to rescue or exacerbate these phenotypes, respectively [Wilson, 2016]. To test if modulation could alter wound closure, we performed wound-repair assays with control and *SPECC1L*-kd U2OS cells and treated with either PI3K inhibitor wortmannin or activator 740 Y-P [Ui, 1995; Derossi, 1998]. In agreement with previous results,

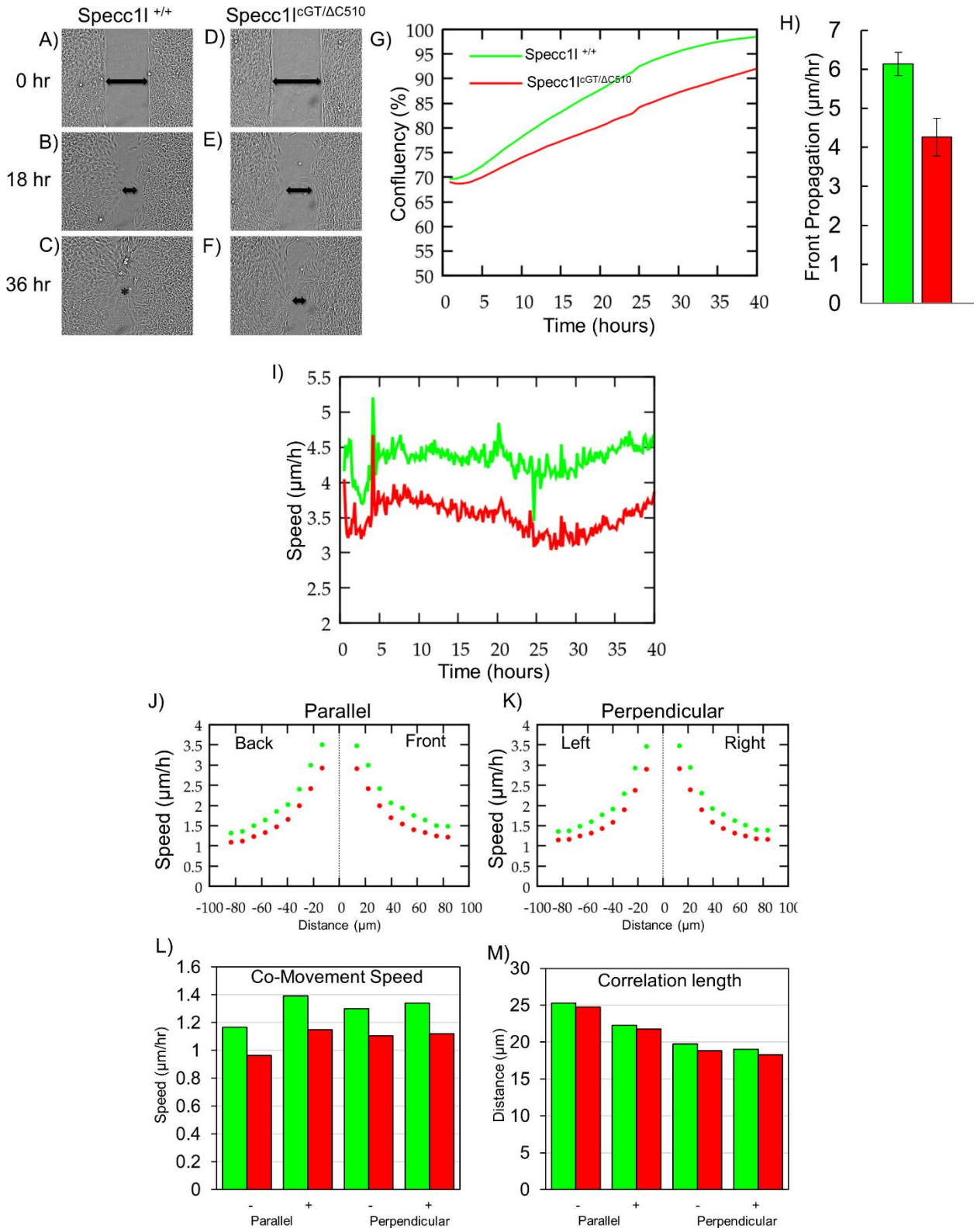
Specc1l +/+
Specc1lcGT/ΔC510
A)
0 hr
B)
18 hr
C)
36 hr
D)
E)
F)
G)
Specc1l +/+
Specc1lcGT/ΔC510
Confluency (%)
Time (hours)
H)
Front Propagation (μm/hr)
I)
Speed (μm/h)
Time (hours)
J)
Parallel
Back
Front
Speed (μm/h)
Distance (μm)
K)
Perpendicular
Left
Right
Speed (μm/h)
Distance (μm)
L)
Co-Movement Speed
Speed (μm/hr)
Parallel
Perpendicular
M)
Correlation length
Distance (μm)
Parallel
Perpendicular

Figure 3.3: *Specc1l*$^{cGT/\Delta C510}$ MEPM cells exhibit defects in wound closure, but not correlation length during wound-repair assays. A-F) Images from wound-repair assays show that wildtype (A-C) MEPM cells close wounds faster than *Specc1l*$^{cGT/\Delta C510}$ (D-F) MEPM cells, similar to U2OS experiments. **G-H)** Mutant MEPM cells (red) show reduced averaged confluency curves and front propagation compared to wildtype (green). **I)** Average displacement of wildtype MEPM cells is higher compared to mutant at all stages of wound closure. **J-K)** PIV flow plots show no differences between the four directions with slightly reduced speed in mutant MEPMs compared to wildtype. **L)** Co-movement speed of mutant wounds is reduced, but correlation lengths are unchanged compared to wildtype.

wortmannin treatment severely impaired the rate of U2OS cell wound closure **(Fig. 3.4A-B)**. The speed of control wound front propagation was reduced to the speed of untreated knockdown cells, while wortmannin-treated knockdown cell propagation speed was even further reduced **(Fig. 3.4A-B)**. In contrast, treatment with 740 Y-P had little effect on control wound closure, but rescued the rate of knockdown wound closure to control levels **(Fig. 3.4A,B)**. Next, we treated MEPM cell wounds with 740 Y-P to see if it would result in a similar effect. PI3K activation did indeed rescue the wound closure defect in *Specc1l*$^{cGT/\Delta C510}$ mutant MEPM cultures **(Fig. 3.4C-D)**. However, unlike U2OS cells, 740 Y-P treatment of both wildtype and mutant MEPM cells increased the rate of wound closure beyond untreated wildtype levels, possibly owing to increased baseline levels of the pathway in U2OS cancer cells **(Fig. 3.4C-D)**.

To determine what aspect of cell behavior was improved by the rescue experiments, we compared cell tracking results from untreated U2OS and MEPM cells to those treated with 740 Y-P **(Fig. 3.5)**. A subtle decrease in dispersion was observed upon PI3K activation in *SPECC1L*-kd U2OS wounds, but this change was restricted to the early stages of closure **(Fig. 3.5A-C)**. To evaluate movement speed, we calculated displacement over time from both the PIV and manual tracking data **(Fig. 3.5D-E)**. PIV analysis shows a slight rescue at mid-closure upon 740 Y-P treatment **(Fig. 3.5D)**. However manual tracking speed did not show a significant change apart from an initial spike in mutant cells **(Fig 3.5G)**. To more easily visualize the differences in these data, we plotted both total displacement **(Fig. 3.5F; thick lines)** and x-axis displacement **(Fig. 3.5F thin lines)** over time. We also divided x-axis displacement (movement into the wound) by total displacement **(Fig. 3.5G)**. This value shows the proportion of total movement that can attributed to movement into the wound, thereby acting as a measure of directed movement. Knockdown cells showed a reduction in all three measures compared to control that was rescued

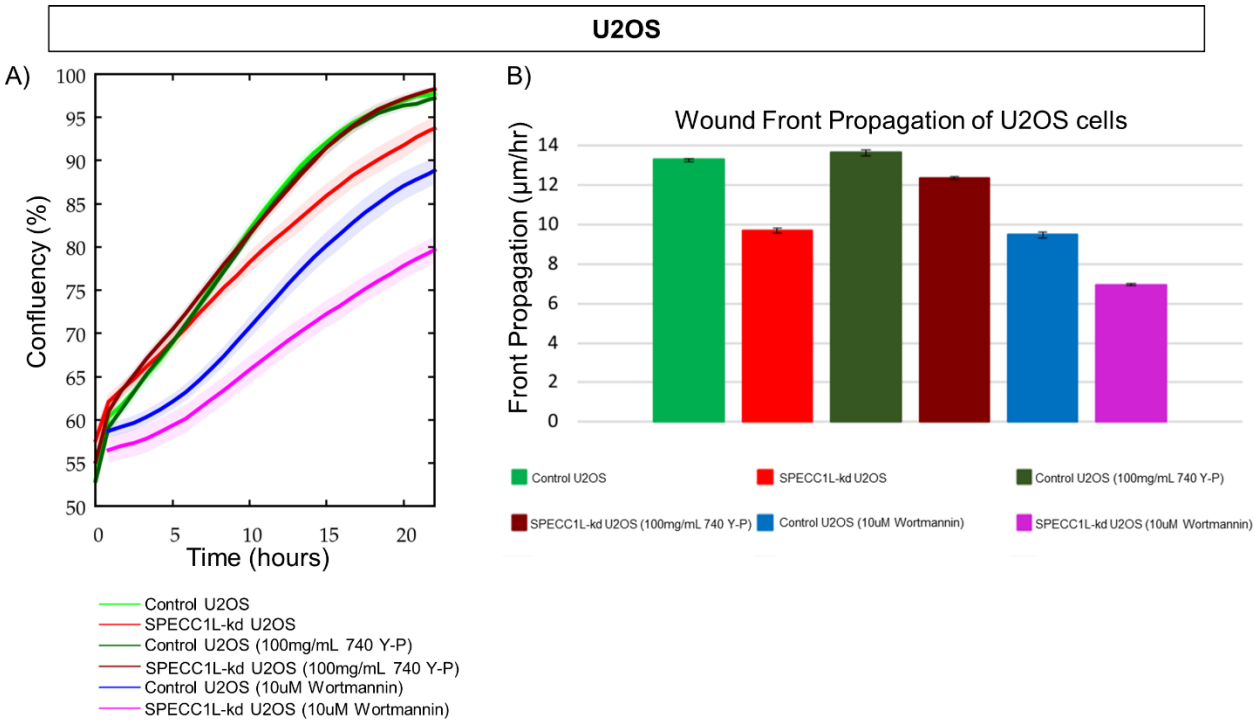
U2OS
A)
Confluency (%)
Time (hours)
Control U2OS
SPECC1L-kd U2OS
Control U2OS (100mg/mL 740 Y-P)
SPECC1L-kd U2OS (100mg/mL 740 Y-P)
Control U2OS (10uM Wortmannin)
SPECC1L-kd U2OS (10uM Wortmannin)
B)
Wound Front Propagation of U2OS cells
Front Propagation (µm/hr)
Control U2OS
SPECC1L-kd U2OS
Control U2OS (100mg/mL 740 Y-P)
SPECC1L-kd U2OS (100mg/mL 740 Y-P)
Control U2OS (10uM Wortmannin)
SPECC1L-kd U2OS (10uM Wortmannin)

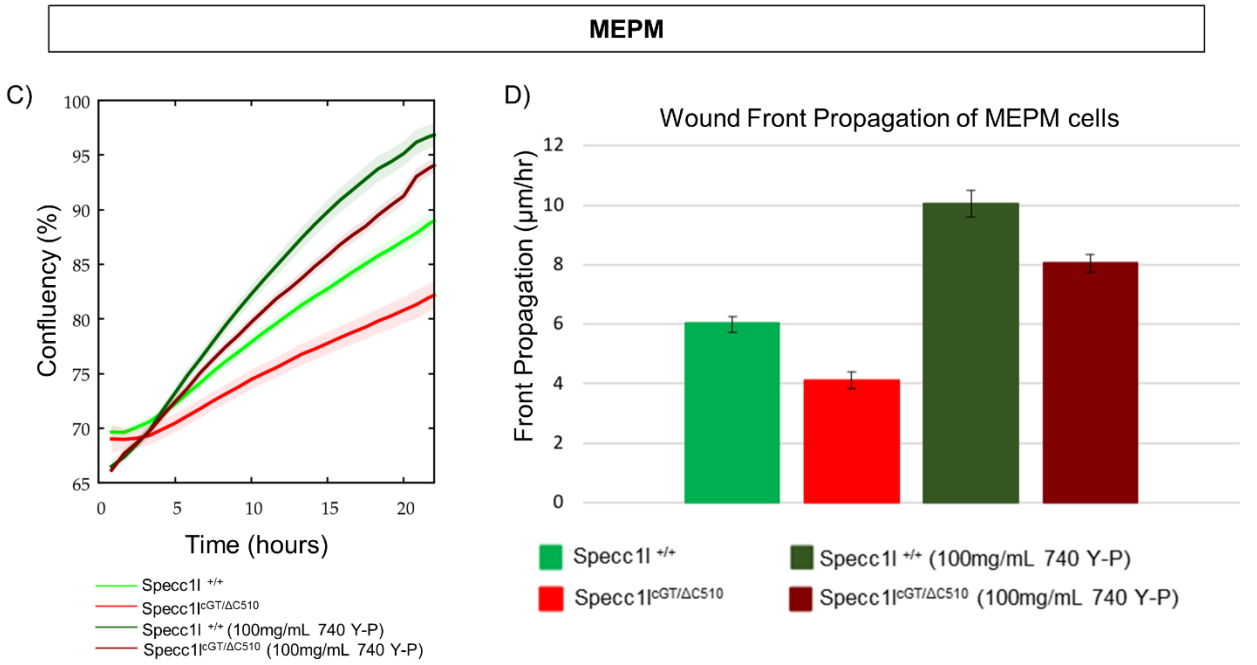
MEPM
C)
Confluency (%)
Time (hours)
Specc1l +/+
Specc1l cGT/ΔC510
Specc1l +/+ (100mg/mL 740 Y-P)
Specc1l cGT/ΔC510 (100mg/mL 740 Y-P)
D)
Wound Front Propagation of MEPM cells
Front Propagation (µm/hr)
Specc1l +/+
Specc1l +/+ (100mg/mL 740 Y-P)
Specc1l cGT/ΔC510
Specc1l cGT/ΔC510 (100mg/mL 740 Y-P)

Figure 3.4: Activation of PI3K-AKT signaling rescues wound closure defects of SPECC1L-deficient cells. A-B) Confluency curves and front propagation of control (green, dark green, blue) and *SPECC1L*-kd (red, brown, pink) U2OS cell wound-repair assays treated with vehicle, 740 Y-P, and wortmannin. 740 Y-P treatment rescues knockdown closure (brown), and has no effect on control (dark green). Conversely, wortmannin treatment decreases closure speed in both control (blue) and knockdown wounds **(pink)**. **C-D)** Confluency curves and front propagation of wildtype (green, dark green) and *Specc1l*$^{cGT/\Delta C510}$ (red, dark red) MEPM cell wound-repair assays treated with vehicle and 740 Y-P. Treatment with 740 Y-P increases wound closure speed in mutant wounds (dark red), but also wildtype wounds (dark green).

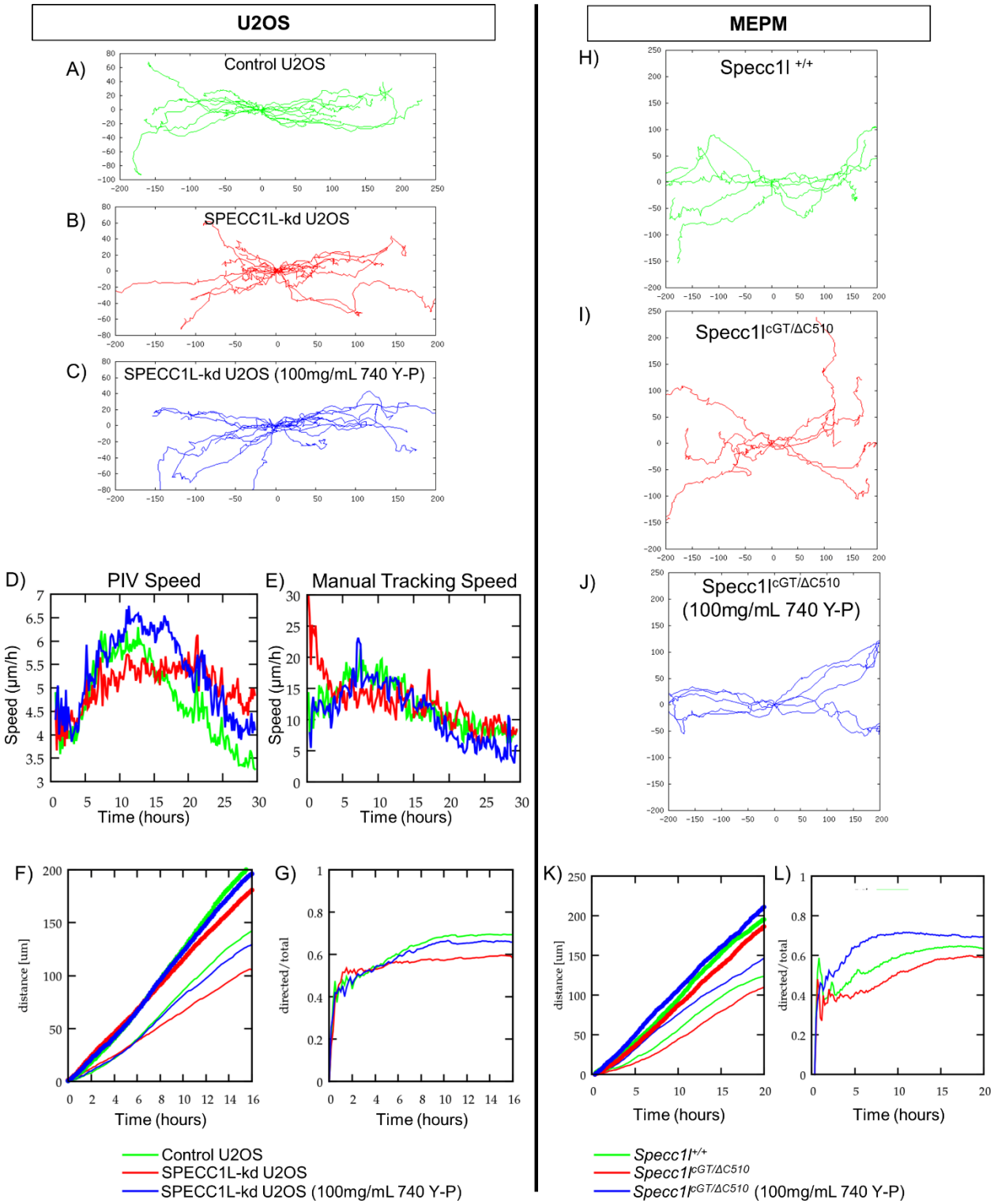
U2OS
A)
Control U2OS
B)
SPECC1L-kd U2OS
C)
SPECC1L-kd U2OS (100mg/mL 740 Y-P)
D)
PIV Speed
Speed (µm/h)
Time (hours)
E)
Manual Tracking Speed
Speed (µm/h)
Time (hours)
F)
distance [um]
Time (hours)
G)
directed/total
Time (hours)
Control U2OS
SPECC1L-kd U2OS
SPECC1L-kd U2OS (100mg/mL 740 Y-P)
MEPM
H)
Specc1l +/+
I)
Specc1lcGT/ΔC510
J)
Specc1lcGT/ΔC510
(100mg/mL 740 Y-P)
K)
distance [um]
Time (hours)
L)
directed/total
Time (hours)
Specc1l+/+
Specc1lcGT/ΔC510
Specc1lcGT/ΔC510 (100mg/mL 740 Y-P)

Figure 3.5: Activation of PI3K-AKT signaling increases cell movement into wound. A-C) Manual cell tracking plots of control (green), *SPECC1L-kd* (red), and 740 Y-P-treated (blue) *SPECC1L-kd* U2OS wound-repair assays. **D-E)** Displacement values from PIV (D) and manual tracking (E). An initial spike in knockdown movement speed is present in the manual tracking graph, but not PIV displacement. **F)** Average total displacement (F; thick lines) and movement directed into the wound (F, thin lines) overtime calculated from manual tracking data to show cell speed and directed movement. Knockdown cells show a reduction in both, but this is rescued upon 740 Y-P treatment. **G)** Ratio of these values shows directed movement into the wound normalized to total displacement. Knockdown cultures show reduced directed movement compared to wildtype, but directed movement is increased in knockdown cultures teated with 740 Y-P. **H-J)** Manual cell tracking plots of *Specc1l*$^{+/+}$ (H; green) *Specc1l*$^{cGT/\Delta C510}$ (I; red), and 740 Y-P-treated *Specc1l*$^{cGT/\Delta C510}$ (J; blue) MEPM wound-repair assays. **K-L)** Total displacement (K; thick lines), wound-directed displacement (K; thin lines), and directionality (L) is reduced in mutant cultures, but rescued upon 740 Y-P treatment.

upon treatment with 740 Y-P. Contrary to the subtle change seen in the U2OS migration plots, cell tracking of MEPM cells showed a substantially reduced dispersion pattern in the rescue wounds **(Fig. 3.5H-J)**. Furthermore, plotting total and x-axis displacement **(Fig. 3.5K,L)** showed the same pattern as the U2OS tracking data, where the displacement and directionality of mutant MEPM cells was reduced compared to wildtype cells. However, mutant cultures treated with 740 Y-P displayed a marked increase in directed movement into the wound that surpassed untreated wildtype cells. Taken together, these data show that PI3K activation rescues wound closure defects in SPECC1L-deficient cells through improvement of both cell speed and directed movement.

3.5 Discussion

Generation of mutant mouse models have been very helpful in characterizing the various cellular and molecular mechanisms underlying palatogenesis [Gritli-Linde, 2008]. Though palate outgrowth and fusion have been well-characterized, the mechanisms driving the elevation of the palatal shelves remain elusive. Much of what we know about palate development stems from analysis of fixed tissues, but the dynamic and rapid nature of palate elevation renders this process difficult to study using this method. Tissue culture of E13.5 embryo heads has been used to directly observe elevation, thereby circumventing some limitations of fixed tissue [Iseki, 2007; Okano, 2012; Song, 2013; Lan, 2016; Lai, 2016]. For example, removal of the jaw can be used to determine whether an elevation defect is intrinsic to the shelves. This method also allows testing the effect of various inhibitory compounds, growth factors, and even gene expression plasmids on palate development [Brinkley, 1982; Shimizu, 2001; Kosazuma, 2004; Tang, 2015]. Isolation of primary MEPM cells has also been used for similar purposes [Liu, 2014; Fantauzzo, 2014; Vasudevan, 2014; Fantauzzo, 2016; Iyyanar, 2017; Jiang, 2017; Gao, 2019]. The uniform

monolayer facilitates the assessment of cellular and molecular processes in highly standardized manner, and so this technique has been popular in exploring the various pathways contributing to mesenchymal proliferation and differentiation. However, only a few studies have investigated the migration of MEPM cells [He, 2013; Fantauzzo, 2017; Gao, 2019], and none, to our knowledge, have examined if they can migrate collectively. We identify the presence of stream formation in MEPM cells, a behavior generally thought to be a feature of collective migration [Szabo, 2010; Czirok, 2013; Scarpa, 2016]. This process requires the active communication through cell adhesions, as well as the dynamic reorganization of the cytoskeleton to direct movement in response to signals from neighboring cells [Czirok, 2013; Theveneau, 2013; Tang, 2017]. The higher correlation lengths seen in the high-density MEPM cultures are consistent with this contact-dependent mechanism.

SPECC1L deficiency has been previously shown to result in defects in cell adhesion and cytoskeletal organization [Saadi, 2011; Wilson, 2016]. In this study we provide a detailed account of cell migration in SPECC1L-deficient MEPM cells. Importantly, we used these cells to successfully replicate the previously reported *SPECC1L*-kd wound closure defects, supporting a palate-specific role for SPECC1L in cell migration [Saadi, 2011; Wilson, 2016]. Our analyses offer three non-exclusive mechanisms that may contribute to these wound closure defects. First, the decreased displacement we assessed by PIV analysis suggest an overall reduction in movement speed of mutant cells. This mechanism is the easiest to explain, as slower-moving cells would predictably result in slower wound closure. Next, the increased dispersion pattern demonstrated by cell tracking shows that the cells do not move persistently to close the wound. If we assume that cell movement in any direction has a maximum speed, any movement not directly towards the wound would decrease the rate of closure. Finally, the reduced correlation lengths we measured

imply that mutant cells have a diminished capacity to respond to the movement of their neighbors, therefore resulting in cells that do not travel with the "flow" into the wound. The latter two findings are likely related, as poor collective movement of the culture may lead to poor directed movement of individual cells. However, we did not see a reduction in correlation length in mutant MEPM wound-repair assays. It is possible that the directionality of wound closure obscures the collective movement of MEPM cells. Each of these mechanisms together or alone could reduce the efficiency of wound closure.

Studies of palatogenesis have demonstrated that remodeling is a primary feature of the elevation process [Yu, 2011; Chiquet, 2016; Li, 2017]. Initial examination of *Specc1l*$^{cGT/\Delta C510}$ mutants suggested that their delay in palate elevation was due to transient epithelial adhesions [Chapter 2]. However, given the migration defects we identified in *Specc1l*$^{cGT/\Delta C510}$ mutant MEPM cells, it is likely that deficiencies in mesenchymal remodeling are also contributing to this delay. Moreover, there remain several mouse mutants with elevation defects for which the underlying pathogenic mechanisms have not been fully elucidated [Reviewed in Gritli-Linde, 2007; Gritli-Linde, 2008; Bush, 2012; Funato, 2015; Li, 2017]. Future inquiries of these mutants may benefit from using MEPM cell migration as a proxy for mesenchymal remodeling during palatal shelf elevation.

Our final analyses showed that activation of PI3K-AKT signaling rescued the wound closure defects in both *SPECC1L*-kd U2OS cells and *Specc1l*$^{cGT/\Delta C510}$ mutant MEPM cells. These results are in agreement with the rescue of cell shape and cell adhesion phenotypes in *SPECC1L*-kd U2OS cells with PI3K-AKT activation that was previously shown [Wilson, 2016]. Interestingly, 740 Y-P treatment increased the front propagation speed of wildtype MEPM cells, but not control U2OS cells. Many cancers already have elevated PI3K-AKT signaling [Altomare,

2005; Testa, 2005], so it is possible that the pathway may have been at capacity before treatment with the activator. Furthermore, cell tracking revealed that increased cell speed and wound-directed movement contributed to this rescue. Given that AKT is a pro-migratory factor [Xue, 2013], the increase in cell speed can be easily explained. However, further studies will be required to determine if the increase in wound-directed movement is due to an improvement in the cells' ability to maintain their direction, or simply an emergent effect of the increased cell speed into the wound. Nevertheless, these experiments collectively demonstrate that SPECC1L regulates cell migration through PI3K-AKT signaling.

CHAPTER FOUR:

IDENTIFICATION OF FUSION DEFECTS IN MOUSE MODEL WITH SPECC1L MUTATION FROM OPITZ G/BBB SYNDROME PATIENT

Authors
Everett G. Hall, Luke W. Wenger, Jeremy P. Goering, Dona Greta Isai, Andras Czirok, Irfan Saadi

Contributions
EGH, LWW, JPG, and IS conceived and designed the experiments. EGH, LWW, and JPG performed the experiments. DGI and AC performed the time-lapse imaging analysis. EGH wrote the paper. EGH and IS edited the manuscript. All authors reviewed the manuscript.

4.1 Abstract

SPECC1L is a cytoskeletal protein implicated in the regulation of cell adhesions and migration. Heterozygous mutations in *SPECC1L* have been identified in patients with a spectrum of phenotypes overlapping Teebi Hypertelorism and Opitz G/BBB syndromes. These disorders consist of midline defects including hypertelorism, cleft lip and/or palate (CL/P), and ventral body wall anomalies. Previous mouse models with *Specc1l* truncation alleles have not recapitulated these malformations. Notably, all *SPECC1L* mutations identified thus far lie within the second coiled-coil domain (CCD2) or calponin homology domain (CHD). We therefore asked if these point mutations would result in palate-specific phenotypes compared to the other alleles. In this study, we generated a knock-in *Specc1l* allele with a mutation in CCD2, T397P, from a patient originally diagnosed with autosomal-dominant Opitz G/BBB syndrome. The resultant homozygous mutant embryos displayed omphaloceles and cleft palate. Cleft palate was also observed in some heterozygous mutants, aptly recapitulating the human condition. To understand the etiology of the cleft palate, we assessed both palate epithelium and mesenchyme, defects in which were also identified in truncation mutants. We found that mutant epithelium showed increased staining of filamentous actin (F-actin), and that mutant protein strongly colocalized with F-actin. Our analysis of mutant mouse embryonic palate mesenchyme (MEPM) cells showed poor migration in wound repair assays. Thus, our findings show that a *SPECC1L* human point mutation in CCD2 is dominant negative. T397P appears to have a more severe effect on both palatogenesis

than *Specc1l* truncation alleles, indicating that the mutation is gain-of-function. In addition, the T397P mutation also recapitulated the ventral body wall closure defect (omphalocele) that is found in 32% of patients with *SPECC1L* mutations.

4.2 Introduction

Clefts of the lip and/or palate (CL/P) are one the most common craniofacial defects, occurring in approximately 1 in 800 live births [Rahimov, 2012; Mossey, 2012]. In most cases, cleft palate occurs in conjunction with other malformations as part of a clinical syndrome, while the remainder are isolated, non-syndromic clefts. Opitz G/BBB syndrome, one such craniofacial disorder, presents with anomalies including hypertelorism, laryngeal defects, and CL/P, as well as urogenital and heart defects [Cappa, 1987]. Opitz syndrome cases have been reported to have both an autosomal dominant and X-linked inheritance pattern and have been associated with mutations in cytoskeletal genes *SPECC1L* and *MID1* (midline-1), respectively. [Taylor, 2010; Bhoj, 2015; Kruszka, 2015; Bhoj, 2018]. *SPECC1L* mutations have also been identified in patients with Teebi hypertelorism syndrome, another autosomal dominant disorder that presents with similar facial features [Bhoj, 2015]. MID1 is responsible for assembling a microtubule-associated complex [Taylor, 2010; Winter, 2016], whereas SPECC1L plays a role in both microtubule stability and F-actin organization [Saadi, 2011; Wilson, 2016; Chapter 2]. Recently, a comprehensive analysis of *SPECC1L* and *MID1* mutations identified a partially overlapping, but distinct spectrum of anomalies between the two groups, and suggested delineation between *MID1* and *SPECC1L*-related syndromes [Bhoj, 2018].

Characterizing the cellular and developmental function of these proteins is imperative to understanding how they contribute to these disorders. Additionally, not all polymorphisms are

deleterious to gene function [Janssen, 2012; Leslie, 2012; Charzewska, 2015]. Therefore, model systems must be utilized to validate the developmental consequences of candidate gene deficiency. Gene trap (RRH, DTM, and cGT) and truncation (ΔC510) mutant *Specc1l* mouse alleles were previously generated to investigate the role of SPECC1L in craniofacial development [Wilson, 2016; Chapter 2]. Embryos homozygous for the gene trap alleles undergo embryonic lethality at embryonic day 9.5 (E9.5) along with defects in cranial neural crest cell (CNCC) delamination [Wilson, 2016]. In contrast, $Specc1l^{cGT/\Delta C510}$ compound heterozygotes die perinatally and exhibit a delay in palatal shelf elevation with over 60% penetrance [Chapter 2]. This delay is only temporary, as the palates of most compound heterozygotes elevate by E15.5 [Chapter 2]. These mutants also show transient oral adhesions and ectopic apical expression of adherens junction markers at the apical surface of periderm cells, representing a potential mechanism for the elevation delay [Chapter 2]. Furthermore, live-imaging analysis showed migration defects in $Specc1l^{cGT/\Delta C510}$ mouse embryonic palatal mesenchyme (MEPM) cells [Chapter 3]. These results are consistent with a role for SPECC1L in palatogenesis in both the palate epithelium and mesenchyme.

SPECC1L contains 8 coiled-coil domains (CCD) and a C-terminal calponin homology domain (CHD). CHDs are known for their affinity for F-actin [Gimona, 2002; Korenbaum, 2002]. In agreement with this cytoskeletal role, examination of SPECC1L cellular expression shows association with both the F-actin and microtubule components of the cytoskeleton [Saadi, 2011; Wilson, 2016]. Syndromic *SPECC1L* variants cluster within, or immediately adjacent to, the second CCD (CCD2) and the CHD [Saadi, 2011; Kruszka, 2015; Bhoj, 2015; Bhoj, 2018]. The addition of mutations from either region disrupts SPECC1L association with microtubules, suggesting that both regions are critical for SPECC1L function [Saadi, 2011; Kruszka, 2015].

The ΔC510 truncation allele removes most of the C-terminal half of the protein, including the CHD [Chapter 2]. However, this model does not recapitulate the orofacial clefting seen in patients with *SPECC1L* mutations. Thus, we hypothesized that the human mutations may have a gain-of-function effect on SPECC1L function. In this study we report the generation of a knock-in mouse line containing a CCD2 mutation from an Opitz Syndrome family [Kruszka, 2015]. Mutant embryos from this line display a high penetrance of cleft palate. We also show that the mutation results in palatal mesenchyme migration defects and alters SPECC1L localization. In sum, these results show that SPECC1L mutations within CCD2 have a qualitatively different impact on SPECC1L function compared to the truncation.

4.3 Materials and Methods

4.3.1 Allele generation, mouse crosses and embryo processing

T397P allele was made with CRISPR/Cas9 with guide RNA (TCTGGTGAATCCGTTCTGTCNGG) targeting the CCD2 region. Heterozygous matings (*Specc1l*$^{T397P/+}$ x *Specc1l*$^{T397P/+}$) were used to generate all analyses, apart from the lineage tracing experiments. To generate mice for those experiments, the T397P allele was separately crossed with the ROSA^{mTmG} (Jax #007576) and Sox10-Cre (Jax # 025807) lines. The ROSA^{mTmG} line was then bred one additional time to generate *Specc1l*$^{T397P/+}$; ROSA$^{mTmG/mTmG}$ mice. Lastly, *Specc1l*$^{T397P/+}$; Sox10-Cre and *Specc1l*$^{T397P/+}$; ROSA$^{mTmG/mTmG}$ mice were crossed together. Embryo harvest and histology processing was performed as previous stated [Chapter 2]. All euthanasia was performed using a primary and secondary method as approved by the institutional IACUC.

4.3.2 Whole mount imaging

Method for DAPI-stained embryos was adapted from published methods [Sandell, 2012]. Briefly, harvested embryos were fixed and permeabilized in 4% PFA at 4°C (overnight for E14.5; 8 hours for E9.5). Next, embryos were washed three times in 1x PBS and then stained in 500nM DAPI dilactate overnight at 4°C. Embryos were submerged in 1x PBS for all imaging. Fluorescent images of lineage tracing at E9.5 were captured on a Nikon Eclipse 80i upright microscope, while all other brightfield and E14.5 DAPI palate images were captured on a Nikon SMZ 1500 stereomicroscope.

4.3.3 Skeletal Preparations

Skeletal stains were performed as dictated by published methods [Rigueur, 2014]. Briefly, E19.5 embryos were harvested, washed in 1x PBS, skinned and eviscerated, and then fixed in 95% ethanol overnight. Embryos were then placed in acetone overnight for additional fixation and permeabilization followed by staining with Alcian blue overnight (product#). After staining, embryos were washed in several ethanol solutions and then cleared in 1% potassium hydroxide (KOH). Next, bones were stained in a 1% KOH/Alizarin red solution. Lastly, stained embryos were acclimated and washed in a 50% glycerol:50% 1% KOH solution for several days, followed by long term storage in 100% glycerol. Images were taken on a Nikon SMZ 1500 stereomicroscope.

4.3.4 MEPM wound-repair assays

MEPM isolation, culture, and wound-repair assays were performed as previously described [Chapter 3]. Briefly, embryos from heterozygous T397P matings were harvested at E13.5. Palatal

shelves were removed from the embryos and dissociated in trypsin before culture in 10% DMEM. For wound-repair assays, MEPM cells were seeded in silicone inserts (Ibidi, 81176) on tissue culture treated plastic dishes at a density of 1.4 x 103 cells/mm2 and cultured for 48 hours. After insert removal to create the wound, imaging was performed using the EVOS FL Auto Imaging System (ThermoFisher, AMAFD1000) with the EVOS Onstage Incubator (ThermoFisher, AMC1000). Cell cultures were kept in a humidified, 5% CO2 environment at 37°C during imaging. Analysis of the live imaging was performed using software developed at the University of Kansas Medical Center by Dr. András Czirók, Ph.D.

4.3.5 Immunofluorescence analysis

For cryosections, samples were permeabilized with 0.5% Triton X-100 in 1x PBS for 30 minutes, washed in PBS, then blocked in 10% NGS (ThermoFisher, #50062Z). Mouse IgG's were blocked with goat anti-mouse antigen-binding fragments (Jackson Immunoresearch, #115-007-003). Primary Rabbit anti-SPECC1L antibody (Proteintech, #25390-1-AP) was incubated overnight at 4°C. Secondary Alexa 488 Goat anti-Rabbit antibody (Invitrogen, A-11008) and Acti-stain 555 phalloidin (Cytoskeleton, #PHDH1-A) incubated for 1 hour at room temperature. Slides were mounted with Prolong Gold with DAPI (Invitrogen, #P36931). Confocal images were captured on a Nikon A1R confocal laser microscope.

4.4 Results

4.4.1 Generation of knock-in T397P Specc1l mouse allele

We utilized CRISPR-Cas9 technology to generate a mouse line containing the p.Thr397Pro (NP_056145) *SPECC1L* mutation that was previously identified in a multigenerational family with

autosomal dominant Opitz G/BBB Syndrome [Kruszka, 2015; Qin, 2016]. Affected members of this family exhibited several malformations including ocular hypertelorism, CL/P, and micrognathia. [Kruszka, 2015]. They also presented with diaphragmatic, inguinal, and umbilical hernias [Kruszka, 2015]. This mutation was chosen for the high proportion of orofacial clefting among the affected members relative to those with other *SPECC1L* variants, as well as for its proximity to CCD2 [Kruszka, 2015; Bhoj, 2018]. To create this mutation, we created a CRISPR targeting oligo that contains two alterations from the original sequence **(Fig. 4.1)**. The first is a synonymous substitution (NM_153406.3:c.1372C>T) that eliminates a Cac8I restriction site **(Fig. 4.1A; green text)**, while the second (NM_153406.3:c.1376A>C) results in the threonine to proline change (NP_700455.3:p.Thr398Pro) **(Fig. 4.1A; red text)**. Note that compared to human SPECC1L, the murine protein contains an additional valine at amino acid position 228 that shifts the amino acid number forward by one. However, for consistency we still refer to the allele as *Specc1l*^{T397P}. We designed forward primers that mapped to the region of either the WT or mutant sequence with one added mismatch, allowing us to genotype each allele without needing to use restriction enzymes or sequencing **(Fig. 4.1B)**.

4.4.2 T397P homozygote embryos show highly penetrant cleft palate

To evaluate the developmental impact of the T397P mutation, we set up heterozygous matings and harvested embryos at mid-gestational **(Fig. 4.2A,B,C,E,F,G)** and perinatal stages **(Fig. 4.2D,H)**. We identified omphaloceles, characterized by improperly externalized gut and liver [Weber, 2002; Torres, 2015], in ~87% of *Specc1l*$^{T397P/T397P}$ embryos (**Fig. 4.2E-H; arrows)**. Homozygotes also displayed occasional edema **(Fig. 4.2I,J; arrowheads)**, exencephaly **(Fig. 4.2I; arrow)**, and vascular defects **(Fig. 4.2J; arrow)**. Examination of the palate showed clefts of the

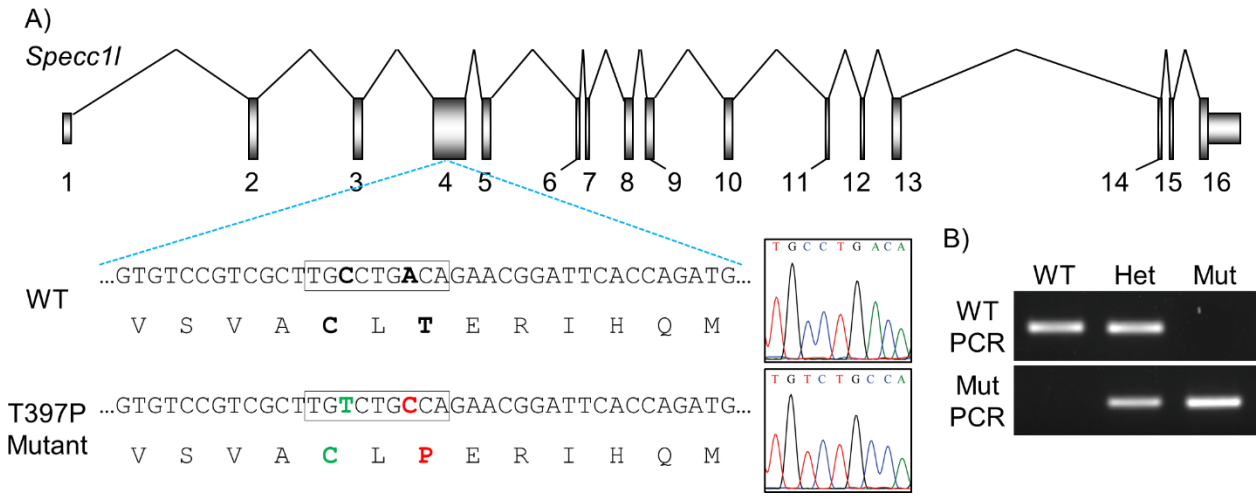

Figure 4.1: Generation of T397P *Specc1l* allele with CRISPR/Cas9. A) Schematic of *Specc1l* depicting the location of the T397P knock-in changes. Gray boxes represent exons. The silent and missense changes are shown in green and red, respectively. The boxes around each DNA sequence are matched with the adjacent sanger chromatogram. **B)** Representative images of wildtype and mutant allele PCRs with wildtype, heterozygote, and mutant samples. WT=wildtype; Het=Heterozygote; Mut=Mutant/Homozygote.

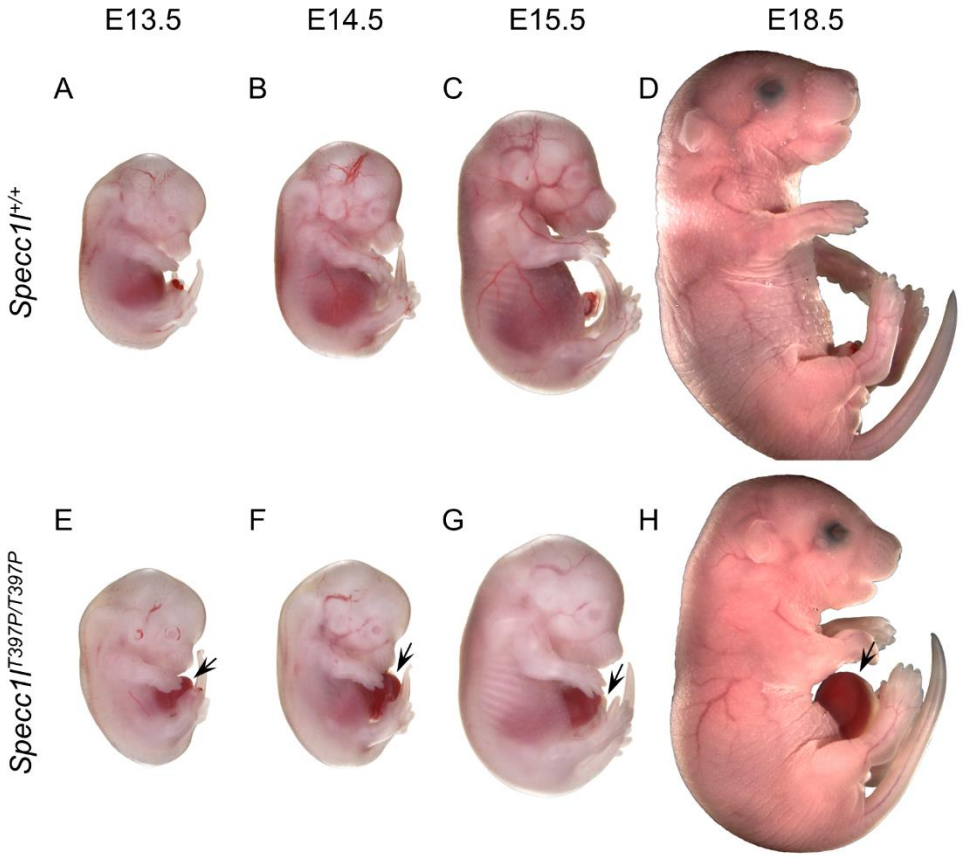

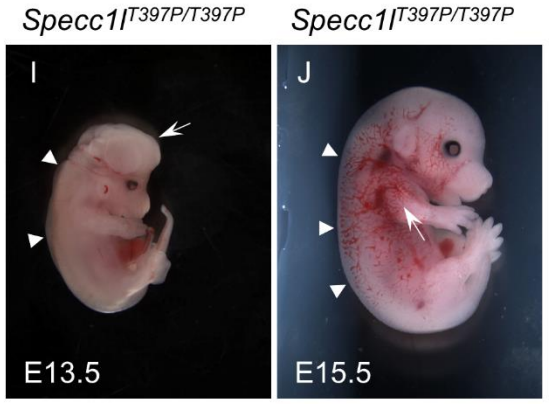

Defect	WT	Het	Mutant
VBW Closure*	0% n=30	22% n=65	87% n=38
Cleft Palate**	0% n=12	27% n=15	100% n=9

* Stages E13.5+
** Stages E14.5+

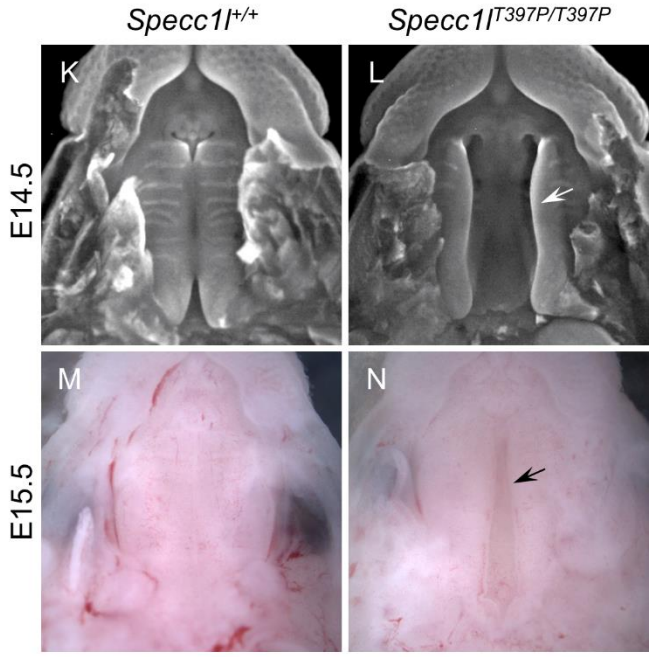

Figure 4.2: T397P mutation causes cleft palate and ventral body wall defects. A-H) Representative images of wildtype (A-D) and T397P homozygote (E-H) embryos at E13.5, E14.5, E15.5, and E18.5. Homozygotes exhibit omphaloceles that contain gut and liver (E-H; arrows). **I-J)** Representative images of the exencephaly (I; arrow), vasculature defects (J; arrow), and edema (I,J; arrowheads) identified in some T397P homozygotes. **K-N)** Oral view of wildtype (K,M) and T397P homozygote (L,N) palates at E14.5 and E15.5. At E14.5, palates of homozygotes are not elevated (L; arrow) compared to controls (K). At E15.5, the shelves are elevated but still do not make contact (N; arrow). E14.5 palates are stained with DAPI, while E15.5 images are brightfield. Bottom-left graph displays compilation of omphalocele and cleft palate phenotypes.

secondary palate in 100% of homozygotes **(Fig. 4.2L,N; arrows)** compared to wildtypes, which showed no palate defects **(Fig. 4.2K,M)**. Omphaloceles and cleft palate were found in 22% and 27% of heterozygotes, respectively **(Fig. 4.2 Table)**. Late-stage mutants would also occasionally show eye-closure defects (data not shown). To determine if the mutation affected bone and cartilage development, we made skeletal preparations of E19.5 embryos. WT **(Fig. 4.3A,C,E)** and heterozygote **(Fig. 4.3B,D,F)** littermates were comparable in size with no obvious changes in staining intensity. However, examination of a heterozygote palate showed defects of the palatine processes of the palatine bone **(Fig. 4.3F; dotted lines)** and palatine processes of the maxilla **(Fig. 4.3F; arrowheads)** compared to wildtype control **(Fig. 4.3E)**, consistent with the cleft palate phenotype. Additionally, one heterozygote (1/4; n=4) had a partial cleft sternum with malformed ribs **(Fig. 4.3D; arrows)**. This defect may have been caused by the severe omphalocele, wherein midline fusion was physically obstructed by the herniated viscera during ribcage development.

4.4.3 T397P homozygote embryos have normal CNCC contribution to craniofacial primordia

Homozygous *Specc1l*$^{genetrap/genetrap}$ embryos exhibit defects in CNCC delamination [Wilson, 2016]. Given that defects in CNCC function can lead to craniofacial malformations, including orofacial clefts [Etchevers, 2006; Achilleos, 2015], we asked if this was the case in *Specc1l*$^{T397P/T397P}$ homozygotes. To achieve this, we performed lineage tracing by crossing the T397P allele with the ROSA$^{mT/mG}$ two-color Cre-reporter [Muzumdar, 2007] and Sox10-Cre allele [Matsuoka, 2005]. ROSA$^{mT/mG}$ ubiquitously expresses membrane-localized tdTomato until Cre recombination, after which it expresses membrane-localized EGFP. Sox10-Cre is expressed in the migratory neural crest, allowing the visualization of this population in embryos [Matsuoka, 2005]. Embryos from these crosses were harvested at E9.5, fixed, and stained with DAPI to assess

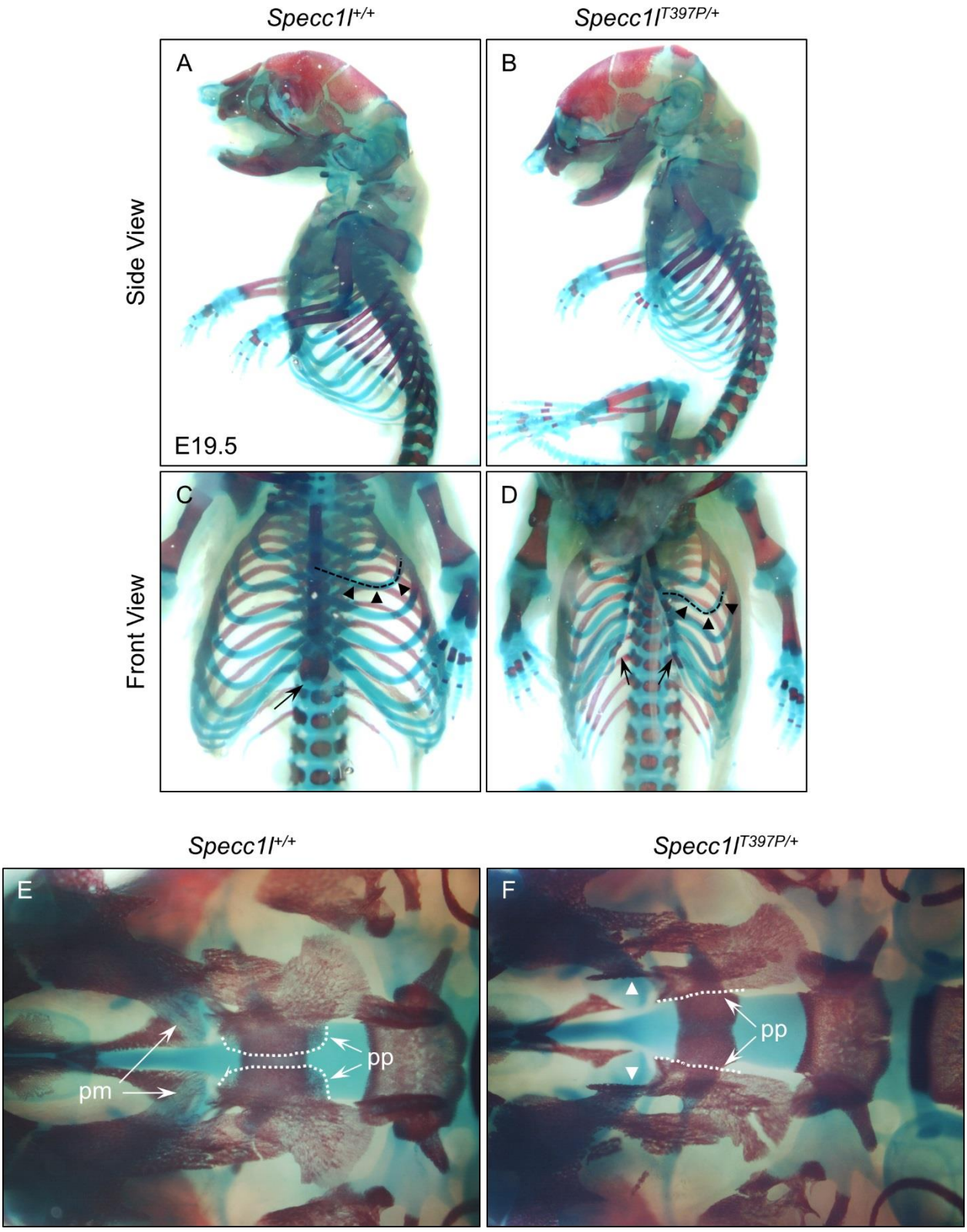
Specc1l+/+
Specc1lT397P/+
Side View
Front View
A
B
C
D
E19.5
Specc1l+/+
Specc1lT397P/+
E
F
pm
pp
pp

Figure 4.3: Identification of sternal cleft in T397P heterozygote. Skeletal preparations of E19.5 embryos stained with Alcian blue for cartilage and Alizarin red for bone. **A-B)** Side view shows that ribcage of T397P heterozygous embryo (B) is slightly smaller compared to the wildtype (A). **C-D)** Front view shows that the inferior sternum is not fused in the heterozygote (D; arrows) with malformed ribs (C vs. D; arrowheads and dotted line) compared to wildtype (C; arrow). **E-F)** Oral view reveals palatine processes of the palatine bone (pp; dotted lines) and palatine processes of the maxilla (pm; arrowheads) are much smaller in the heterozygote with cleft palate (F) compared to wildtype (E).

morphology [Sandell, 2012] **(Fig. 4.4)**. There were no gross differences in size between WT **(Fig. 4.4A-C)** and *Specc1l*$^{T397P/T397P}$ homozygous **(Fig. 4.4D-F)** embryos, but a lack of lateral turning was observed in both heterozygotes (not shown) and homozygotes **(Fig. 4.4A,B vs. D,E; arrowheads)**. GFP expression in homozygotes **(Fig. 4.4D,F; arrows)** was similarly distributed in the frontonasal process and first pharyngeal arch compared to WT **(Fig. 4.4A,C; arrows)**, suggesting that CNCC migration to the craniofacial regions is not impaired in T397P mutants.

4.4.4 T397P mutant MEPM cells show defects in migration

Previously, we showed that SPECC1L deficiency can lead to migration defects in cultured primary mouse embryonic palate mesenchyme (MEPM) cells [Saadi, 2011; Chapter 3]. Since CNCC migration was largely unchanged, we asked if the T397P mutation would affect the migration of CNCC-derived palatal mesenchyme. To test this, we harvested MEPM cells from E13.5 embryos and performed wound-repair assays as previously described [Chapter 3]. Both *Specc1l*$^{T397P/+}$ and *Specc1l*$^{T397P/T397P}$ MEPM cells closed the wound more slowly compared to WT **(Fig. 4.5A,B)**, consistent with the migration defects seen in *Specc1l*$^{cGT/\Delta C510}$ compound heterozygote MEPMs [Chapter 3]. Together with the linage tracing, these data suggest that while CNCCs populate the craniofacial structures normally, defects in palatal mesenchyme remodeling may be contributing to the palate defects in T397P mutants.

4.4.5 Palates of T397P homozygotes show aberrant SPECC1L and F-actin staining

Lastly, we wanted to examine if the palate *Specc1l*$^{T397P/T397P}$ embryos showed similar molecular changes to those seen in *Specc1l*$^{cGT/\Delta C510}$ compound heterozygotes [Chapter 2]. We examined SPECC1L expression and co-stained with phalloidin to assess F-actin staining **(Fig.**

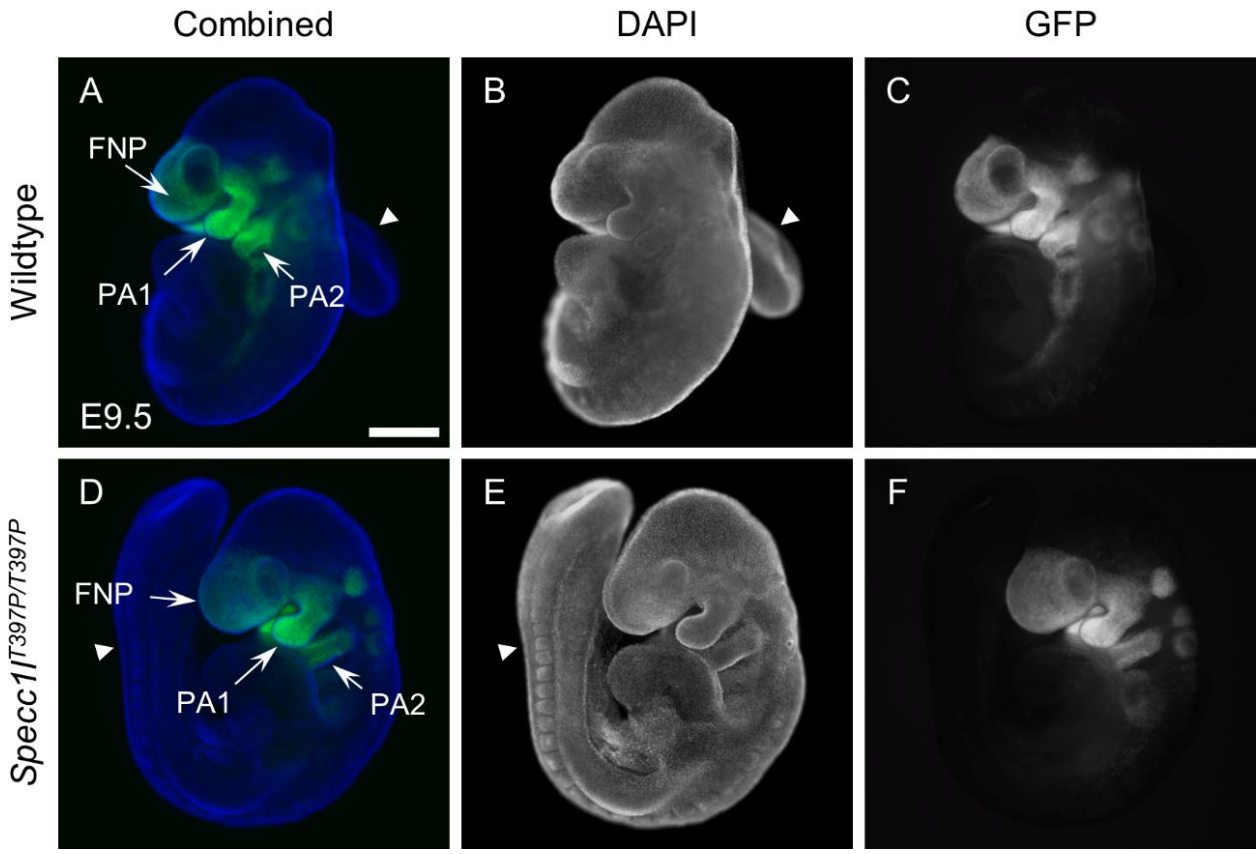

Figure 4.4: Neural crest cell lineage tracing with *Sox10*-Cre shows no changes in T397P homozygotes. Whole mount epifluorescent images of DAPI-stained E9.5 embryos with GFP-labeled migratory neural crest cells. **A-C)** Wildtype embryos are turned (arrowheads) with GFP expression in FNP, PA1, and PA2 (arrows). **D-F)** GFP distribution is similar in T397P homozygote (arrows) but turning is less robust (arrowheads). FNP=frontonasal prominence; PA=Pharyngeal arch. Scale bar is 500µm.

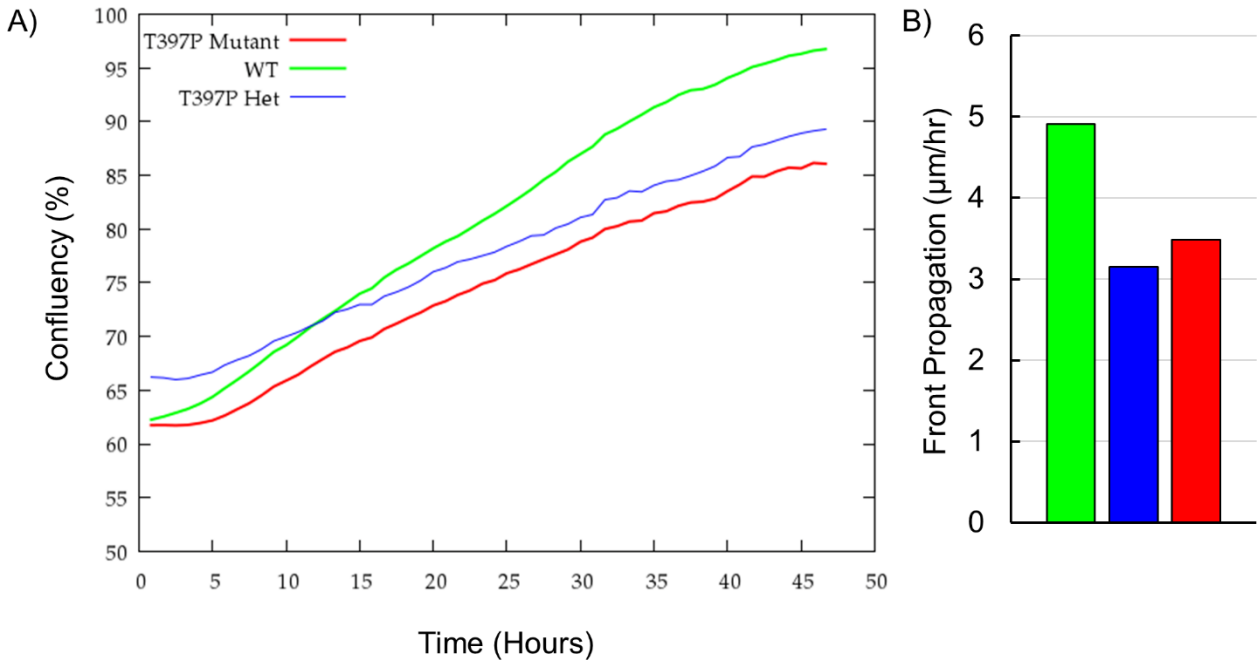

Figure 4.5: Primary mouse palatal mesenchyme cells from T397P mutants have impaired migration. A-B) Graphs depicting average percentage closure (A) and average front propagation (B) of MEPM cell wound-repair assays. MEPM cells from homozygous (red) and heterozygous (blue) embryos exhibit a reduced rate of wound closure compared to wildtype cultures (green).

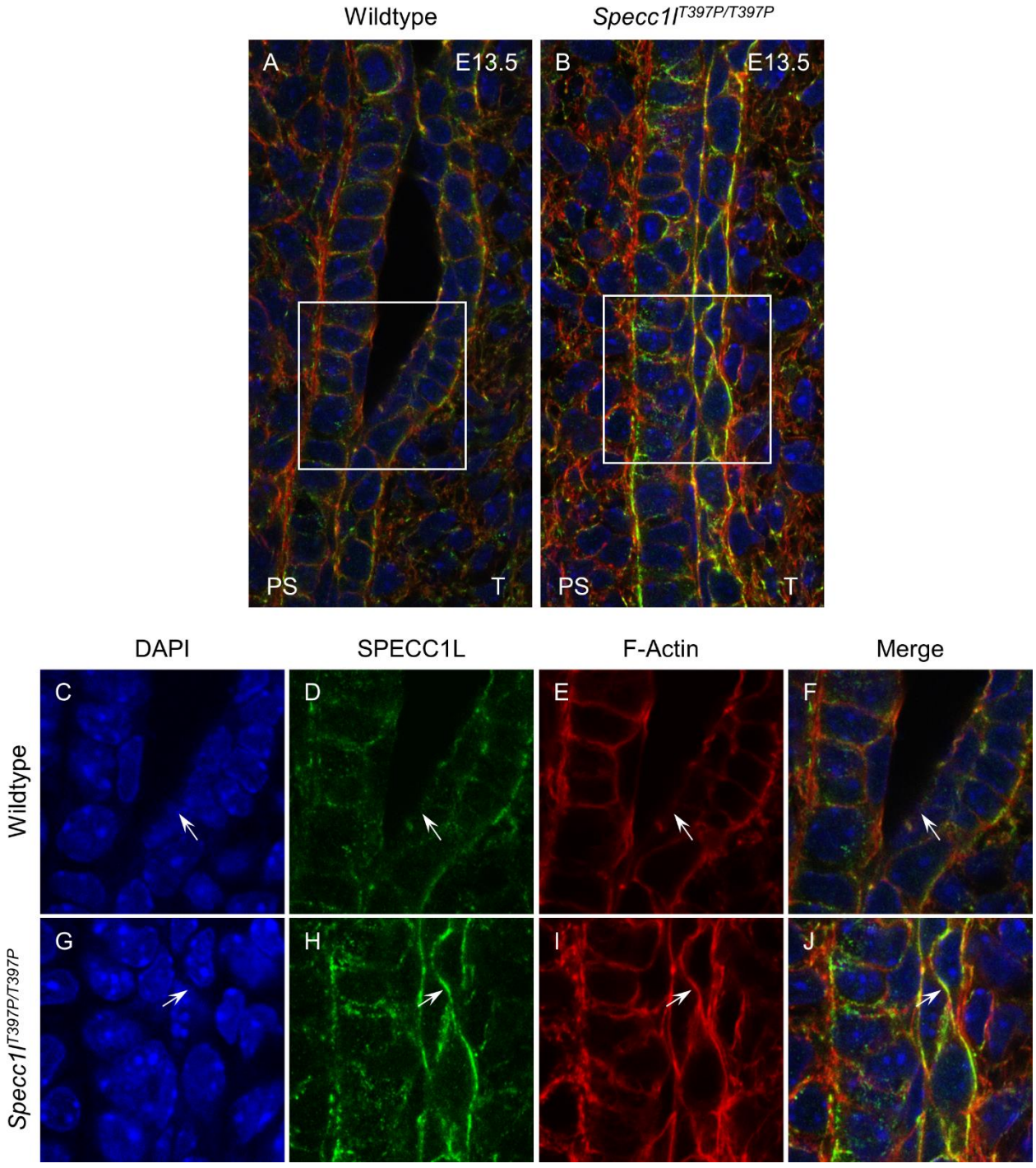
Wildtype
Specc1l T397P/T397P
A
E13.5
PS
T
B
E13.5
PS
T
DAPI
SPECC1L
F-Actin
Merge
Wildtype
Specc1l T397P/T397P
C
D
E
F
G
H
I
J

Figure 4.6: Oral epithelium of T397P homozygotes show altered SPECC1L localization. **A-B)** Confocal images E13.5 wildtype (A) and *Specc1l*$^{T397P/T397P}$ (B) coronal sections stained for SPECC1L (green) and F-actin (red). **C-J)** Zoomed in regions of A and B. Wildtype SPECC1L expression is punctate in the wildtype with little apical expression (D; arrow). In contrast, staining in T397P homozygotes show increased localization of SPECC1L to the cell membrane (H; arrow). This change in localization coincides with increased F-actin staining (E vs. I; arrows). PS=palatal shelf; T=tongue.

4.6). SPECC1L staining in the wildtype embryo exhibited a punctate pattern that was distributed throughout the cells with some concentrations along F-actin and cell-cell contacts **(Fig. 4.6A)** [Saadi, 2011; Wilson, 2016]. In contrast, *Specc1l*$^{T397P/T397P}$ palates showed an increased staining intensity of both SPECC1L and F-actin, particularly at the cell border. **(Fig. 4.6B)**. This increased staining intensity was also present at the apical surface of flattened periderm cells **(Fig. 4.6G-J vs C-F; arrows)**. These results partially reproduce the changes in *Specc1l*$^{cGT/\Delta C510}$. Additionally, these data suggest that the T397P mutation may alter SPECC1L localization, as well as its affinity for F-actin.

4.5 Discussion

This study presents the first example of a human *SPECC1L* mutation in a mouse model. The cleft palate and omphaloceles identified in these embryos **(Fig. 4.2)** recapitulate congenital anomalies seen in patients with *SPECC1L* mutations, further solidifying a causal role for SPECC1L disruption in these disorders [Kruszka, 2015; Bhoj, 2015; Bhoj, 2018].

The edema and palate elevation delay in *Specc1l*$^{cGT/\Delta C510}$ compound heterozygotes shows that loss of SPECC1L function can lead to developmental defects [Chapter 2]. While we did identify edema in some *Specc1l*$^{T397P/T397P}$ mutants, the other malformations seen in these embryos indicate that the impact of this mutation on SPECC1L function is different from the loss of function models [Wilson, 2016; Chapter 2]. Haploinsufficiency of *Specc1l* is tolerated in mice as indicated by the very rare incidence of malformations in *Specc1l* gene trap heterozygotes [Wilson, 2016]. In contrast, embryos with only one T397P allele often exhibited malformations, consistent with a gain-of-function mutation. This also reproduces the autosomal dominant inheritance pattern of the family in which the mutation was identified [Kruszka, 2015].

We showed that the palatal shelves of *Specc1l*$^{T397P/T397P}$ embryos are unelevated at E14.5 compared to wildtype littermates **(Fig. 4.2K,L)**. This is similar to the elevation delay present in the majority of *Specc1l*$^{cGT/\Delta C510}$ embryos [Chapter 2]. However, unlike the compound heterozygote model, the palates of *Specc1l*$^{T397P/T397P}$ embryos do not make contact after elevation at E15.5 **(Fig. 4.2M,N)**, resulting in cleft palate in all the embryos we evaluated. Palatogenesis requires the outgrowth, elevation, and fusion of the secondary palatal shelves, and disruption to any of these steps can lead to cleft palate [Bush, 2012]. For instance, analyses of cleft palate in other mouse models show that reduced proliferation can lead to smaller palatal shelves that fail to make contact [Liu, 2008]. Reduced CNCC contribution to the craniofacial structures can lead to similar outcomes, but lineage tracing with Sox10-Cre in our mutants suggests that this is not the case **(Fig. 4.4)** [Dixon, 2006]. Additionally, the middle and posterior palate has been shown to undergo extensive remodeling, and deficiencies in this process, especially during elevation, may lead to palate defects [Yu, 2011]. Indeed, *Zfhx1a* null mice exhibit delays in palate elevation and cleft palate without obvious changes to palatal shelf growth [Jin, 2008]. The migration defect in MEPM cells from *Specc1l*$^{T397P/T397P}$ embryos suggests that deficient remodeling may also be a contributing factor in our model **(Fig. 4.5)**. Furthermore, increased SPECC1L staining at the membrane in *Specc1l*$^{T397P/T397P}$ embryos **(Fig. 4.6)** is reminiscent of the pattern seen in high density cultures [Wilson, 2016]. This pattern has been shown to overlap with adherens junction markers [Wilson, 2016]. Considering that improper adhesions and abnormal cell junction staining were shown in *Specc1l*$^{cGT/\Delta C510}$ mutants, it follows that they may also occur in *Specc1l*$^{T397P/T397P}$ mutants [Chapter 2]. Lastly, it is possible that the cleft palate in these embryos is not solely intrinsic to the palatal shelves. Roughly a third of patients with SPECC1L mutations were noted to have micrognathia, a condition characterized by an undersized jaw [Bhoj, 2018]. It has been demonstrated in mouse

models with this malformation that obstruction by the tongue is sufficient to cause palate defects [Song, 2013; Reviewed in Okano, 2014]. However, we have no consistent evidence for this phenotype in our mutants. The mechanisms suggested here are not mutually exclusive. Further studies into the morphological and molecular changes in T397P mutant embryos must be performed to determine which are contributing to these palate defects.

Ventral body wall defects, including omphaloceles, comprise a group of rare congenital anomalies characterized by the herniation of viscera through an opening in the anterior body wall [Weber, 2002; Torres, 2015]. In humans, omphaloceles occur as isolated cases or as part of a syndrome with a prevalence of approximately 1 per 5000 pregnancies [Stoll, 2001; Benjamin, 2014]. The omphaloceles in our T397P mouse model faithfully reproduce those reported in 32% (10 out of 31) of patients with *SPECC1L* mutations [Bhoj, 2018]. Many mouse models with defects of the ventral body wall have been analyzed [Reviewed in Brewer, 2004; Williams, 2008; Takahashi; 2018]. However, mutants for proteins involved in cell migration and adhesion, particularly through regulation of cytoskeletal dynamics, display phenotypes that match closely with our model. Loss of Rho-associated kinase I/II (ROCK-I/II) results in impaired eyelid closure and omphaloceles stemming from defects in actomyosin cable formation [Shimizu, 2005; Thumkeo, 2005]. A similar example can be seen in mice with a point mutation in non-muscle Myosin II-B (NMII-B), which exhibit cleft palate, omphalocele, edema, and inferior sternal cleft [Ma, 2014]. Umbilical ring closure requires the contractility of actomyosin structures, and it has been proposed that the ventral body wall defects in ROCK-I/II KO mice are due to deficiencies in this process [Shimizu, 2005; Thumkeo, 2005]. SPECC1L deficiency has been shown to result in defects in actin reorganization [Saadi, 2011; Wilson, 2016; Chapter 2]. This is consistent with our immunostaining of palatal epithelium showing that the T397P mutation changes SPECC1L

localization and F-actin association **(Fig. 4.6)**. Thus, it is reasonable to hypothesize that several malformations in T397P mutant mice are due to impairment of the actomyosin structures, especially with respect to umbilical ring closure.

Taken together, we can conclude that the T397P mutation is indeed gain-of-function in nature. The high penetrance of cleft palate in *Specc1l*$^{T397P/T397P}$ embryos solidly established a role for SPECC1L in palatogenesis. Future analyses into the functional consequences of CCD2 disruption will shed light onto the pathogenetic mechanisms of the craniofacial disorders in patients with *SPECC1L* mutations.

CHAPTER FIVE:

DISCUSSION, FUTURE DIRECTIONS, AND SIGNIFICANCE

5.1 Discussion

5.1.1 A validated role for SPECC1L in palatogenesis

Genetic analysis of patients with orofacial clefts provides an ever-growing list of associated genes. However, association alone is not enough – a causal link in a model system is critical for understanding the underlying mechanisms of these defects. After the two initial patients with oblique facial clefts, *SPECC1L* variants were identified in 31 other individuals diagnosed with either Opitz G/BBB or Teebi hypertelorism syndrome [Saadi, 2011; Kruszka, 2015; Bhoj, 2015; Bhoj, 2018]. While many models of SPECC1L-deficiency have been studied, the palate defects in these patients have yet to be recapitulated in a mammalian system [Saadi, 2011; Gfrerer, 2014; Wilson, 2016]. Utilizing three novel *Specc1l* mutant mouse alleles, we were able to generate embryos with impaired palate development. Our analyses suggest defects in palatal epithelium and mesenchyme are at play in these mutants [Chapter 2; Chapter 3]. We also extend the SPECC1L-deficient phenotype to ventral body wall defects seen in patients with *SPECC1L* patients [Chapter 4]. These studies are the first to establish a direct role for SPECC1L in the development of the mammalian palate.

5.1.2 Palate elevation delay as a model of cleft palate predisposition

Histological analysis of E14.5 embryos showed that ~66% of *Specc1l*$^{cGT/\Delta 510}$ mutant palates had not elevated compared to littermate controls [Chapter 2]. Numerous mouse mutants with palate elevation defects have been described [Reviewed in Gritli-Linde, 2007; Gritli-Linde, 2008; Bush, 2012; Funato, 2015; Li, 2017]. In some mutants, the shelves completely fail to reorient and remain in a horizontal position, as in seen in *Golgb1* deficient mice [Lan, 2016]. However, cleft palate due to incomplete or delayed elevation is more commonly observed [Chapter 1.2.3; Reviewed in

Gritli-Linde, 2008]. In contrast with these other mouse mutants, we found that most *Specc1l*$^{cGT/\Delta 510}$ embryos do not exhibit cleft palate. This phenomenon – a delay in elevation with rare or absent cleft palate phenotypes – has only a few examples in the literature. For instance, *Arhgap29* heterozygotes showed no evidence of cleft palate, but elevation delay was found in 28% of embryos [Paul, 2017]. Another example can be seen in embryos heterozygous for a gain-of-function *Fgfr2* allele, which show delayed elevation and cleft palate with 49% and 4% penetrance, respectively [Snyder-Warwick, 2010]. It is likely that delays in other mouse mutants remain unreported due to the transient nature of the phenotype, especially if they do not result in cleft palate.

Delays in palate elevation have also been identified in the A/J inbred mouse strain, which naturally shows a low incidence of CL/P [Walker, 1956; Reviewed in Juriloff, 2008]. A comparison analysis found that A/J embryos closed palates approximately 10-12 hours after C57BL/Fr embryos of the same developmental stage [Walker, 1956]. Previous studies also found that A/J mice are more likely than other strains to develop CL/P upon exposure to teratogens [Vekemans, 1979; Sonawane, 1981; Gasser, 1992; Yamada, 2006; Juriloff, 2008].

Together, these models demonstrate that even if an elevation delay is not sufficient to cause cleft palate, it can render palatogenesis more susceptible to other insults. Consistent with this, numerous genetic and environmental factors have been shown to confer an increased risk of CL/P [Leslie, 2013]. Thus, we posit that a palate elevation delay might serve as a predisposing factor to orofacial clefting, only resulting in cleft palate upon further perturbation. This is especially applicable to the incomplete penetrance of nonsyndromic CL/P [Jugessur, 2009; Pengelly, 2016].

5.1.3 Abnormalities in both the palatal epithelium and mesenchyme of Specc1l mutants contribute to elevation delay

In Chapter 2, analysis of *Specc1l*$^{cGT/\Delta 510}$ mutants revealed an abnormal oral epithelium with transient adhesions and ectopic localization of adherens junction proteins. We also showed that SPECC1L lies downstream of IRF6. Similar epithelial and elevation defects are seen in mouse mutants for *Irf6* and *Arhgap29* [Ingraham, 2006; Richardson, 2006; Paul, 2017]. If the palatal shelves are impeded with sufficient force during elevation, it is likely to delay this process. Next, Chapter 3 showed reduced speed and correlation length in wound repair assays and in an open field of *Specc1l* mutant MEPM cells. Previous studies have shown that the middle and posterior sections of the palate undergo remodeling during elevation [Yu, 2011]. Furthermore, *ex vivo* experiments have shown that palatal mesenchyme can migrate in the context of the shelves [He, 2008]. If the movement of the palatal mesenchyme is disrupted, it may also result in decreased elevation efficiency. Together, our analysis of *Specc1l*$^{cGT/\Delta C510}$ mutant embryos offers two probable roles for SPECC1L in palatogenesis: prevention of epithelial cell adhesion and regulation of mesenchymal remodeling.

5.1.4 Specc1l mouse mutants exhibit a broad spectrum of phenotypes

5.1.4.1 Evaluating the phenotypes of the Specc1l allelic series

Three kinds of novel *Specc1l* mutant alleles have been presented in this work: gene trap (cGT), truncation (ΔC510), and CCD2 point mutation (T397P). During the process of generating the T397P allele, we also created a series of in-frame deletion alleles (data not shown). One results in the deletion of just the 397th threonine (ΔT397), while the other deletes the entire CCD2 (ΔCCD2). Phenotypic analysis thus far indicates these mutants show similar phenotypes to T397P

mutants. A third allele deletes exon 4 and introduces a stop codon that truncates the majority of SPECC1L (ΔC1016) including CCD2, and initial matings suggest it results in similar phenotypes to the ΔC510 truncation mutant, i.e. no permanent cleft palate. Despite some overlap, each "category" of allele resulted in some unique phenotypes not seen in the others. Comparing these phenotypes across mutants should provide clues as to the specific processes disrupted by each allele.

5.1.4.2 Explaining the embryonic lethality in Specc1l gene trap homozygotes

The DTM, cGT, and RRH gene trap constructs reside within *Specc1l* introns 1, 2, and 15, respectively [Wilson, 2016]. In Chapter 2, we showed that *Specc1l*$^{cGT/cGT}$ homozygotes undergo embryonic lethality with open neural folds, consistent with other gene trap mutants [Wilson, 2016]. In contrast, homozygotes (and compound heterozygotes in the case of *Specc1l*$^{cGT/\Delta C510}$ embryos) with truncation or CCD2 disruption alleles die perinatally [Chapter 2; Chapter 4]. This difference is even more surprising given that the ΔC1016 deletion removes all but the first ~100 amino acids of SPECC1L, while the RRH allele only removes the CHD with a β-galactosidase tag. There are several possible reasons for the discrepancy in lethality phenotypes between truncation and gene trap.

The truncated alleles of SPECC1L (ΔC510; ΔC1016) may have some residual function that is lost upon fusion with β-galactosidase by the gene traps. We have shown in Western blots that ΔC510 is indeed expressed [Chapter 2]. Another important factor is the strain background of the alleles. The genetrap alleles were generated on a mixed 129 and C57BL/6J background and backcrossed onto the C57BL/6J. The ΔC510 and ΔC1016 were created on a mixed FVB and C57BL/6J background. As we backcross these alleles onto the C57BL/6J background, the

homozygous phenotype has become more severe. It is also feasible that an additional cryptic splice site bypasses the stop codons we identified in these alleles. Our RT-PCR and western blot data on the ΔC510 allele show no evidence for this, but the ΔC1016 allele requires additional investigation. Alternatively, molecular consequences of the gene trap construct insertion and function may be important to explain why the gene traps have a more detrimental effect on embryonic development. The perinatal phenotypes in truncation mutants could represent the true *Specc1l* null phenotype, while the gene traps confer a dominant-negative effect during embryonic development. There may also be a chance that the insertion of these gene traps not only disrupts *Specc1l,* but also neighboring genes. *Adora2a* (NM_009630) encodes a G protein-coupled receptor and is located just downstream of *Specc1l* in the mouse genome. Screens of human transcripts have identified a SPECC1L-ADORA2A fusion transcript (NR_103546). Though this transcript has been categorized for nonsense mediated decay, a gene trap in *Specc1l* could also disrupt an equivalent transcript in the mouse. However, *Adora2a* knockout mouse models do not exhibit embryonic lethality, reducing the likelihood of this supposition [Ledent, 1997; Chen, 1999]. Lastly, *Specc1l* introns may contain regulatory elements for other genes that are disrupted upon gene trap insertion.

5.1.4.3 Mutation of CCD2 may disrupt actomyosin networks

Perhaps the most intriguing comparison is between the truncation and CCD2 disruption alleles. In Chapter 2, we identified a palate elevation delay phenotype in *Specc1l*$^{cGT/\Delta C510}$ mutant embryos. In contrast, *Specc1l*$^{T397P/T397P}$ mutant mice show cleft palate with ~100% penetrance [Chapter 4]. Disruption of CCD2 also results in other defects not seen in truncation mutants, including omphaloceles, eye closure defects, and exencephaly. Together, these phenotypes represent deficiencies in tissue fusion or closure.

It is established that changes in cellular organization during development are largely driven by actomyosin networks [Munjal, 2014; Heer, 2017]. Through adhesions with neighboring cells, these networks utilize myosin motors and crosslinking proteins to generate contractile forces across multiple cells [Munjal, 2014; Heer, 2017]. These cumulative forces direct tissue stiffness and contractility, thus giving rise to the phenomenon of tissue morphogenesis [Heer, 2017]. Given its association with cell junctions and cytoskeletal components, SPECC1L would likely be in close vicinity with this molecular machinery [Saadi, 2011; Mattison, 2011; Wilson, 2016]. Indeed, the fusion defects we observed in T397P mutants have all been linked to cytoskeleton-related genes [Ma, 2014; Reviewed in Brewer, 2004; Harris, 2007; Copp, 2010; Funato, 2015]. As discussed in Chapter 4, ROCK-I and ROCK-II knockout mice show impaired umbilical ring closure and eye closure defects with defects in actin cable formation [Shimizu, 2005; Thumkeo, 2005]. The "zippering" process by which the neural folds come together during neurulation has also been shown to rely on actomyosin networks [Galea, 2017]. Finally, analyses of F-actin patterning during palate elevation are beginning to implicate these networks in palate elevation, and there is no shortage of cleft palate models with mutations in actin regulators [Chiquet, 2016, Reviewed in Funato, 2015]. While the exact mechanisms are unclear, changes in tissue contractility or stiffness are probable explanations for the defects in CCD2 mutants.

5.1.4.4 IRF6 may regulate SPECC1L in both the neural tube and palatal shelves

There are several examples of mouse mutants that present with both cleft palate and neural tube defects, suggesting similar etiologies [Reviewed in Harris, 2007]. A recent review of the implicated genes and subsequent bioinformatic analysis found several common gene networks between the two processes [Kousa, 2017]. This overlap was then demonstrated in a follow-up

study that crossed together *Tfap2a* (Transcription Factor Activation Protein 2A), *Irf6*, and *Grhl3* mutant mouse alleles – all transcription factors implicated in human orofacial clefting syndromes – to evaluate genetic interactions [Kousa, 2019]. The resultant embryos showed neural tube defects of variable severity depending on the allelic combination, ranging from a mild curly tail phenotype to complete neural tube closure failure [Kousa, 2019]. In addition, the study also showed that IRF6 is expressed in the neural folds and early migrating neural crest cells [Kousa, 2019]. This is consistent with SPECC1L expression in early embryogenesis [Wilson, 2016], as well as our finding that SPECC1L requires IRF6 in the palate [Chapter 2]. Together, these results further support a connection between SPECC1L and IRF6 during both neurulation and palate development. However, determining if CCD2 mutants develop neural tube defects through the same mechanisms as gene trap homozygotes will require further investigation.

5.1.4.5 Sternal cleft in T397P heterozygote is consistent with midline syndromes

In Chapter 4, we showed an inferior sternal cleft in a T397P heterozygote. In humans, this extremely rare defect can occur alone or with other anomalies with an incidence of approximately 1 per 100,000 births [Alshomer, 2017]. Though no sternal clefts have been identified in patients with *SPECC1L* mutations, this is not unexpected due to the rarity of the malformation [Saadi, 2011; Kruszka, 2015; Bhoj, 2015; Bhoj, 2018]. Examination of the sternum was not routine prior to the identification of this defect in our mice, so the penetrance of the phenotype in T397P mutants is currently unknown.

Omphaloceles and inferior sternal clefts can be found together in patients with Cantrell syndrome [Marginean, 2018]. Also called pentalogy of Cantrell, this very rare disorder (1 per 65,000-200,000 births) presents with five primary features: defects of the inferior sternum, anterior

diaphragm, apical pericardium, anterior abdominal wall, and intracardial regions [Marginean, 2018]. While these malformations are more severe than Opitz G/BBB and Teebi hypertelorism syndrome, all three disorders are characterized by anomalies of midline structures, implying a similar etiology [Kruszka, 2015; Bhoj, 2015; Bhoj, 2018; Marginean; 2018]. Furthermore, mouse mutants with a mutation in the motor domain of non-muscle Myosin-IIB (NMII-B) phenocopy the defects of Cantrell syndrome, including omphalocele and sternal cleft [Ma, 2014]. These mice also exhibited cleft palate, consistent with a role for actomyosin activity in palatogenesis [Ma, 2014].

Interestingly, the study also examined the phenotypes of null NM-IIB embryos and found that they did not exhibit the palate, sternum, omphalocele, or diaphragm defects that were seen in the motor domain mutants [Ma, 2014]. Drawing from their previous *in vitro* studies [Kim, 2005], they hypothesized that the mutant NM-IIB protein had prolonged binding to actin filaments, thereby hindering any compensatory functionality of NM-IIA [Ma, 2014]. This is curiously analogous to the appearance of fusion defects and increased actin-associated staining in *Specc1l*$^{T397P/T397P}$ mutants when compared to *Specc1l*$^{cGT/\Delta C510}$ mutant phenotypes.

5.1.4.6 Effects of genetic background on Specc1l mutant phenotypes

As standard practice in our lab, newly generated *Specc1l* mutant mice are crossed onto a C57BL/6 background. This has two main benefits. First, mice of a consistent background should have more consistent phenotypes [Doetschman, 2009]. Second, outcrossing from the original founders is important for minimizing off-target effects, especially with mutants generated with CRISPR/Cas9 [Aryal, 2018]. Upon backcrossing the T397P allele, however, we began to see a much lower survival rate of heterozygote pups (data not shown). Previous studies have shown that genetic strain can have a considerable effect on mutant phenotypes, including lethality [Reviewed

in Doetschman, 2009]. One instance of this was found in ROCK-II mutant mice, wherein backcrossing to a C57BL/6N background from a 129/SvJ and C57BL/6N mixed background resulted in omphaloceles, eye closure defects, and increased perinatal lethality [Thumkeo, 2005]. Background strain has also been shown to impact the penetrance of craniofacial defects [Proetzel, 1995; Dixon, 2004]. The possibility that the phenotypes in our *Specc1l* mutant mice may also be influenced by genetic background raises several questions. Could backcrossing our truncation alleles onto a different strain result in palate phenotypes, rather than just a delay in elevation? Additionally, genetic background may explain why homozygotes for the ΔC1016 truncation allele do not show embryonic lethality. Future studies using these mice will need to consider these factors.

5.1.5 Molecular consequences of SPECC1L truncation and CCD2 disruption

5.1.5.1 Technical classification of SPECC1L coiled-coil domains

The structural architecture of coiled-coil domains is highly standardized, allowing moderately accurate predictions from amino acid sequence [Lupas, 1991; Gruber, 2006; Truebestein, 2016]. We derive our current figure of the SPECC1L CCD prediction **(Fig. 5.1A)** from the COILS program (https://embnet.vital-it.ch/software/COILS_form.html) using the following settings: unweighted MTIDK matrix with a scanning window size of 21 and prediction threshold of 50% [Lupas, 1991]. COILS analysis of human and mouse SPECC1L with these settings show identical number, length, and locations of the domains, excluding the additional valine in mouse SPECC1L **(Fig. 5.1B)**. However, the number and sizes of the CCDs may change depending on the algorithm used, as can be seen in other publications on SPECC1L [Saadi, 2011;

A)

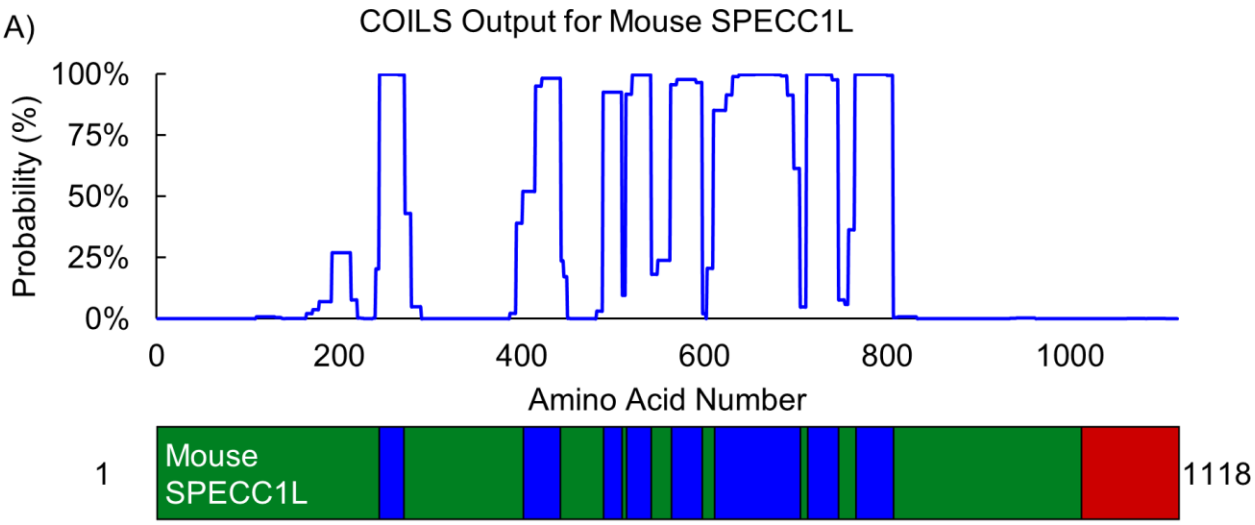

B)

COILS	Human SPECC1L (NP_056145)			Mouse SPECC1L (NP_700455)		
CCD #	Start	End	Length	Start	End	Length
1	243	270	28	244	271	28
2	400	441	42	401	442	42
3	488	508	21	489	509	21
4	513	540	28	514	541	28
5	562	596	35	563	597	35
6	609	703	95	610	704	95
7	711	745	35	712	746	35
8	764	805	42	765	806	42

C)

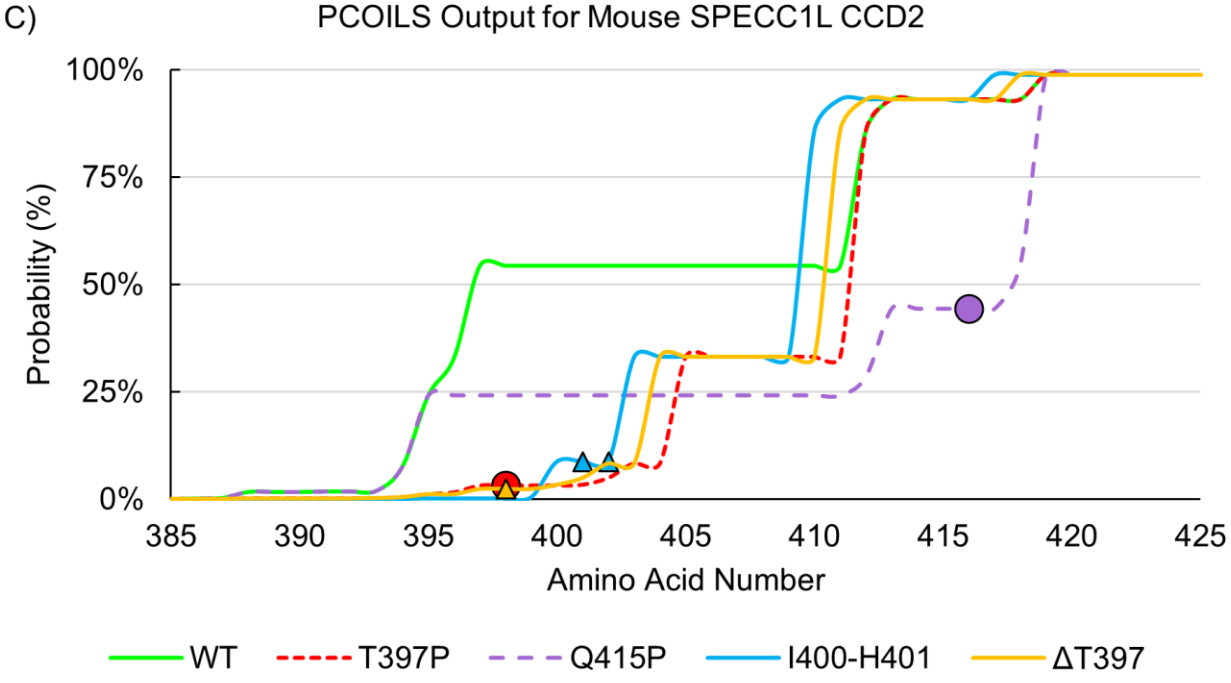

Figure 5.1: Prediction of SPECC1L CCD with *in silico* COILS analyses. A) Line plot showing probability of CCD formation in mouse SPECC1L generated with COILS. Below, SPECC1L diagram lined up with the plot to illustrate the domains. **B)** Chart depicting the amino acid residues of each CCD in human and mouse SPECC1L. C) Line plot showing the probability of CCD formation at the beginning of CCD2 in mouse SPECC1L (aa 385-425) with wildtype (green), T397P (red), Q415P (purple), I400-H401 (blue), or ΔT397 (yellow) mutations. Circles and triangles on lines represent location of mutations and deletions, respectively.

Mattison, 2011; Gfrerer, 2014; Bhoj, 2015; Kruszka, 2015]. For the purposes of this discussion, we will use our classification of eight CCDs when mentioning previous work.

5.1.5.2 Point mutations may disrupt CCD2 structure

To predict the impact of various mutations on CCD2 structure, we input mouse SPECC1L sequences (NP_700455) into PCOILS, an updated version of COILS, using the default MTIDK weighted settings [Gruber, 2006]. Included in the analysis were the T397P, Q415P, and I400-H401del variants from the patients with *SPECC1L* mutations [Saadi, 2011; Kruszka, 2015; Bhoj, 2015], as well as the ΔT397 deletion. Results from the wildtype CCD2 predict the beginning of CCD2 at amino acid 397 **(Fig. 5.1C; green line)**, compared to 401 in the original COILS **(Fig. 5.1B)**. Addition of the T397P mutation drastically changes this prediction, not passing 50% probability until amino acid 412 **(Fig. 5.1C; red line)**. Similar results are seen upon addition of the Q415P, I400-H401, and ΔT397 mutations with 50% probability at amino acids 418, 410, and 411, respectively **(Fig. 5.1C; purple, blue, and yellow lines)**. Stereotypical coiled-coil structure consists of heptad repeats formed into supercoiled α-helices, with hydrophobic residues typically at the points of contact between the coils [Truebestein, 2016]. Given that the T397P and Q415P mutations both convert a polar, non-charged amino acid into a hydrophilic proline, it is possible that this may compromise the integrity of the domain. Similarly, the two deletions may disrupt the structure by forcing a "shift" in the heptad sequence that does not recover until the next intact heptad. In addition, the Q415P mutation is predicted to disrupt a larger portion of the domain compared to the other mutations, consistent with the more severe atypical clefts identified in the patient with the Q415P mutation [Saadi, 2011]. This is possibly because it lies further into the domain, and the ~2 heptad repeats between the Q415P mutation and the others may not be able to

form a stable coil. Though these are just *in silico* results, they provide a basis for understanding the structural and functional impacts of mutations in CCD2.

5.1.5.3 Disruption of SPECC1L association with microtubules, but not with the actin cytoskeleton, results in cleft palate phenotypes

The differences in phenotypes between truncation and CCD2 disruption mutants most likely stem from how the alleles disrupt the function of SPECC1L domains. The ΔC510 truncation results in the loss of CCDs 6-8 and the C-terminal CHD. Previous studies have demonstrated that mutations in the CCD2 or the CHD can ablate the microtubule acetylation phenotype of full-length SPECC1L [Saadi, 2011; Kruszka, 2015]. Furthermore, a study of SPECC1L fragment expression showed that C-terminal third (aa 851-1117) of SPECC1L has an affinity for F-actin, consistent with the actin-binding role for CHDs [Korenbuam, 2002; Gimona, 2002; Mattison, 2011]. However, this study also found that the middle third (aa 351-851), containing CCDs 2-8, showed mild actin association [Mattison, 2011]. From these studies, one could hypothesize that the ΔC510 truncation eliminates the ability for SPECC1L to stabilize microtubules or associate with the actin cytoskeleton. However, whether CCDs 2-5 retain the capacity to associate with the actin cytoskeleton is still unclear.

This work has been expanded by a recent dissertation on the functions of Protein Phosphatase 1 (PP1), in which an interactome screen revealed an association between SPECC1L and PP1-interactor Myosin Phosphatase Targeting Protein (Mypt1) [Mehta, 2017]. This group performed SPECC1L-GFP fragment expression analyses like those seen in other studies, but with two additional refinements: improved partitioning of neighboring domains and examination of both tubulin and F-actin association [Mattison, 2011; Mehta, 2017]. These experiments verified

previous findings that the CCD3-7 (aa 462-890) and CHD (aa 891-1117) fragments associated with the actin cytoskeleton [Mehta, 2017]. More importantly, they showed that the N-terminal CCD1-2 fragment (aa 1-461) associates with tubulin and confirmed direct binding with a subsequent microtubule spin down assay. While the insertion of point mutations has suggested that the N-terminal region mediates microtubule binding, this analysis was the first to demonstrate it clearly [Saadi, 2011; Kruszka, 2015; Mehta, 2017].

Taken together, we can infer that the ΔC510 truncation and CCD2 disruption alleles would have fundamentally different impacts on SPECC1L function, resulting in loss of association with actin and microtubules, respectively. Truncation mutants may also be incapable of SPECC1L-mediated microtubule acetylation. Furthermore, disruption of CCD2 by point mutation or deletion may cause ectopic binding to actin filaments. Indeed, this would be consistent with the increase in SPECC1L co-localization with F-actin in T397P mutant palates and may represent the gain-of-function mechanism of the CCD2 mutations.

5.2 Future directions

5.2.1 Analysis of signaling pathways in wildtype and Specc1l mutant palates

To better understand the molecular changes in our *Specc1l* mutants, we had an antibody microarray screen performed on wildtype and *Specc1l*$^{cGT/\Delta C510}$ palate lysates (Kinexus Bioinformatics Corporation). The resultant dataset provides a broad view on the signaling changes in our *Specc1l* mutants (Table X). This dataset will be useful for identifying new directions of research. For example, we can utilize Ingenuity Pathway Analysis (IPA) software to identify altered signaling networks. Manual scanning of top hits may also provide specific targets for investigation by western blot or immunofluorescence. Furthermore, these data can be used to

explain molecular changes we have already identified, such as changes in cell adhesion markers or increased F-actin staining [Chapter 2]. Indeed, an initial review shows a marked reduction in AKT2 in the mutant lysate, consistent with the reduction in AKT levels found previously [Wilson, 2016].

5.2.2 Analysis of tissue fusion defects in embryos with CCD2 mutations

In Chapter 4, we identified elevation delay and cleft palate in mice with the T397P allele. In order to determine the nature of this defect, future analyses should include paraffin histology and immunofluorescence. The former will allow the assessment of palatal shelf shape and size. If remodeling is affected in our mutants, for example, the palatal shelves may be of similar size, but not properly extended at E15.5. Alternatively, if proliferation defects are a major factor, then the palatal shelf size may be reduced. The palatal shelves by gross examination do not appear to be reduced in size, so we predict the shape will be the primary difference. Paraffin histology can also be used to look for oral adhesions, as we saw in *Specc1l*$^{cGT/\Delta C510}$ mutants [Chapter 2]. Furthermore, immunofluorescence can be used to evaluate adhesion and cytoskeleton components, especially those associated with the actomyosin networks. Proliferation and apoptosis levels should also be examined. Similar analyses can also be performed to investigate fusion defects of the ventral body wall, eye, and neural tube. We hypothesize that an increase in actin filament staining will be observed in these tissues.

5.2.3 Specc1l in-frame deletions: utilizing an allelic series to dissect SPECC1L molecular function

The allelic series we have generated not only allows evaluation of different SPECC1L disruptions on embryonic development, but also provides a unique tool to examine molecular

function of SPECC1L domains. After harvesting craniofacial tissue, we can combine an immunoprecipitation pulldown of SPECC1L with mass spectrometry to screen for differences in protein interactions between wildtype and mutant lysates. For example, comparing how protein interactions between ΔCCD2 and ΔC510 mutant SPECC1L will be informative to determine how each allele effects cellular function.

Primary cells from these mutants can also be cultured to directly examine how each allele impacts cellular processes, such as cell division and migration. These analyses can be paired with treatment with pharmacological compounds, such as 740 Y-P to activate PI3K-AKT signaling. Follow-up immunostaining can be used to show how cytoskeletal and adhesion proteins are impacted.

5.2.4 Investigating the function of SPECC1L in cell division

SPECC1L associated with both the mitotic spindle and actomyosin ring during cell division (**Fig. 5.2A,B; arrows)**. During our analysis of *Specc1l*$^{cGT/\Delta C510}$ MEPM cells, we noted that the cells will often fail to properly divide and try multiple times before succeeding **(Fig 5.2C,D; arrows)**. Preliminary quantification showed that a greater proportion of mutant MEPM cell divisions are incomplete compared to wildtype cells **(Fig. 5.2E,F; orange vs. blue bars)**. Furthermore, we also found a ~20% reduction in total division events in mutant cultures **(Fig. 5.2E)**. This is unexpected, given that we did not find any differences in Ki-67 staining between wildtype and mutant palates [Chapter 2]. However, Ki-67 is expressed during the G1, S, G2, and M phases, so it may only be showing us partial information. Moreover, failed cell divisions may not necessarily influence the rate of cell division itself. We also did not control for cell number in this preliminary division analysis. Previous studies have shown that siRNA knockdown of

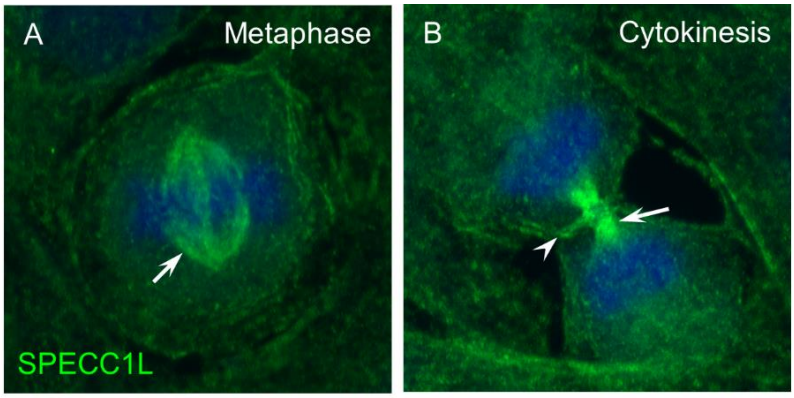
A
Metaphase
SPECC1L
B
Cytokinesis

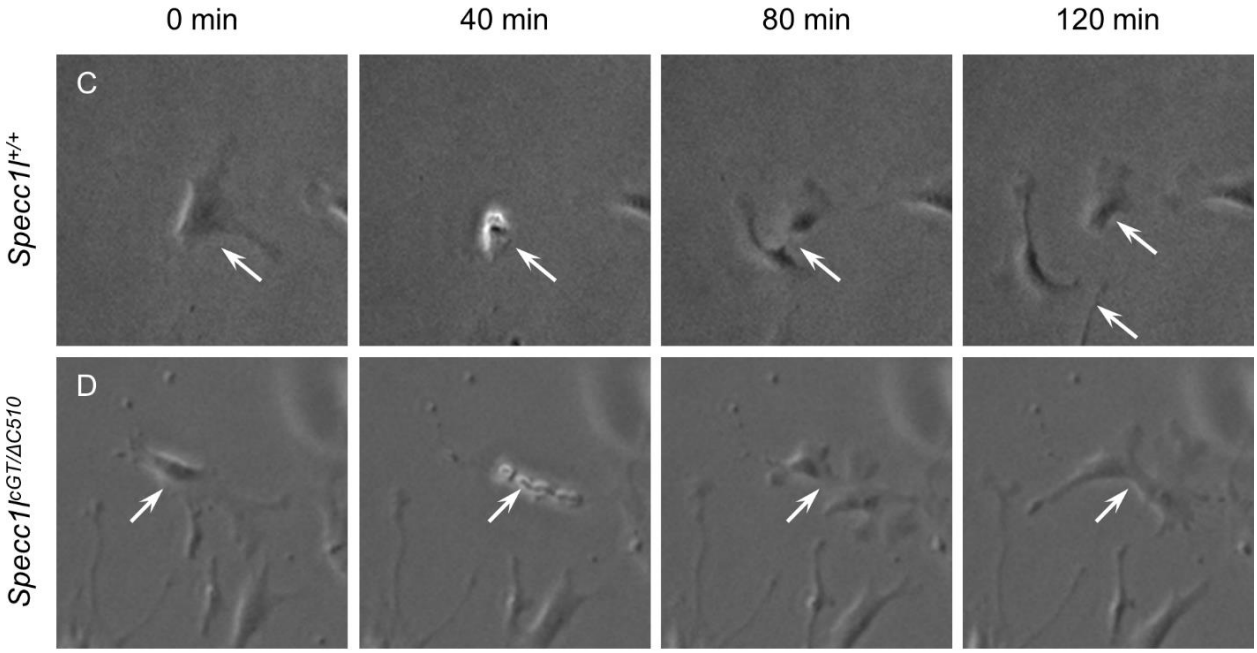
0 min
40 min
80 min
120 min
C
D
Specc1l+/+
Specc1lcGT/ΔC510

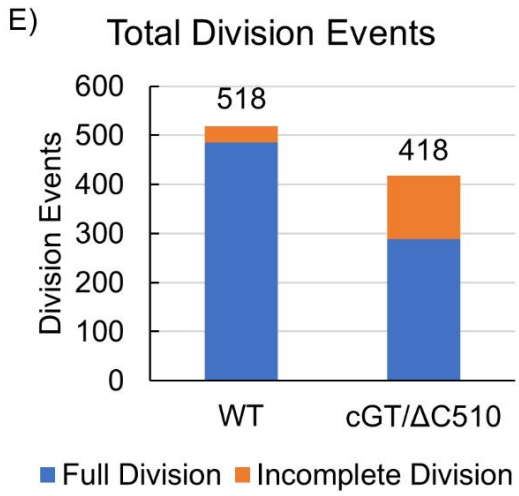
E)
Total Division Events
Division Events
600
500
400
300
200
100
0
518
418
WT
cGT/ΔC510
Full Division
Incomplete Division

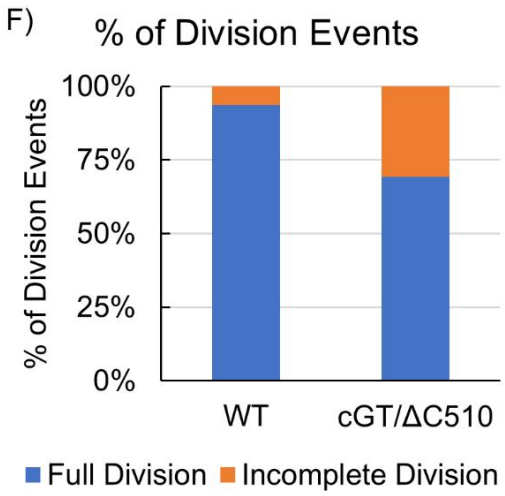
F)
% of Division Events
% of Division Events
100%
75%
50%
25%
0%
WT
cGT/ΔC510
Full Division
Incomplete Division

Figure 5.2: Cell division defects in *Specc1l*$^{cGT/\Delta C510}$ MEPM cells. A-B) Immunofluorescence images of SPECC1L (green) in control U2OS cells showing association with microtubules (A,B; arrows) and actomyosin ring (B; arrowhead) during mitosis. **C-D)** Representative frames from time-lapse videos showing normal cell divison in wildtype MEPM cells (C; arrows) and a failed division in *Specc1l*$^{cGT/\Delta C510}$ mutant MEPM cells (D; arrows). **E-F)** Graphs showing total division events (E) and percentage of failed division events (F) in wildtype and Specc1lcGT/ΔC510 mutant MEPM cells.

SPECC1L causes rocking of cell division [Mattison, 2011]. Taken together with the expression of SPECC1L in the mitotic spindle and peri-midbody region, this result strongly suggests a role in cytokinesis. We hypothesize that this increase in failed cell divisions is due to defects in cytokinesis, possibly resulting in impaired growth of the cell population and aneuploidy. Future analysis should include live imaging analyses to evaluate the division process in detail, as well as immunofluorescence to examine cytoskeletal components important for cell division.

5.2.5 Rescue SPECC1L fusion defects with upregulation of PI3K-AKT pathway

We showed that activation of the PI3K-AKT pathway can rescue the wound closure defects of *Specc1l* mutant MEPM cells [Chapter 3]. Previous studies show that the shape and adherens junction phenotypes of *SPECC1L*-kd U2OS cells can also be improved in a similar manner [Wilson, 2016]. Thus, we hypothesize that activation of this pathway *in vivo* may be able to rescue some of the developmental malformations seen in our *Specc1l* mutant embryos. This could be achieved in two ways. First, pregnant dams could be treated with 740 Y-P by intraperitoneal injection at specific developmental stages prior to the defect we wish to rescue. For neural tube closure defects, injections would be performed from E6.5–E8.5 with embryo harvest and evaluation at E9.5. Likewise, injections from E12.5-E14.5 and subsequent harvest at E15.5 can be used to evaluate rescue of the omphalocele and cleft palate defects. Next, a genetic rescue can also be performed by crossing our *Specc1l* mutants with mice heterozygous for tumor suppressor PTEN, a negative regulator of PI3K-AKT signaling [Majumder, 2005; Podsypanina, 2001; Di Cristofano, 1998]. This allele has already been generated in our colony by crossing a $Pten^{flox}$ (Jax #004597) mouse with a CMV-Cre mouse (Jax #006054), resulting in a global knockout allele. Complete loss of PTEN results in embryonic lethality, so only one parent will contain this allele

in the crosses. Considering that mice deficient in the PI3K-AKT pathway have cleft palate and blebbing phenotypes similar to our *Specc1l* mutants, we would expect that these interventions would partially rescue some of these defects.

5.2.6 Investigating differentiation and patterning in Specc1l mutant palates

Proper ossification and patterning of the palate is critical for normal palatogenesis [Chapter 1.2.5]. Though we did not examine differentiation directly, our skeletal stains of the T397P heterozygote embryo in Chapter 4 indicate that *Specc1l* may play roles in these processes **(Fig. 4.3)**. Inspection of the oral cavity revealed defects of the palatine processes when compared to a wildtype littermate. This finding is consistent with skeletal stains of other cleft palate mouse models [Baek, 2011; Lan, 2016; Strassman, 2017]. Future studies should investigate whether these staining differences are primary differentiation defects, or rather a consequence of the delay in palatal shelf elevation and insufficient horizontal growth. Palate morphology can be investigated by histology as described in 5.2.2, combined with Goldner's trichrome [Wu, 2008] or Van Gieson (van Gieson's picrofuchsin and alcian blue) [Baek, 2011] stains to evaluate mineralization and connective tissue. Ossification can also be investigated by staining for osteogenesis markers, such as alkaline phosphatase [Sweney, 1971], *Runx2* [Ducy, 1997], and *Osterix* [Nakashima, 2002].

Gross examination of wildtype and *Specc1l*$^{\Delta C510/\Delta C510}$ palates at E18.5 also reveal changes in rugae arrangement **(Fig. 5.3)** indicating that SPECC1L may also play a role in patterning. All rugae, apart from 7b, are visible in both palate images [Pantalacci, 2008]. In controls **(Fig 5.3A)**, rugae 1-3 are straight, followed by slanted rugae until the eighth, which lies at the border between the hard and soft palate. In contrast, *Specc1l*$^{\Delta C510/\Delta C510}$ occasionally show abnormal morphology, such as the improperly slanted third ruga **(Fig. 5.3B)**. Additionally, some rugae in the mutant also

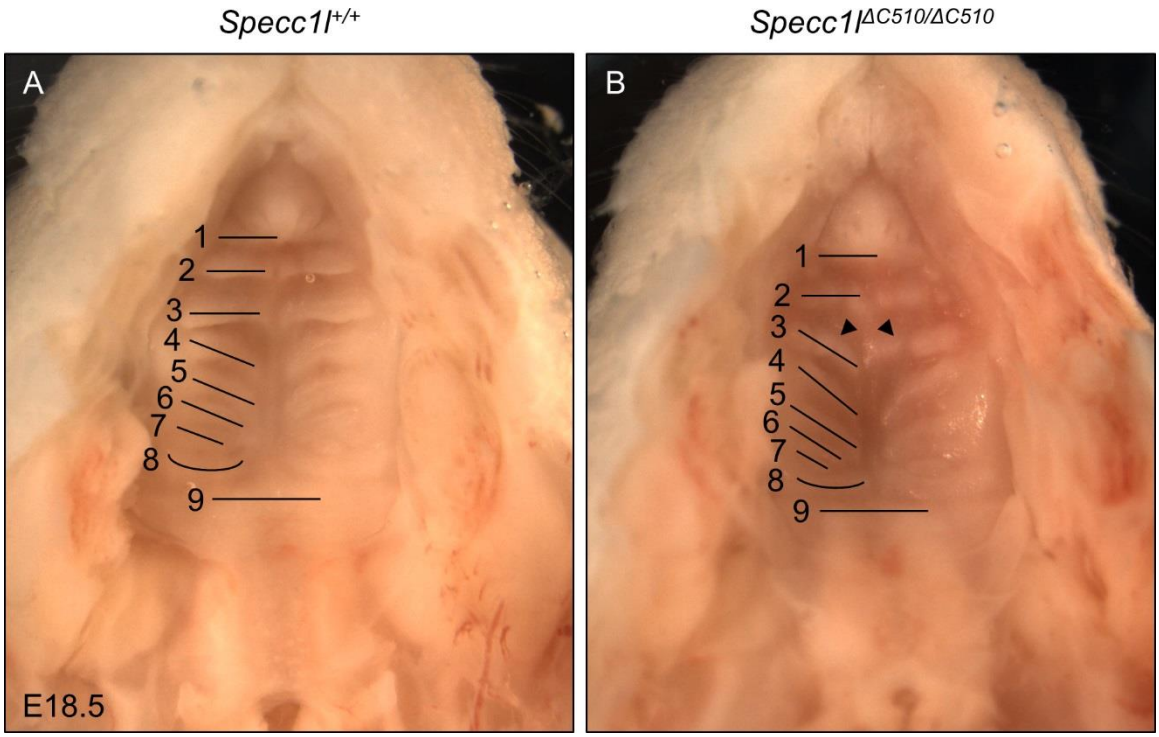

Figure 5.3: *Specc1l* mutants show rugae defects. A-B) Oral view of wildtype (A) and *Specc1l*$^{\Delta C510/\Delta C510}$ mutant (B) palates at E18.5 with all rugae labeled except 7b. The mutant palate shows abnormal rugae morphology, including a slanted third rugae (B; #3) and discontinuous patterning (B; arrowheads) compared to wildtype control (A). Palate designation based on Pantalacci *et al.* 2008.

exhibit a discontinuous morphology **(Fig 5.3B; arrowheads)**. There are several possible causes for these patterning defects. First, changes to the regional proliferation within and between rugae could result in altered morphology [Pantalacci, 2008]. Defects in rugae specification may also be responsible for the discontinuous patterning. Alternatively, it is possible that the defects are not due to a primary change in the rugae, but are instead caused by deficiencies in overall palatal shelf growth and elevation. Future analyses should include whole mount staining for SHH expression, an early marker of rugae formation, by *in situ* hybridization [Rice, 2006; Pantalacci, 2008]. Rugae proliferation and morphology can be visualized through whole mount immunofluorescence and DAPI staining, respectively [Pantalacci, 2008; Sandell, 2012].

5.3 Significance

The consequences of orofacial clefts are multifold, posing not only a considerable financial burden on the family, but also a significant strain on the quality of life and social interactions of the affected patient [Reviewed in Wehby, 2010]. Thus, it is imperative that the various causes of these disorders are identified. The basic concept of an orofacial cleft is relatively straightforward: a gap resulting from the failed fusion between two craniofacial processes. However, even a cursory investigation into the basis of these congenital anomalies reveals that the underlying pathogenetic mechanisms are far from simple. Indeed, elucidating the etiology of orofacial clefts has remained an immense challenge due to the complex nature of craniofacial morphogenesis.

These studies make multiple contributions to our understanding of orofacial clefting. First, we demonstrated that IRF6 is required for SPECC1L in the palate, thereby inserting *SPECC1L* into the well-characterized IRF6-GRHL3 craniofacial gene network. We also extend the known spectrum of *SPECC1L*-related phenotypes to patients with nonsyndromic clefts. Furthermore, our

analysis revealed oral adhesions and deficiencies of mesenchymal remodeling as two potential mechanisms for the palate elevation delay in *Specc1l* compound heterozygote mice. The former is consistent with previous studies on IRF6-related mouse mutants, while the latter attempts to answer a question that, despite old roots, has only begun to be investigated in recent studies. Lastly, perhaps the most impactful findings in this work come from our examination of T397P mutant mice. By recapitulating the cleft palate and omphalocele defects with a knock-in mutation identical to a human *SPECC1L* variant, we directly establish a causal role for *SPECC1L* in those human phenotypes. Our analyses of these mice also implicate actomyosin networks in palatogenesis, representing yet another mechanism that has been scarcely studied.

References

Abu-Issa, R., Smyth, G., Smoak, I., Yamamura, K., & Meyers, E. N. (2002). Fgf8 is required for pharyngeal arch and cardiovascular development in the mouse. *Development, 129*(19), 4613-4625.

Achilleos, A., & Trainor, P. A. (2015). Mouse Models of Rare Craniofacial Disorders. *Curr Top Dev Biol, 115*, 413-458. doi:10.1016/bs.ctdb.2015.07.011

Adams, D., Baldock, R., Bhattacharya, S., Copp, A. J., Dickinson, M., Greene, N. D., . . . West, D. (2013). Bloomsbury report on mouse embryo phenotyping: recommendations from the IMPC workshop on embryonic lethal screening. *Dis Model Mech, 6*(3), 571-579. doi:10.1242/dmm.011833

Adeyemo, W. L., & Butali, A. (2017). Genetics and genomics etiology of nonsyndromic orofacial clefts. *Mol Genet Genomic Med, 5*(1), 3-7. doi:10.1002/mgg3.272

Adzhubei, I. A., Schmidt, S., Peshkin, L., Ramensky, V. E., Gerasimova, A., Bork, P., . . . Sunyaev, S. R. (2010). A method and server for predicting damaging missense mutations. *Nat Methods, 7*(4), 248-249. doi:10.1038/nmeth0410-248

Alshomer, F., Aldaghri, F., Alohaideb, N., Aljehani, R., Murad, M. A., & Hashem, F. (2017). Reconstruction of Congenital Sternal Clefts: Surgical Experience and Literature Review. *Plast Reconstr Surg Glob Open, 5*(11), e1567. doi:10.1097/GOX.0000000000001567

Altomare, D. A., & Testa, J. R. (2005). Perturbations of the AKT signaling pathway in human cancer. *Oncogene, 24*(50), 7455-7464. doi:10.1038/sj.onc.1209085

Aryal, N. K., Wasylishen, A. R., & Lozano, G. (2018). CRISPR/Cas9 can mediate high-efficiency off-target mutations in mice in vivo. *Cell Death Dis, 9*(11), 1099. doi:10.1038/s41419-018-1146-0

Baek, J. A., Lan, Y., Liu, H., Maltby, K. M., Mishina, Y., & Jiang, R. (2011). Bmpr1a signaling plays critical roles in palatal shelf growth and palatal bone formation. *Dev Biol, 350*(2), 520-531. doi:10.1016/j.ydbio.2010.12.028

Bajpai, R., Chen, D. A., Rada-Iglesias, A., Zhang, J., Xiong, Y., Helms, J., . . . Wysocka, J. (2010). CHD7 cooperates with PBAF to control multipotent neural crest formation. *Nature, 463*(7283), 958-962. doi:10.1038/nature08733

Barriga, E. H., & Mayor, R. (2015). Embryonic cell-cell adhesion: a key player in collective neural crest migration. *Curr Top Dev Biol, 112*, 301-323. doi:10.1016/bs.ctdb.2014.11.023

Basch, M. L., Bronner-Fraser, M., & Garcia-Castro, M. I. (2006). Specification of the neural crest occurs during gastrulation and requires Pax7. *Nature, 441*(7090), 218-222. doi:10.1038/nature04684

Beaty, T. H., Murray, J. C., Marazita, M. L., Munger, R. G., Ruczinski, I., Hetmanski, J. B., . . . Scott, A. F. (2010). A genome-wide association study of cleft lip with and without cleft palate identifies risk variants near MAFB and ABCA4. *Nat Genet, 42*(6), 525-529. doi:10.1038/ng.580

Benjamin, B., & Wilson, G. N. (2014). Anomalies associated with gastroschisis and omphalocele: analysis of 2825 cases from the Texas Birth Defects Registry. *J Pediatr Surg, 49*(4), 514-519. doi:10.1016/j.jpedsurg.2013.11.052

Bezanilla, M., Gladfelter, A. S., Kovar, D. R., & Lee, W. L. (2015). Cytoskeletal dynamics: a view from the membrane. *J Cell Biol, 209*(3), 329-337. doi:10.1083/jcb.201502062

Bhoj, E. J., Haye, D., Toutain, A., Bonneau, D., Nielsen, I. K., Lund, I. B., . . . Verloes, A. (2018). Phenotypic spectrum associated with SPECC1L pathogenic variants: new families and critical review of the nosology of Teebi, Opitz GBBB, and Baraitser-Winter syndromes. *Eur J Med Genet*. doi:10.1016/j.ejmg.2018.11.022

Bhoj, E. J., Li, D., Harr, M. H., Tian, L., Wang, T., Zhao, Y., . . . Zackai, E. H. (2015). Expanding the SPECC1L mutation phenotypic spectrum to include Teebi hypertelorism syndrome. *Am J Med Genet A, 167A*(11), 2497-2502. doi:10.1002/ajmg.a.37217

Biggs, L. C., Naridze, R. L., DeMali, K. A., Lusche, D. F., Kuhl, S., Soll, D. R., . . . Dunnwald, M. (2014). Interferon regulatory factor 6 regulates keratinocyte migration. *J Cell Sci, 127*(Pt 13), 2840-2848. doi:10.1242/jcs.139246

Bjork, B. C., Turbe-Doan, A., Prysak, M., Herron, B. J., & Beier, D. R. (2010). Prdm16 is required for normal palatogenesis in mice. *Human Molecular Genetics, 19*(5), 774-789. doi:10.1093/hmg/ddp543

Bolande, R. (1974). The neurocristopathiesA unifying concept of disease arising in neural crest maldevelopment. *Human Pathology, 5*(4), 409-429. doi:10.1016/s0046-8177(74)80021-3

Botti, E., Spallone, G., Moretti, F., Marinari, B., Pinetti, V., Galanti, S., . . . Costanzo, A. (2011). Developmental factor IRF6 exhibits tumor suppressor activity in squamous cell carcinomas. *Proc Natl Acad Sci U S A, 108*(33), 13710-13715. doi:10.1073/pnas.1110931108

Brewer, S., & Williams, T. (2004). Finally, a sense of closure? Animal models of human ventral body wall defects. *Bioessays, 26*(12), 1307-1321. doi:10.1002/bies.20137

Brinkley, L. L., & Bookstein, F. L. (1986). Cell distribution during mouse secondary palate closure. II. Mesenchymal cells. *J Embryol Exp Morphol, 96*, 111-130.

Brinkley, L. L., & Morris-Wiman, J. (1987). Computer-assisted analysis of hyaluronate distribution during morphogenesis of the mouse secondary palate. *Development, 100*(4), 629-635.

Brock, L. J., Economou, A. D., Cobourne, M. T., & Green, J. B. (2016). Mapping cellular processes in the mesenchyme during palatal development in the absence of Tbx1 reveals complex proliferation changes and perturbed cell packing and polarity. *J Anat, 228*(3), 464-473. doi:10.1111/joa.12425

Brunet, C. L., Sharpe, P. M., & Ferguson, M. W. (1995). Inhibition of TGF-beta 3 (but not TGF-beta 1 or TGF-beta 2) activity prevents normal mouse embryonic palate fusion. *Int J Dev Biol, 39*(2), 345-355.

Brunskill, E. W., Potter, A. S., Distasio, A., Dexheimer, P., Plassard, A., Aronow, B. J., & Potter, S. S. (2014). A gene expression atlas of early craniofacial development. *Dev Biol, 391*(2), 133-146. doi:10.1016/j.ydbio.2014.04.016

Burdick, A. B., Bixler, D., & Puckett, C. L. (1985). Genetic analysis in families with van der Woude syndrome. *J Craniofac Genet Dev Biol, 5*(2), 181-208.

Burkhard, P., Stetefeld, J., & Strelkov, S. V. (2001). Coiled coils: a highly versatile protein folding motif. *Trends Cell Biol, 11*(2), 82-88.

Busche, A., Hehr, U., Sieg, P., & Gillessen-Kaesbach, G. (2016). Van der Woude and Popliteal Pterygium Syndromes: Broad intrafamilial variability in a three generation family with mutation in IRF6. *Am J Med Genet A, 170*(9), 2404-2407. doi:10.1002/ajmg.a.37791

Bush, J. O., & Jiang, R. (2012). Palatogenesis: morphogenetic and molecular mechanisms of secondary palate development. *Development, 139*(2), 231-243. doi:10.1242/dev.067082

Bush, W. S., & Moore, J. H. (2012). Chapter 11: Genome-wide association studies. *PLoS Comput Biol, 8*(12), e1002822. doi:10.1371/journal.pcbi.1002822

Cappa, M., Borrelli, P., Marini, R., & Neri, G. (1987). The Opitz syndrome: a new designation for the clinically indistinguishable BBB and G syndromes. *Am J Med Genet, 28*(2), 303-309. doi:10.1002/ajmg.1320280207

Carballo, G. B., Honorato, J. R., de Lopes, G. P. F., & Spohr, Tclse. (2018). A highlight on Sonic hedgehog pathway. *Cell Commun Signal, 16*(1), 11. doi:10.1186/s12964-018-0220-7

Carmona-Fontaine, C., Matthews, H. K., Kuriyama, S., Moreno, M., Dunn, G. A., Parsons, M., . . . Mayor, R. (2008). Contact inhibition of locomotion in vivo controls neural crest directional migration. *Nature, 456*(7224), 957-961. doi:10.1038/nature07441

Caruana, G., Farlie, P. G., Hart, A. H., Bagheri-Fam, S., Wallace, M. J., Dobbie, M. S., . . . Bertram, J. F. (2013). Genome-wide ENU mutagenesis in combination with high density SNP analysis and exome sequencing provides rapid identification of novel mouse models of developmental disease. *PLoS One, 8*(3), e55429. doi:10.1371/journal.pone.0055429

Casey, L. M., Lan, Y., Cho, E. S., Maltby, K. M., Gridley, T., & Jiang, R. (2006). Jag2-Notch1 signaling regulates oral epithelial differentiation and palate development. *Dev Dyn, 235*(7), 1830-1844. doi:10.1002/dvdy.20821

Charles, C., Pantalacci, S., Peterkova, R., Peterka, M., Laudet, V., & Viriot, L. (2007). Disruption of the palatal rugae pattern in Tabby (eda) mutant mice. *Eur J Oral Sci, 115*(6), 441-448. doi:10.1111/j.1600-0722.2007.00482.x

Charzewska, A., Obersztyn, E., Hoffman-Zacharska, D., Lenart, J., Poznanski, J., & Bal, J. (2015). Novel Mutations in the IRF6 Gene on the Background of Known Polymorphisms in Polish Patients With Orofacial Clefting. *Cleft Palate Craniofac J, 52*(5), e161-167. doi:10.1597/14-030

Chen, J. F., Huang, Z., Ma, J., Zhu, J., Moratalla, R., Standaert, D., . . . Schwarzschild, M. A. (1999). A(2A) adenosine receptor deficiency attenuates brain injury induced by transient focal ischemia in mice. *J Neurosci, 19*(21), 9192-9200.

Chiquet, M., Blumer, S., Angelini, M., Mitsiadis, T. A., & Katsaros, C. (2016). Mesenchymal Remodeling during Palatal Shelf Elevation Revealed by Extracellular Matrix and F-Actin Expression Patterns. *Front Physiol, 7*, 392. doi:10.3389/fphys.2016.00392

Coleman, R. D. (1965). Development of the Rat Palate. *Anat Rec, 151*, 107-117.

Copp, A. J. (1995). Death before birth: clues from gene knockouts and mutations. *Trends Genet, 11*(3), 87-93. doi:10.1016/S0168-9525(00)89008-3

Copp, A. J., & Greene, N. D. (2010). Genetics and development of neural tube defects. *J Pathol, 220*(2), 217-230. doi:10.1002/path.2643

Cordero, D. R., Brugmann, S., Chu, Y., Bajpai, R., Jame, M., & Helms, J. A. (2011). Cranial neural crest cells on the move: their roles in craniofacial development. *Am J Med Genet A, 155A*(2), 270-279. doi:10.1002/ajmg.a.33702

Cuervo, R., & Covarrubias, L. (2004). Death is the major fate of medial edge epithelial cells and the cause of basal lamina degradation during palatogenesis. *Development, 131*(1), 15-24. doi:10.1242/dev.00907

Czirok, A., Varga, K., Mehes, E., & Szabo, A. (2013). Collective cell streams in epithelial monolayers depend on cell adhesion. *New J Phys, 15*, 75006. doi:10.1088/1367-2630/15/7/075006

Dasouki, M., Barr, M., Jr., Erickson, R. P., & Cox, B. (1988). Translocation (1;22) in a child with bilateral oblique facial clefts. *J Med Genet, 25*(6), 427-429. doi:10.1136/jmg.25.6.427

Davy, A., Aubin, J., & Soriano, P. (2004). Ephrin-B1 forward and reverse signaling are required during mouse development. *Genes Dev, 18*(5), 572-583. doi:10.1101/gad.1171704

De Groote, P., Tran, H. T., Fransen, M., Tanghe, G., Urwyler, C., De Craene, B., . . . Declercq, W. (2015). A novel RIPK4-IRF6 connection is required to prevent epithelial fusions characteristic for popliteal pterygium syndromes. *Cell Death Differ, 22*(6), 1012-1024. doi:10.1038/cdd.2014.191

de la Garza, G., Schleiffarth, J. R., Dunnwald, M., Mankad, A., Weirather, J. L., Bonde, G., . . . Cornell, R. A. (2013). Interferon regulatory factor 6 promotes differentiation of the periderm by activating expression of Grainyhead-like 3. *J Invest Dermatol, 133*(1), 68-77. doi:10.1038/jid.2012.269

de Lima, R. L., Hoper, S. A., Ghassibe, M., Cooper, M. E., Rorick, N. K., Kondo, S., . . . Schutte, B. C. (2009). Prevalence and nonrandom distribution of exonic mutations in interferon regulatory factor 6 in 307 families with Van der Woude syndrome and 37 families with popliteal pterygium syndrome. *Genet Med, 11*(4), 241-247. doi:10.1097/GIM.0b013e318197a49a

Delon, I., & Brown, N. H. (2007). Integrins and the actin cytoskeleton. *Curr Opin Cell Biol, 19*(1), 43-50. doi:10.1016/j.ceb.2006.12.013

Depew, M. J., Liu, J. K., Long, J. E., Presley, R., Meneses, J. J., Pedersen, R. A., & Rubenstein, J. L. (1999). Dlx5 regulates regional development of the branchial arches and sensory capsules. *Development, 126*(17), 3831-3846.

Depew, M. J., Lufkin, T., & Rubenstein, J. L. (2002). Specification of jaw subdivisions by Dlx genes. *Science, 298*(5592), 381-385. doi:10.1126/science.1075703

Derossi, D., Williams, E. J., Green, P. J., Dunican, D. J., & Doherty, P. (1998). Stimulation of mitogenesis by a cell-permeable PI 3-kinase binding peptide. *Biochem Biophys Res Commun, 251*(1), 148-152. doi:10.1006/bbrc.1998.9444

Di Cristofano, A., Pesce, B., Cordon-Cardo, C., & Pandolfi, P. P. (1998). Pten is essential for embryonic development and tumour suppression. *Nat Genet, 19*(4), 348-355. doi:10.1038/1235

Dixon, J., & Dixon, M. J. (2004). Genetic background has a major effect on the penetrance and severity of craniofacial defects in mice heterozygous for the gene encoding the nucleolar protein Treacle. *Dev Dyn, 229*(4), 907-914. doi:10.1002/dvdy.20004

Dixon, J., Jones, N. C., Sandell, L. L., Jayasinghe, S. M., Crane, J., Rey, J. P., . . . Trainor, P. A. (2006). Tcof1/Treacle is required for neural crest cell formation and proliferation deficiencies that cause craniofacial abnormalities. *Proc Natl Acad Sci U S A, 103*(36), 13403-13408. doi:10.1073/pnas.0603730103

Dixon, M. J., Marazita, M. L., Beaty, T. H., & Murray, J. C. (2011). Cleft lip and palate: understanding genetic and environmental influences. *Nat Rev Genet, 12*(3), 167-178. doi:10.1038/nrg2933

Doetschman, T. (2009). Influence of genetic background on genetically engineered mouse phenotypes. *Methods Mol Biol, 530*, 423-433. doi:10.1007/978-1-59745-471-1_23

Dottori, M., Gross, M. K., Labosky, P., & Goulding, M. (2001). The winged-helix transcription factor Foxd3 suppresses interneuron differentiation and promotes neural crest cell fate. *Development, 128*(21), 4127-4138.

Ducy, P., Zhang, R., Geoffroy, V., Ridall, A. L., & Karsenty, G. (1997). Osf2/Cbfa1: a transcriptional activator of osteoblast differentiation. *Cell, 89*(5), 747-754.

Dudas, M., Li, W. Y., Kim, J., Yang, A., & Kaartinen, V. (2007). Palatal fusion - where do the midline cells go? A review on cleft palate, a major human birth defect. *Acta Histochem, 109*(1), 1-14. doi:10.1016/j.acthis.2006.05.009

Duncan, K. M., Mukherjee, K., Cornell, R. A., & Liao, E. C. (2017). Zebrafish models of orofacial clefts. *Dev Dyn, 246*(11), 897-914. doi:10.1002/dvdy.24566

Dzamba, B. J., Jakab, K. R., Marsden, M., Schwartz, M. A., & DeSimone, D. W. (2009). Cadherin adhesion, tissue tension, and noncanonical Wnt signaling regulate fibronectin matrix organization. *Dev Cell, 16*(3), 421-432. doi:10.1016/j.devcel.2009.01.008

Etchevers, H. C., Amiel, J., & Lyonnet, S. (2006). Molecular bases of human neurocristopathies. *Adv Exp Med Biol, 589*, 213-234. doi:10.1007/978-0-387-46954-6_14

Fakhouri, W. D., Rhea, L., Du, T., Sweezer, E., Morrison, H., Fitzpatrick, D., . . . Schutte, B. C. (2012). MCS9.7 enhancer activity is highly, but not completely, associated with expression of Irf6 and p63. *Dev Dyn, 241*(2), 340-349. doi:10.1002/dvdy.22786

Fantauzzo, K. A., & Soriano, P. (2014). PI3K-mediated PDGFRalpha signaling regulates survival and proliferation in skeletal development through p53-dependent intracellular pathways. *Genes Dev, 28*(9), 1005-1017. doi:10.1101/gad.238709.114

Fantauzzo, K. A., & Soriano, P. (2016). PDGFRbeta regulates craniofacial development through homodimers and functional heterodimers with PDGFRalpha. *Genes Dev, 30*(21), 2443-2458. doi:10.1101/gad.288746.116

Fantauzzo, K. A., & Soriano, P. (2017). Generation of an immortalized mouse embryonic palatal mesenchyme cell line. *PLoS One, 12*(6), e0179078. doi:10.1371/journal.pone.0179078

Ferguson, M. W. (1978). Palatal shelf elevation in the Wistar rat fetus. *J Anat, 125*(Pt 3), 555-577.

Ferguson, M. W. (1988). Palate development. *Development, 103 Suppl*, 41-60.

Fitzpatrick, D. R., Denhez, F., Kondaiah, P., & Akhurst, R. J. (1990). Differential expression of TGF beta isoforms in murine palatogenesis. *Development, 109*(3), 585-595.

Fletcher, D. A., & Mullins, R. D. (2010). Cell mechanics and the cytoskeleton. *Nature, 463*(7280), 485-492. doi:10.1038/nature08908

Friedel, Roland H., & Soriano, Philippe. (2010). Gene Trap Mutagenesis in the Mouse. In Paul M. Wassarman & Philippe M. Soriano (Eds.), *Guide to Techniques in Mouse Development, Part B: Mouse Molecular Genetics, 2nd Edition* (Vol. 477, pp. 243-269): Academic Press.

Funato, N., Nakamura, M., & Yanagisawa, H. (2015). Molecular basis of cleft palates in mice. *World J Biol Chem, 6*(3), 121-138. doi:10.4331/wjbc.v6.i3.121

Galea, G. L., Cho, Y. J., Galea, G., Mole, M. A., Rolo, A., Savery, D., . . . Copp, A. J. (2017). Biomechanical coupling facilitates spinal neural tube closure in mouse embryos. *Proc Natl Acad Sci U S A, 114*(26), E5177-E5186. doi:10.1073/pnas.1700934114

Gammill, L. S., Gonzalez, C., & Bronner-Fraser, M. (2007). Neuropilin 2/semaphorin 3F signaling is essential for cranial neural crest migration and trigeminal ganglion condensation. *Dev Neurobiol, 67*(1), 47-56. doi:10.1002/dneu.20326

Gao, L., Xu, J., Li, X., Wang, T., Wu, W., & Cao, J. (2019). 2,3,7,8-Tetrachlorodibenzo-p-dioxin and TGFbeta3-Mediated Mouse Embryonic Palatal Mesenchymal Cells. *Dose Response, 17*(1), 1559325818786822. doi:10.1177/1559325818786822

Gasser, D. L., Yang, P., & Buetow, K. H. (1992). Palate teratogenicity and embryotoxicity of cyclosporin A in mice. *J Craniofac Genet Dev Biol, 12*(3), 155-158.

Gendron-Maguire, M., Mallo, M., Zhang, M., & Gridley, T. (1993). Hoxa-2 mutant mice exhibit homeotic transformation of skeletal elements derived from cranial neural crest. *Cell, 75*(7), 1317-1331.

Gfrerer, L., Shubinets, V., Hoyos, T., Kong, Y., Nguyen, C., Pietschmann, P., . . . Liao, E. C. (2014). Functional analysis of SPECC1L in craniofacial development and oblique facial cleft pathogenesis. *Plast Reconstr Surg, 134*(4), 748-759. doi:10.1097/PRS.0000000000000517

Gimona, M., Djinovic-Carugo, K., Kranewitter, W. J., & Winder, S. J. (2002). Functional plasticity of CH domains. *FEBS Lett, 513*(1), 98-106.

Goudy, S., Law, A., Sanchez, G., Baldwin, H. S., & Brown, C. (2010). Tbx1 is necessary for palatal elongation and elevation. *Mech Dev, 127*(5-6), 292-300. doi:10.1016/j.mod.2010.03.001

Gowans, L. J., Busch, T. D., Mossey, P. A., Eshete, M. A., Adeyemo, W. L., Aregbesola, B., . . . Butali, A. (2017). The prevalence, penetrance, and expressivity of etiologic IRF6 variants in orofacial clefts patients from sub-Saharan Africa. *Mol Genet Genomic Med, 5*(2), 164-171. doi:10.1002/mgg3.273

Gritli-Linde, A. (2007). Molecular control of secondary palate development. *Dev Biol, 301*(2), 309-326. doi:10.1016/j.ydbio.2006.07.042

Gritli-Linde, A. (2008). The etiopathogenesis of cleft lip and cleft palate: usefulness and caveats of mouse models. *Curr Top Dev Biol, 84*, 37-138. doi:10.1016/S0070-2153(08)00602-9

Gruber, M., Soding, J., & Lupas, A. N. (2006). Comparative analysis of coiled-coil prediction methods. *J Struct Biol, 155*(2), 140-145. doi:10.1016/j.jsb.2006.03.009

Han, J., Mayo, J., Xu, X., Li, J., Bringas, P., Jr., Maas, R. L., . . . Chai, Y. (2009). Indirect modulation of Shh signaling by Dlx5 affects the oral-nasal patterning of palate and rescues cleft palate in Msx1-null mice. *Development, 136*(24), 4225-4233. doi:10.1242/dev.036723

Harris, M. J., & Juriloff, D. M. (2007). Mouse mutants with neural tube closure defects and their role in understanding human neural tube defects. *Birth Defects Res A Clin Mol Teratol, 79*(3), 187-210. doi:10.1002/bdra.20333

He, F., & Soriano, P. (2013). A critical role for PDGFRalpha signaling in medial nasal process development. *PLoS Genet, 9*(9), e1003851. doi:10.1371/journal.pgen.1003851

He, F., Xiong, W., Yu, X., Espinoza-Lewis, R., Liu, C., Gu, S., . . . Chen, Y. (2008). Wnt5a regulates directional cell migration and cell proliferation via Ror2-mediated noncanonical pathway in mammalian palate development. *Development, 135*(23), 3871-3879. doi:10.1242/dev.025767

Heer, N. C., & Martin, A. C. (2017). Tension, contraction and tissue morphogenesis. *Development, 144*(23), 4249-4260. doi:10.1242/dev.151282

Heisenberg, C. P., & Bellaiche, Y. (2013). Forces in tissue morphogenesis and patterning. *Cell, 153*(5), 948-962. doi:10.1016/j.cell.2013.05.008

Hill, C. R., Yuasa, M., Schoenecker, J., & Goudy, S. L. (2014). Jagged1 is essential for osteoblast development during maxillary ossification. *Bone, 62*, 10-21. doi:10.1016/j.bone.2014.01.019

Hsu, P., Ma, A., Wilson, M., Williams, G., Curotta, J., Munns, C. F., & Mehr, S. (2014). CHARGE syndrome: a review. *J Paediatr Child Health, 50*(7), 504-511. doi:10.1111/jpc.12497

Ingraham, C. R., Kinoshita, A., Kondo, S., Yang, B., Sajan, S., Trout, K. J., . . . Schutte, B. C. (2006). Abnormal skin, limb and craniofacial morphogenesis in mice deficient for interferon regulatory factor 6 (Irf6). *Nat Genet, 38*(11), 1335-1340. doi:10.1038/ng1903

Iseki, S., Ishii-Suzuki, M., Tsunekawa, N., Yamada, Y., Eto, K., & Obata, K. (2007). Experimental induction of palate shelf elevation in glutamate decarboxylase 67-deficient mice with cleft palate due to vertically oriented palatal shelf. *Birth Defects Res A Clin Mol Teratol, 79*(10), 688-695. doi:10.1002/bdra.20400

Ishizaki, K., Sakurai, K., Tazaki, M., & Inoue, T. (2006). Response of Merkel cells in the palatal rugae to the continuous mechanical stimulation by palatal plate. *Somatosens Mot Res, 23*(1-2), 63-72. doi:10.1080/08990220600741069

Iwata, J., Suzuki, A., Pelikan, R. C., Ho, T. V., Sanchez-Lara, P. A., Urata, M., . . . Chai, Y. (2013). Smad4-Irf6 genetic interaction and TGFbeta-mediated IRF6 signaling cascade are crucial for palatal fusion in mice. *Development, 140*(6), 1220-1230. doi:10.1242/dev.089615

Iyyanar, P. P. R., & Nazarali, A. J. (2017). Hoxa2 Inhibits Bone Morphogenetic Protein Signaling during Osteogenic Differentiation of the Palatal Mesenchyme. *Front Physiol, 8*, 929. doi:10.3389/fphys.2017.00929

Janssen, N., Bergman, J. E., Swertz, M. A., Tranebjaerg, L., Lodahl, M., Schoots, J., . . . Hoefsloot, L. H. (2012). Mutation update on the CHD7 gene involved in CHARGE syndrome. *Hum Mutat, 33*(8), 1149-1160. doi:10.1002/humu.22086

Jiang, R., Lan, Y., Chapman, H. D., Shawber, C., Norton, C. R., Serreze, D. V., . . . Gridley, T. (1998). Defects in limb, craniofacial, and thymic development in Jagged2 mutant mice. *Genes Dev, 12*(7), 1046-1057.

Jiang, Z., Pan, L., Chen, X., Chen, Z., & Xu, D. (2017). Wnt6 influences the viability of mouse embryonic palatal mesenchymal cells via the beta-catenin pathway. *Exp Ther Med, 14*(6), 5339-5344. doi:10.3892/etm.2017.5240

Jin, J. Z., & Ding, J. (2006). Analysis of cell migration, transdifferentiation and apoptosis during mouse secondary palate fusion. *Development, 133*(17), 3341-3347. doi:10.1242/dev.02520

Jin, J. Z., & Ding, J. (2006). Analysis of Meox-2 mutant mice reveals a novel postfusion-based cleft palate. *Dev Dyn, 235*(2), 539-546. doi:10.1002/dvdy.20641

Jin, J. Z., Li, Q., Higashi, Y., Darling, D. S., & Ding, J. (2008). Analysis of Zfhx1a mutant mice reveals palatal shelf contact-independent medial edge epithelial differentiation during palate fusion. *Cell Tissue Res, 333*(1), 29-38. doi:10.1007/s00441-008-0612-x

Jin, J. Z., Tan, M., Warner, D. R., Darling, D. S., Higashi, Y., Gridley, T., & Ding, J. (2010). Mesenchymal cell remodeling during mouse secondary palate reorientation. *Dev Dyn, 239*(7), 2110-2117. doi:10.1002/dvdy.22339

Jo, H., Mondal, S., Tan, D., Nagata, E., Takizawa, S., Sharma, A. K., . . . Luo, H. R. (2012). Small molecule-induced cytosolic activation of protein kinase Akt rescues ischemia-elicited neuronal death. *Proc Natl Acad Sci U S A, 109*(26), 10581-10586. doi:10.1073/pnas.1202810109

Jones, J. L., Canady, J. W., Brookes, J. T., Wehby, G. L., L'Heureux, J., Schutte, B. C., . . . Dunnwald, M. (2010). Wound complications after cleft repair in children with Van der Woude syndrome. *J Craniofac Surg, 21*(5), 1350-1353. doi:10.1097/SCS.0b013e3181ec6aad

Jugessur, A., Farlie, P. G., & Kilpatrick, N. (2009). The genetics of isolated orofacial clefts: from genotypes to subphenotypes. *Oral Dis, 15*(7), 437-453. doi:10.1111/j.1601-0825.2009.01577.x

Juriloff, D. M., & Harris, M. J. (2008). Mouse genetic models of cleft lip with or without cleft palate. *Birth Defects Res A Clin Mol Teratol, 82*(2), 63-77. doi:10.1002/bdra.20430

Kaartinen, V., Cui, X. M., Heisterkamp, N., Groffen, J., & Shuler, C. F. (1997). Transforming growth factor-beta3 regulates transdifferentiation of medial edge epithelium during palatal fusion and associated degradation of the basement membrane. *Dev Dyn, 209*(3), 255-260. doi:10.1002/(SICI)1097-0177(199707)209:3<255::AID-AJA1>3.0.CO;2-H

Kadakia, S., Helman, S. N., Badhey, A. K., Saman, M., & Ducic, Y. (2014). Treacher Collins Syndrome: the genetics of a craniofacial disease. *Int J Pediatr Otorhinolaryngol, 78*(6), 893-898. doi:10.1016/j.ijporl.2014.03.006

Ke, C. Y., Xiao, W. L., Chen, C. M., Lo, L. J., & Wong, F. H. (2015). IRF6 is the mediator of TGFbeta3 during regulation of the epithelial mesenchymal transition and palatal fusion. *Sci Rep, 5*, 12791. doi:10.1038/srep12791

Kenny, S. E., Tam, P. K., & Garcia-Barcelo, M. (2010). Hirschsprung's disease. *Semin Pediatr Surg, 19*(3), 194-200. doi:10.1053/j.sempedsurg.2010.03.004

Kerameddin, S., Namipashaki, A., Ebrahimi, S., & Ansari-Pour, N. (2015). IRF6 Is a Marker of Severity in Nonsyndromic Cleft Lip/Palate. *J Dent Res, 94*(9 Suppl), 226S-232S. doi:10.1177/0022034515581013

Kindberg, A. A., & Bush, J. O. (2019). Cellular organization and boundary formation in craniofacial development. *Genesis, 57*(1), e23271. doi:10.1002/dvg.23271

Kitase, Y., & Shuler, C. F. (2013). Microtubule disassembly prevents palatal fusion and alters regulation of the E-cadherin/catenin complex. *Int J Dev Biol, 57*(1), 55-60. doi:10.1387/ijdb.120117yk

Kondo, S., Schutte, B. C., Richardson, R. J., Bjork, B. C., Knight, A. S., Watanabe, Y., . . . Murray, J. C. (2002). Mutations in IRF6 cause Van der Woude and popliteal pterygium syndromes. *Nat Genet, 32*(2), 285-289. doi:10.1038/ng985

Korenbaum, E., & Rivero, F. (2002). Calponin homology domains at a glance. *J Cell Sci, 115*(Pt 18), 3543-3545.

Kosazuma, T., Hashimoto, S., Ohno, H., Chou, M. J., & Shiota, K. (2004). Organ culture of the fetal mouse palate for screening the developmental toxicity of chemicals: a validation study. *Congenit Anom (Kyoto), 44*(2), 60-71. doi:10.1111/j.1741-4520.2004.00010.x

Kousa, Y. A., Mansour, T. A., Seada, H., Matoo, S., & Schutte, B. C. (2017). Shared molecular networks in orofacial and neural tube development. *Birth Defects Res, 109*(2), 169-179. doi:10.1002/bdra.23598

Kousa, Y. A., Moussa, D., & Schutte, B. C. (2017). IRF6 expression in basal epithelium partially rescues Irf6 knockout mice. *Dev Dyn, 246*(9), 670-681. doi:10.1002/dvdy.24537

Kousa, Y. A., Roushangar, R., Patel, N., Walter, A., Marangoni, P., Krumlauf, R., . . . Schutte, B. C. (2017). IRF6 and SPRY4 Signaling Interact in Periderm Development. *J Dent Res, 96*(11), 1306-1313. doi:10.1177/0022034517719870

Kousa, Y. A., & Schutte, B. C. (2016). Toward an orofacial gene regulatory network. *Dev Dyn, 245*(3), 220-232. doi:10.1002/dvdy.24341

Kousa, Y. A., Zhu, H., Fakhouri, W. D., Lei, Y., Kinoshita, A., Roushangar, R. R., . . . Schutte, B. C. (2019). The TFAP2A-IRF6-GRHL3 genetic pathway is conserved in neurulation. *Hum Mol Genet*. doi:10.1093/hmg/ddz010

Kouskoura, T., Kozlova, A., Alexiou, M., Blumer, S., Zouvelou, V., Katsaros, C., . . . Graf, D. (2013). The etiology of cleft palate formation in BMP7-deficient mice. *PLoS One, 8*(3), e59463. doi:10.1371/journal.pone.0059463

Kruszka, P., Li, D., Harr, M. H., Wilson, N. R., Swarr, D., McCormick, E. M., . . . Zackai, E. H. (2015). Mutations in SPECC1L, encoding sperm antigen with calponin homology and coiled-coil domains 1-like, are found in some cases of autosomal dominant Opitz G/BBB syndrome. *J Med Genet, 52*(2), 104-110. doi:10.1136/jmedgenet-2014-102677

Kulesa, P. M., Bailey, C. M., Kasemeier-Kulesa, J. C., & McLennan, R. (2010). Cranial neural crest migration: new rules for an old road. *Dev Biol, 344*(2), 543-554. doi:10.1016/j.ydbio.2010.04.010

Lai, Y., Xie, C., Zhang, S., Gan, G., Wu, D., & Chen, W. (2016). Bone morphogenetic protein type I receptor inhibition induces cleft palate associated with micrognathia and cleft lower lip in mice. *Birth Defects Res A Clin Mol Teratol, 106*(7), 612-623. doi:10.1002/bdra.23504

Lan, Y., & Jiang, R. (2009). Sonic hedgehog signaling regulates reciprocal epithelial-mesenchymal interactions controlling palatal outgrowth. *Development, 136*(8), 1387-1396. doi:10.1242/dev.028167

Lan, Y., Ovitt, C. E., Cho, E. S., Maltby, K. M., Wang, Q., & Jiang, R. (2004). Odd-skipped related 2 (Osr2) encodes a key intrinsic regulator of secondary palate growth and morphogenesis. *Development, 131*(13), 3207-3216. doi:10.1242/dev.01175

Lan, Y., Xu, J., & Jiang, R. (2015). Cellular and Molecular Mechanisms of Palatogenesis. *Curr Top Dev Biol, 115*, 59-84. doi:10.1016/bs.ctdb.2015.07.002

Lan, Y., Zhang, N., Liu, H., Xu, J., & Jiang, R. (2016). Golgb1 regulates protein glycosylation and is crucial for mammalian palate development. *Development, 143*(13), 2344-2355. doi:10.1242/dev.134577

Lane, J., Yumoto, K., Azhar, M., Ninomiya-Tsuji, J., Inagaki, M., Hu, Y., . . . Kaartinen, V. (2015). Tak1, Smad4 and Trim33 redundantly mediate TGF-beta3 signaling during palate development. *Dev Biol, 398*(2), 231-241. doi:10.1016/j.ydbio.2014.12.006

Ledent, C., Vaugeois, J. M., Schiffmann, S. N., Pedrazzini, T., El Yacoubi, M., Vanderhaeghen, J. J., . . . Parmentier, M. (1997). Aggressiveness, hypoalgesia and high blood pressure in mice lacking the adenosine A2a receptor. *Nature, 388*(6643), 674-678. doi:10.1038/41771

Lek, M., Karczewski, K. J., Minikel, E. V., Samocha, K. E., Banks, E., Fennell, T., . . . Exome Aggregation, Consortium. (2016). Analysis of protein-coding genetic variation in 60,706 humans. *Nature, 536*(7616), 285-291. doi:10.1038/nature19057

Leslie, E. J., Koboldt, D. C., Kang, C. J., Ma, L., Hecht, J. T., Wehby, G. L., . . . Marazita, M. L. (2016). IRF6 mutation screening in non-syndromic orofacial clefting: analysis of 1521 families. *Clin Genet, 90*(1), 28-34. doi:10.1111/cge.12675

Leslie, E. J., Liu, H., Carlson, J. C., Shaffer, J. R., Feingold, E., Wehby, G., . . . Marazita, M. L. (2016). A Genome-wide Association Study of Nonsyndromic Cleft Palate Identifies an Etiologic Missense Variant in GRHL3. *Am J Hum Genet, 98*(4), 744-754. doi:10.1016/j.ajhg.2016.02.014

Leslie, E. J., Mansilla, M. A., Biggs, L. C., Schuette, K., Bullard, S., Cooper, M., . . . Murray, J. C. (2012). Expression and mutation analyses implicate ARHGAP29 as the etiologic gene for the cleft lip with or without cleft palate locus identified by genome-wide association on chromosome 1p22. *Birth Defects Res A Clin Mol Teratol, 94*(11), 934-942. doi:10.1002/bdra.23076

Leslie, E. J., & Marazita, M. L. (2013). Genetics of cleft lip and cleft palate. *Am J Med Genet C Semin Med Genet, 163C*(4), 246-258. doi:10.1002/ajmg.c.31381

Leslie, E. J., Standley, J., Compton, J., Bale, S., Schutte, B. C., & Murray, J. C. (2013). Comparative analysis of IRF6 variants in families with Van der Woude syndrome and popliteal pterygium syndrome using public whole-exome databases. *Genet Med, 15*(5), 338-344. doi:10.1038/gim.2012.141

Leslie, E. J., Taub, M. A., Liu, H., Steinberg, K. M., Koboldt, D. C., Zhang, Q., . . . Murray, J. C. (2015). Identification of functional variants for cleft lip with or without cleft palate in or near PAX7, FGFR2, and NOG by targeted sequencing of GWAS loci. *Am J Hum Genet, 96*(3), 397-411. doi:10.1016/j.ajhg.2015.01.004

Letra, A., Maili, L., Mulliken, J. B., Buchanan, E., Blanton, S. H., & Hecht, J. T. (2014). Further evidence suggesting a role for variation in ARHGAP29 variants in nonsyndromic cleft lip/palate. *Birth Defects Res A Clin Mol Teratol, 100*(9), 679-685. doi:10.1002/bdra.23286

Li, C., Lan, Y., & Jiang, R. (2017). Molecular and Cellular Mechanisms of Palate Development. *J Dent Res, 96*(11), 1184-1191. doi:10.1177/0022034517703580

Li, L., Lin, M., Wang, Y., Cserjesi, P., Chen, Z., & Chen, Y. (2011). BmprIa is required in mesenchymal tissue and has limited redundant function with BmprIb in tooth and palate development. *Dev Biol, 349*(2), 451-461. doi:10.1016/j.ydbio.2010.10.023

Li, Q., & Ding, J. (2007). Gene expression analysis reveals that formation of the mouse anterior secondary palate involves recruitment of cells from the posterior side. *Int J Dev Biol, 51*(2), 167-172. doi:10.1387/ijdb.062212ql

Liu, H., Busch, T., Eliason, S., Anand, D., Bullard, S., Gowans, L. J. J., . . . Butali, A. (2017). Exome sequencing provides additional evidence for the involvement of ARHGAP29 in Mendelian orofacial clefting and extends the phenotypic spectrum to isolated cleft palate. *Birth Defects Res, 109*(1), 27-37. doi:10.1002/bdra.23596

Liu, J. P., & Jessell, T. M. (1998). A role for rhoB in the delamination of neural crest cells from the dorsal neural tube. *Development, 125*(24), 5055-5067.

Liu, W., Lan, Y., Pauws, E., Meester-Smoor, M. A., Stanier, P., Zwarthoff, E. C., & Jiang, R. (2008). The Mn1 transcription factor acts upstream of Tbx22 and preferentially regulates posterior palate growth in mice. *Development, 135*(23), 3959-3968. doi:10.1242/dev.025304

Liu, X., Zhang, H., Gao, L., Yin, Y., Pan, X., Li, Z., . . . Yu, Z. (2014). Negative interplay of retinoic acid and TGF-beta signaling mediated by TG-interacting factor to modulate mouse embryonic palate mesenchymal-cell proliferation. *Birth Defects Res B Dev Reprod Toxicol, 101*(6), 403-409. doi:10.1002/bdrb.21130

Lumsden, A., Sprawson, N., & Graham, A. (1991). Segmental origin and migration of neural crest cells in the hindbrain region of the chick embryo. *Development, 113*(4), 1281-1291.

Lupas, A., Van Dyke, M., & Stock, J. (1991). Predicting coiled coils from protein sequences. *Science, 252*(5009), 1162-1164. doi:10.1126/science.252.5009.1162

Ma, X., & Adelstein, R. S. (2014). A point mutation in Myh10 causes major defects in heart development and body wall closure. *Circ Cardiovasc Genet, 7*(3), 257-265. doi:10.1161/CIRCGENETICS.113.000455

Machado, R. G., & Eames, B. F. (2017). Using Zebrafish to Test the Genetic Basis of Human Craniofacial Diseases. *J Dent Res, 96*(11), 1192-1199. doi:10.1177/0022034517722776

Majumder, P. K., & Sellers, W. R. (2005). Akt-regulated pathways in prostate cancer. *Oncogene, 24*(50), 7465-7474. doi:10.1038/sj.onc.1209096

Mangold, E., Ludwig, K. U., & Nothen, M. M. (2011). Breakthroughs in the genetics of orofacial clefting. *Trends Mol Med, 17*(12), 725-733. doi:10.1016/j.molmed.2011.07.007

Manning, B. D., & Toker, A. (2017). AKT/PKB Signaling: Navigating the Network. *Cell, 169*(3), 381-405. doi:10.1016/j.cell.2017.04.001

Mansouri, A., Stoykova, A., Torres, M., & Gruss, P. (1996). Dysgenesis of cephalic neural crest derivatives in Pax7-/- mutant mice. *Development, 122*(3), 831-838.

Marazita, M. L. (2012). The evolution of human genetic studies of cleft lip and cleft palate. *Annu Rev Genomics Hum Genet, 13*, 263-283. doi:10.1146/annurev-genom-090711-163729

Marginean, C., Marginean, C. O., Gozar, L., Melit, L. E., Suciu, H., Gozar, H., . . . Cucerea, M. (2018). Cantrell Syndrome-A Rare Complex Congenital Anomaly: A Case Report and Literature Review. *Front Pediatr, 6*, 201. doi:10.3389/fped.2018.00201

Martelli-Junior, H., Chaves, M. R., Swerts, M. S., de Miranda, R. T., Bonan, P. R., & Coletta, R. D. (2007). Clinical and genetic features of Van der Woude syndrome in two large families in Brazil. *Cleft Palate Craniofac J, 44*(3), 239-243. doi:10.1597/06-064

Mateer, S. C., Morris, L. E., Cromer, D. A., Bensenor, L. B., & Bloom, G. S. (2004). Actin filament binding by a monomeric IQGAP1 fragment with a single calponin homology domain. *Cell Motil Cytoskeleton, 58*(4), 231-241. doi:10.1002/cm.20013

Matsumura, K., Taketomi, T., Yoshizaki, K., Arai, S., Sanui, T., Yoshiga, D., . . . Nakamura, S. (2011). Sprouty2 controls proliferation of palate mesenchymal cells via fibroblast growth factor signaling. *Biochem Biophys Res Commun, 404*(4), 1076-1082. doi:10.1016/j.bbrc.2010.12.116

Matsuoka, T., Ahlberg, P. E., Kessaris, N., Iannarelli, P., Dennehy, U., Richardson, W. D., . . . Koentges, G. (2005). Neural crest origins of the neck and shoulder. *Nature, 436*(7049), 347-355. doi:10.1038/nature03837

Mattison, C. P., Stumpff, J., Wordeman, L., & Winey, M. (2011). Mip1 associates with both the Mps1 kinase and actin, and is required for cell cortex stability and anaphase spindle positioning. *Cell Cycle, 10*(5), 783-793. doi:10.4161/cc.10.5.14955

McLennan, R., Teddy, J. M., Kasemeier-Kulesa, J. C., Romine, M. H., & Kulesa, P. M. (2010). Vascular endothelial growth factor (VEGF) regulates cranial neural crest migration in vivo. *Dev Biol, 339*(1), 114-125. doi:10.1016/j.ydbio.2009.12.022

Mehta, Virja. (2017). *A Comprehensive Analysis of PP1c Leads to the Identification and Characterization of a Novel Family of Regulators for the Mypt1/PP1β Phosphatase.* Université d'Ottawa/University of Ottawa,

Meng, L., Bian, Z., Torensma, R., & Von den Hoff, J. W. (2009). Biological mechanisms in palatogenesis and cleft palate. *J Dent Res, 88*(1), 22-33. doi:10.1177/0022034508327868

Minoux, M., & Rijli, F. M. (2010). Molecular mechanisms of cranial neural crest cell migration and patterning in craniofacial development. *Development, 137*(16), 2605-2621. doi:10.1242/dev.040048

Moretti, F., Marinari, B., Lo Iacono, N., Botti, E., Giunta, A., Spallone, G., . . . Costanzo, A. (2010). A regulatory feedback loop involving p63 and IRF6 links the pathogenesis of 2 genetically different human ectodermal dysplasias. *J Clin Invest, 120*(5), 1570-1577. doi:10.1172/JCI40267

Morris-Wiman, J., & Brinkley, L. (1992). An extracellular matrix infrastructure provides support for murine secondary palatal shelf remodelling. *Anat Rec, 234*(4), 575-586. doi:10.1002/ar.1092340413

Mossey, P. A., Little, J., Munger, R. G., Dixon, M. J., & Shaw, W. C. (2009). Cleft lip and palate. *Lancet, 374*(9703), 1773-1785. doi:10.1016/S0140-6736(09)60695-4

Mossey, P. A., & Modell, B. (2012). Epidemiology of oral clefts 2012: an international perspective. *Front Oral Biol, 16*, 1-18. doi:10.1159/000337464

Munjal, A., & Lecuit, T. (2014). Actomyosin networks and tissue morphogenesis. *Development, 141*(9), 1789-1793. doi:10.1242/dev.091645

Murdoch, B., DelConte, C., & Garcia-Castro, M. I. (2012). Pax7 lineage contributions to the mammalian neural crest. *PLoS One, 7*(7), e41089. doi:10.1371/journal.pone.0041089

Murray, J. C. (1995). Face facts: genes, environment, and clefts. *Am J Hum Genet, 57*(2), 227-232.

Muzumdar, M. D., Tasic, B., Miyamichi, K., Li, L., & Luo, L. (2007). A global double-fluorescent Cre reporter mouse. *Genesis, 45*(9), 593-605. doi:10.1002/dvg.20335

Nagy, Andras, Gertsenstein, Marina, Vintersten, Kristina, & Behringer, Richard. (2003). *Manipulating the mouse embryo: a laboratory manual*: Firefly Books.

Nakajima, A., C, F. Shuler, Gulka, A. O. D., & Hanai, J. I. (2018). TGF-beta Signaling and the Epithelial-Mesenchymal Transition during Palatal Fusion. *Int J Mol Sci, 19*(11). doi:10.3390/ijms19113638

Nakashima, K., Zhou, X., Kunkel, G., Zhang, Z., Deng, J. M., Behringer, R. R., & de Crombrugghe, B. (2002). The novel zinc finger-containing transcription factor osterix is required for osteoblast differentiation and bone formation. *Cell, 108*(1), 17-29.

Narasimha, Maithreyi, & Brown, Nicholas H. (2013). Integrins and associated proteins in Drosophila development. In *Madame Curie Bioscience Database [Internet]*: Landes Bioscience.

Nawshad, A. (2008). Palatal seam disintegration: to die or not to die? that is no longer the question. *Dev Dyn, 237*(10), 2643-2656. doi:10.1002/dvdy.21599

Noack Watt, K. E., Achilleos, A., Neben, C. L., Merrill, A. E., & Trainor, P. A. (2016). The Roles of RNA Polymerase I and III Subunits Polr1c and Polr1d in Craniofacial Development and in Zebrafish Models of Treacher Collins Syndrome. *PLoS Genet, 12*(7), e1006187. doi:10.1371/journal.pgen.1006187

Noritake, J., Watanabe, T., Sato, K., Wang, S., & Kaibuchi, K. (2005). IQGAP1: a key regulator of adhesion and migration. *J Cell Sci, 118*(Pt 10), 2085-2092. doi:10.1242/jcs.02379

Nunzi, M. G., Pisarek, A., & Mugnaini, E. (2004). Merkel cells, corpuscular nerve endings and free nerve endings in the mouse palatine mucosa express three subtypes of vesicular glutamate transporters. *J Neurocytol, 33*(3), 359-376. doi:10.1023/B:NEUR.0000044196.45602.92

Okano, J., Kimura, W., Papaionnou, V. E., Miura, N., Yamada, G., Shiota, K., & Sakai, Y. (2012). The regulation of endogenous retinoic acid level through CYP26B1 is required for elevation of palatal shelves. *Dev Dyn, 241*(11), 1744-1756. doi:10.1002/dvdy.23862

Okano, J., Udagawa, J., & Shiota, K. (2014). Roles of retinoic acid signaling in normal and abnormal development of the palate and tongue. *Congenit Anom (Kyoto), 54*(2), 69-76. doi:10.1111/cga.12049

Pantalacci, S., Prochazka, J., Martin, A., Rothova, M., Lambert, A., Bernard, L., . . . Laudet, V. (2008). Patterning of palatal rugae through sequential addition reveals an anterior/posterior boundary in palatal development. *BMC Dev Biol, 8*, 116. doi:10.1186/1471-213X-8-116

Papaioannou, V. E., & Behringer, R. R. (2012). Early embryonic lethality in genetically engineered mice: diagnosis and phenotypic analysis. *Vet Pathol, 49*(1), 64-70. doi:10.1177/0300985810395725

Paul, B. J., Palmer, K., Sharp, J. C., Pratt, C. H., Murray, S. A., & Dunnwald, M. (2017). ARHGAP29 Mutation Is Associated with Abnormal Oral Epithelial Adhesions. *J Dent Res, 96*(11), 1298-1305. doi:10.1177/0022034517726079

Payapilly, A., & Malliri, A. (2018). Compartmentalisation of RAC1 signalling. *Curr Opin Cell Biol, 54*, 50-56. doi:10.1016/j.ceb.2018.04.009

Pengelly, R. J., Arias, L., Martinez, J., Upstill-Goddard, R., Seaby, E. G., Gibson, J., . . . Briceno, I. (2016). Deleterious coding variants in multi-case families with non-syndromic cleft lip and/or palate phenotypes. *Sci Rep, 6*, 30457. doi:10.1038/srep30457

Peterkova, R., Klepacek, I., & Peterka, M. (1987). Prenatal development of rugae palatinae in mice: scanning electron microscopic and histologic studies. *J Craniofac Genet Dev Biol, 7*(2), 169-189.

Peyrard-Janvid, M., Leslie, E. J., Kousa, Y. A., Smith, T. L., Dunnwald, M., Magnusson, M., . . . Schutte, B. C. (2014). Dominant mutations in GRHL3 cause Van der Woude Syndrome and disrupt oral periderm development. *Am J Hum Genet, 94*(1), 23-32. doi:10.1016/j.ajhg.2013.11.009

Podsypanina, K., Lee, R. T., Politis, C., Hennessy, I., Crane, A., Puc, J., . . . Parsons, R. (2001). An inhibitor of mTOR reduces neoplasia and normalizes p70/S6 kinase activity in Pten+/- mice. *Proc Natl Acad Sci U S A, 98*(18), 10320-10325. doi:10.1073/pnas.171060098

Proetzel, G., Pawlowski, S. A., Wiles, M. V., Yin, M., Boivin, G. P., Howles, P. N., . . . Doetschman, T. (1995). Transforming growth factor-beta 3 is required for secondary palate fusion. *Nat Genet, 11*(4), 409-414. doi:10.1038/ng1295-409

Qin, W., Kutny, P. M., Maser, R. S., Dion, S. L., Lamont, J. D., Zhang, Y., . . . Wang, H. (2016). Generating Mouse Models Using CRISPR-Cas9-Mediated Genome Editing. *Curr Protoc Mouse Biol, 6*(1), 39-66. doi:10.1002/9780470942390.mo150178

Qiu, M., Bulfone, A., Ghattas, I., Meneses, J. J., Christensen, L., Sharpe, P. T., . . . Rubenstein, J. L. (1997). Role of the Dlx homeobox genes in proximodistal patterning of the branchial arches: mutations of Dlx-1, Dlx-2, and Dlx-1 and -2 alter morphogenesis of proximal skeletal and soft tissue structures derived from the first and second arches. *Dev Biol, 185*(2), 165-184. doi:10.1006/dbio.1997.8556

Rahimov, F., Jugessur, A., & Murray, J. C. (2012). Genetics of nonsyndromic orofacial clefts. *Cleft Palate Craniofac J, 49*(1), 73-91. doi:10.1597/10-178

Rahimov, F., Marazita, M. L., Visel, A., Cooper, M. E., Hitchler, M. J., Rubini, M., . . . Murray, J. C. (2008). Disruption of an AP-2alpha binding site in an IRF6 enhancer is associated with cleft lip. *Nat Genet, 40*(11), 1341-1347. doi:10.1038/ng.242

Restivo, G., Nguyen, B. C., Dziunycz, P., Ristorcelli, E., Ryan, R. J., Ozuysal, O. Y., . . . Dotto, G. P. (2011). IRF6 is a mediator of Notch pro-differentiation and tumour suppressive function in keratinocytes. *EMBO J, 30*(22), 4571-4585. doi:10.1038/emboj.2011.325

Rice, R., Connor, E., & Rice, D. P. (2006). Expression patterns of Hedgehog signalling pathway members during mouse palate development. *Gene Expr Patterns, 6*(2), 206-212. doi:10.1016/j.modgep.2005.06.005

Rice, R., Spencer-Dene, B., Connor, E. C., Gritli-Linde, A., McMahon, A. P., Dickson, C., . . . Rice, D. P. (2004). Disruption of Fgf10/Fgfr2b-coordinated epithelial-mesenchymal interactions causes cleft palate. *J Clin Invest, 113*(12), 1692-1700. doi:10.1172/JCI20384

Richardson, R. J., Dixon, J., Jiang, R., & Dixon, M. J. (2009). Integration of IRF6 and Jagged2 signalling is essential for controlling palatal adhesion and fusion competence. *Hum Mol Genet, 18*(14), 2632-2642. doi:10.1093/hmg/ddp201

Richardson, R. J., Dixon, J., Malhotra, S., Hardman, M. J., Knowles, L., Boot-Handford, R. P., . . . Dixon, M. J. (2006). Irf6 is a key determinant of the keratinocyte proliferation-differentiation switch. *Nat Genet, 38*(11), 1329-1334. doi:10.1038/ng1894

Richardson, R. J., Hammond, N. L., Coulombe, P. A., Saloranta, C., Nousiainen, H. O., Salonen, R., . . . Dixon, M. J. (2014). Periderm prevents pathological epithelial adhesions during embryogenesis. *J Clin Invest, 124*(9), 3891-3900. doi:10.1172/JCI71946

Rigueur, D., & Lyons, K. M. (2014). Whole-mount skeletal staining. *Methods Mol Biol, 1130*, 113-121. doi:10.1007/978-1-62703-989-5_9

Rijli, F. M., Mark, M., Lakkaraju, S., Dierich, A., Dolle, P., & Chambon, P. (1993). A homeotic transformation is generated in the rostral branchial region of the head by disruption of Hoxa-2, which acts as a selector gene. *Cell, 75*(7), 1333-1349.

Romano, R. A., Smalley, K., Magraw, C., Serna, V. A., Kurita, T., Raghavan, S., & Sinha, S. (2012). DeltaNp63 knockout mice reveal its indispensable role as a master regulator of epithelial development and differentiation. *Development, 139*(4), 772-782. doi:10.1242/dev.071191

Saadi, I., Alkuraya, F. S., Gisselbrecht, S. S., Goessling, W., Cavallesco, R., Turbe-Doan, A., . . . Maas, R. L. (2011). Deficiency of the cytoskeletal protein SPECC1L leads to oblique facial clefting. *Am J Hum Genet, 89*(1), 44-55. doi:10.1016/j.ajhg.2011.05.023

Samson, E. B., Tsao, D. S., Zimak, J., McLaughlin, R. T., Trenton, N. J., Mace, E. M., . . . Diehl, M. R. (2017). The coordinating role of IQGAP1 in the regulation of local, endosome-specific actin networks. *Biol Open, 6*(6), 785-799. doi:10.1242/bio.022624

Sandell, L. L., Iulianella, A., Melton, K. R., Lynn, M., Walker, M., Inman, K. E., . . . Trainor, P. A. (2011). A phenotype-driven ENU mutagenesis screen identifies novel alleles with functional roles in early mouse craniofacial development. *Genesis, 49*(4), 342-359. doi:10.1002/dvg.20727

Sandell, L. L., Kurosaka, H., & Trainor, P. A. (2012). Whole mount nuclear fluorescent imaging: convenient documentation of embryo morphology. *Genesis, 50*(11), 844-850. doi:10.1002/dvg.22344

Sato, A., Scholl, A. M., Kuhn, E. N., Stadt, H. A., Decker, J. R., Pegram, K., . . . Kirby, M. L. (2011). FGF8 signaling is chemotactic for cardiac neural crest cells. *Dev Biol, 354*(1), 18-30. doi:10.1016/j.ydbio.2011.03.010

Savastano, C. P., Brito, L. A., Faria, A. C., Seto-Salvia, N., Peskett, E., Musso, C. M., . . . Passos-Bueno, M. R. (2017). Impact of rare variants in ARHGAP29 to the etiology of oral clefts: role of loss-of-function vs missense variants. *Clin Genet, 91*(5), 683-689. doi:10.1111/cge.12823

Scarpa, E., & Mayor, R. (2016). Collective cell migration in development. *J Cell Biol, 212*(2), 143-155. doi:10.1083/jcb.201508047

Scarpa, E., Szabo, A., Bibonne, A., Theveneau, E., Parsons, M., & Mayor, R. (2015). Cadherin Switch during EMT in Neural Crest Cells Leads to Contact Inhibition of Locomotion via Repolarization of Forces. *Dev Cell, 34*(4), 421-434. doi:10.1016/j.devcel.2015.06.012

Schmierer, B., & Hill, C. S. (2007). TGFbeta-SMAD signal transduction: molecular specificity and functional flexibility. *Nat Rev Mol Cell Biol, 8*(12), 970-982. doi:10.1038/nrm2297

Schnutgen, F., De-Zolt, S., Van Sloun, P., Hollatz, M., Floss, T., Hansen, J., . . . von Melchner, H. (2005). Genomewide production of multipurpose alleles for the functional analysis of the mouse genome. *Proc Natl Acad Sci U S A, 102*(20), 7221-7226. doi:10.1073/pnas.0502273102

Schutte, B. C., Saal, H. M., Goudy, S., & Leslie, E. (1993). IRF6-Related Disorders. In M. P. Adam, H. H. Ardinger, R. A. Pagon, S. E. Wallace, L. J. H. Bean, K. Stephens, & A. Amemiya (Eds.), *GeneReviews((R))*. Seattle (WA).

Schwarz, Q., Vieira, J. M., Howard, B., Eickholt, B. J., & Ruhrberg, C. (2008). Neuropilin 1 and 2 control cranial gangliogenesis and axon guidance through neural crest cells. *Development, 135*(9), 1605-1613. doi:10.1242/dev.015412

Serbedzija, G. N., Bronner-Fraser, M., & Fraser, S. E. (1992). Vital dye analysis of cranial neural crest cell migration in the mouse embryo. *Development, 116*(2), 297-307.

Shellard, A., & Mayor, R. (2016). Chemotaxis during neural crest migration. *Semin Cell Dev Biol, 55*, 111-118. doi:10.1016/j.semcdb.2016.01.031

Shimizu, N., Aoyama, H., Hatakenaka, N., Kaneda, M., & Teramoto, S. (2001). An in vitro screening system for characterizing the cleft palate-inducing potential of chemicals and underlying mechanisms. *Reprod Toxicol, 15*(6), 665-672.

Shimizu, Y., Thumkeo, D., Keel, J., Ishizaki, T., Oshima, H., Oshima, M., . . . Narumiya, S. (2005). ROCK-I regulates closure of the eyelids and ventral body wall by inducing assembly of actomyosin bundles. *J Cell Biol, 168*(6), 941-953. doi:10.1083/jcb.200411179

Shiomi, N., Cui, X. M., Yamamoto, T., Saito, T., & Shuler, C. F. (2006). Inhibition of SMAD2 expression prevents murine palatal fusion. *Dev Dyn, 235*(7), 1785-1793. doi:10.1002/dvdy.20819

Shoval, I., Ludwig, A., & Kalcheim, C. (2007). Antagonistic roles of full-length N-cadherin and its soluble BMP cleavage product in neural crest delamination. *Development, 134*(3), 491-501. doi:10.1242/dev.02742

Sim, N. L., Kumar, P., Hu, J., Henikoff, S., Schneider, G., & Ng, P. C. (2012). SIFT web server: predicting effects of amino acid substitutions on proteins. *Nucleic Acids Res, 40*(Web Server issue), W452-457. doi:10.1093/nar/gks539

Sit, S. T., & Manser, E. (2011). Rho GTPases and their role in organizing the actin cytoskeleton. *J Cell Sci, 124*(Pt 5), 679-683. doi:10.1242/jcs.064964

Snider, T. N., & Mishina, Y. (2014). Cranial neural crest cell contribution to craniofacial formation, pathology, and future directions in tissue engineering. *Birth Defects Res C Embryo Today, 102*(3), 324-332. doi:10.1002/bdrc.21075

Snyder-Warwick, A. K., Perlyn, C. A., Pan, J., Yu, K., Zhang, L., & Ornitz, D. M. (2010). Analysis of a gain-of-function FGFR2 Crouzon mutation provides evidence of loss of function activity in the etiology of cleft palate. *Proc Natl Acad Sci U S A, 107*(6), 2515-2520. doi:10.1073/pnas.0913985107

Sonawane, B. R., & Goldman, A. S. (1981). Susceptibility of mice to phenytoin-induced cleft palate correlated with inhibition of fetal palatal RNA and protein synthesis (41255). *Proc Soc Exp Biol Med, 168*(2), 175-179.

Song, Z., Liu, C., Iwata, J., Gu, S., Suzuki, A., Sun, C., . . . Chen, Y. (2013). Mice with Tak1 deficiency in neural crest lineage exhibit cleft palate associated with abnormal tongue development. *J Biol Chem, 288*(15), 10440-10450. doi:10.1074/jbc.M112.432286

Stanier, P., & Moore, G. E. (2004). Genetics of cleft lip and palate: syndromic genes contribute to the incidence of non-syndromic clefts. *Hum Mol Genet, 13 Spec No 1*, R73-81. doi:10.1093/hmg/ddh052

Steinhart, Z., & Angers, S. (2018). Wnt signaling in development and tissue homeostasis. *Development, 145*(11). doi:10.1242/dev.146589

Stoll, C., Alembik, Y., Dott, B., & Roth, M. P. (2001). Risk factors in congenital abdominal wall defects (omphalocele and gastroschisi): a study in a series of 265,858 consecutive births. *Ann Genet, 44*(4), 201-208.

Strassman, A., Schnutgen, F., Dai, Q., Jones, J. C., Gomez, A. C., Pitstick, L., . . . Bjork, B. C. (2017). Generation of a multipurpose Prdm16 mouse allele by targeted gene trapping. *Dis Model Mech, 10*(7), 909-922. doi:10.1242/dmm.029561

Strobl-Mazzulla, P. H., & Bronner, M. E. (2012). Epithelial to mesenchymal transition: new and old insights from the classical neural crest model. *Semin Cancer Biol, 22*(5-6), 411-416. doi:10.1016/j.semcancer.2012.04.008

Sweney, L. R., & Shapiro, B. L. (1971). Alkaline phosphatase in rodent secondary palate development. A histochemical and biochemical study. *Anat Rec, 170*(2), 235-241. doi:10.1002/ar.1091700208

Szabo, A., Unnep, R., Mehes, E., Twal, W. O., Argraves, W. S., Cao, Y., & Czirok, A. (2010). Collective cell motion in endothelial monolayers. *Phys Biol, 7*(4), 046007. doi:10.1088/1478-3975/7/4/046007

Takahashi, M., Tamura, M., Sato, S., & Kawakami, K. (2018). Mice doubly deficient in Six4 and Six5 show ventral body wall defects reproducing human omphalocele. *Dis Model Mech, 11*(10). doi:10.1242/dmm.034611

Taneyhill, L. A. (2008). To adhere or not to adhere: the role of Cadherins in neural crest development. *Cell Adh Migr, 2*(4), 223-230. doi:10.1038/nrm2825

Taneyhill, L. A., Coles, E. G., & Bronner-Fraser, M. (2007). Snail2 directly represses cadherin6B during epithelial-to-mesenchymal transitions of the neural crest. *Development, 134*(8), 1481-1490. doi:10.1242/dev.02834

Tang, D. D., & Gerlach, B. D. (2017). The roles and regulation of the actin cytoskeleton, intermediate filaments and microtubules in smooth muscle cell migration. *Respir Res, 18*(1), 54. doi:10.1186/s12931-017-0544-7

Tang, Q., Li, L., Jin, C., Lee, J. M., & Jung, H. S. (2015). Role of region-distinctive expression of Rac1 in regulating fibronectin arrangement during palatal shelf elevation. *Cell Tissue Res, 361*(3), 857-868. doi:10.1007/s00441-015-2169-9

Taylor, J., & Aftimos, S. (2010). Congenital diaphragmatic hernia is a feature of Opitz G/BBB syndrome. *Clin Dysmorphol, 19*(4), 225-226. doi:10.1097/MCD.0b013e32833b2bd3

Tessier, P. (1976). Anatomical classification facial, cranio-facial and latero-facial clefts. *J Maxillofac Surg, 4*(2), 69-92. doi:10.1016/S0301-0503(76)80013-6

Testa, J. R., & Tsichlis, P. N. (2005). AKT signaling in normal and malignant cells. *Oncogene, 24*(50), 7391-7393. doi:10.1038/sj.onc.1209100

Theveneau, E., & Mayor, R. (2012). Neural crest delamination and migration: from epithelium-to-mesenchyme transition to collective cell migration. *Dev Biol, 366*(1), 34-54. doi:10.1016/j.ydbio.2011.12.041

Theveneau, E., & Mayor, R. (2013). Collective cell migration of epithelial and mesenchymal cells. *Cell Mol Life Sci, 70*(19), 3481-3492. doi:10.1007/s00018-012-1251-7

Thomason, Helen A., & Dixon, Michael J. (2009). Craniofacial Defects and Cleft Lip and Palate. In *Encyclopedia of Life Sciences*.

Thomason, H. A., Zhou, H. Q., Kouwenhoven, E. N., Dotto, G. P., Restivo, G., Nguyen, B. C., . . . Dixon, J. (2010). Cooperation between the transcription factors p63 and IRF6 is essential to prevent cleft palate in mice. *Journal of Clinical Investigation, 120*(5), 1561-1569. doi:10.1172/Jci40266

Thumkeo, D., Shimizu, Y., Sakamoto, S., Yamada, S., & Narumiya, S. (2005). ROCK-I and ROCK-II cooperatively regulate closure of eyelid and ventral body wall in mouse embryo. *Genes Cells, 10*(8), 825-834. doi:10.1111/j.1365-2443.2005.00882.x

Torres, U. S., Portela-Oliveira, E., Braga Fdel, C., Werner, H., Jr., Daltro, P. A., & Souza, A. S. (2015). When Closure Fails: What the Radiologist Needs to Know About the Embryology, Anatomy, and Prenatal Imaging of Ventral Body Wall Defects. *Semin Ultrasound CT MR, 36*(6), 522-536. doi:10.1053/j.sult.2015.01.001

Trainor, P. A. (2005). Specification of neural crest cell formation and migration in mouse embryos. *Semin Cell Dev Biol, 16*(6), 683-693. doi:10.1016/j.semcdb.2005.06.007

Trainor, P. A. (2010). Craniofacial birth defects: The role of neural crest cells in the etiology and pathogenesis of Treacher Collins syndrome and the potential for prevention. *Am J Med Genet A, 152A*(12), 2984-2994. doi:10.1002/ajmg.a.33454

Truebestein, L., & Leonard, T. A. (2016). Coiled-coils: The long and short of it. *Bioessays, 38*(9), 903-916. doi:10.1002/bies.201600062

Ui, M., Okada, T., Hazeki, K., & Hazeki, O. (1995). Wortmannin as a unique probe for an intracellular signalling protein, phosphoinositide 3-kinase. *Trends Biochem Sci, 20*(8), 303-307. doi:10.1016/S0968-0004(00)89056-8

Van Otterloo, Eric, Williams, Trevor, & Artinger, Kristin Bruk. (2016). The old and new face of craniofacial research: How animal models inform human craniofacial genetic and clinical data. *Developmental Biology, 415*(2), 171-187. doi:10.1016/j.ydbio.2016.01.017

Vasudevan, H. N., & Soriano, P. (2014). SRF regulates craniofacial development through selective recruitment of MRTF cofactors by PDGF signaling. *Dev Cell, 31*(3), 332-344. doi:10.1016/j.devcel.2014.10.005

Vasudevan, K. M., & Garraway, L. A. (2010). AKT signaling in physiology and disease. *Curr Top Microbiol Immunol, 347*, 105-133. doi:10.1007/82_2010_66

Vaziri Sani, F., Hallberg, K., Harfe, B. D., McMahon, A. P., Linde, A., & Gritli-Linde, A. (2005). Fate-mapping of the epithelial seam during palatal fusion rules out epithelial-mesenchymal transformation. *Dev Biol, 285*(2), 490-495. doi:10.1016/j.ydbio.2005.07.027

Vekemans, M., Taylor, B. A., & Fraser, F. C. (1981). The susceptibility to cortisone-induced cleft palate of recombinant inbred strains of mice: lack of association with the H-2 haplotype. *Genet Res, 38*(3), 327-331.

Walker, BE, & Fraser, FC. (1956). Closure of the secondary palate in three strains of mice. *Development, 4*(2), 176-189.

Weber, T. R., Au-Fliegner, M., Downard, C. D., & Fishman, S. J. (2002). Abdominal wall defects. *Curr Opin Pediatr, 14*(4), 491-497.

Wehby, G. L., & Cassell, C. H. (2010). The impact of orofacial clefts on quality of life and healthcare use and costs. *Oral Dis, 16*(1), 3-10. doi:10.1111/j.1601-0825.2009.01588.x

Wheelock, M. J., & Johnson, K. R. (2003). Cadherins as modulators of cellular phenotype. *Annu Rev Cell Dev Biol, 19*, 207-235. doi:10.1146/annurev.cellbio.19.011102.111135

Williams, T. (2008). Animal models of ventral body wall closure defects: a personal perspective on gastroschisis. *Am J Med Genet C Semin Med Genet, 148C*(3), 186-191. doi:10.1002/ajmg.c.30179

Wilson, N. R., Olm-Shipman, A. J., Acevedo, D. S., Palaniyandi, K., Hall, E. G., Kosa, E., . . . Saadi, I. (2016). SPECC1L deficiency results in increased adherens junction stability and reduced cranial neural crest cell delamination. *Sci Rep, 6*, 17735. doi:10.1038/srep17735

Winter, J., Basilicata, M. F., Stemmler, M. P., & Krauss, S. (2016). The MID1 protein is a central player during development and in disease. *Front Biosci (Landmark Ed), 21*, 664-682.

Witkos, T. M., & Lowe, M. (2015). The Golgin Family of Coiled-Coil Tethering Proteins. *Front Cell Dev Biol, 3*, 86. doi:10.3389/fcell.2015.00086

Witte, J. S. (2010). Genome-wide association studies and beyond. *Annu Rev Public Health, 31*, 9-20 24 p following 20. doi:10.1146/annurev.publhealth.012809.103723

Wu, M., Li, J., Engleka, K. A., Zhou, B., Lu, M. M., Plotkin, J. B., & Epstein, J. A. (2008). Persistent expression of Pax3 in the neural crest causes cleft palate and defective osteogenesis in mice. *J Clin Invest, 118*(6), 2076-2087. doi:10.1172/JCI33715

Wu, X., Kodama, A., & Fuchs, E. (2008). ACF7 regulates cytoskeletal-focal adhesion dynamics and migration and has ATPase activity. *Cell, 135*(1), 137-148. doi:10.1016/j.cell.2008.07.045

Xu, J., Liu, H., Lan, Y., Aronow, B. J., Kalinichenko, V. V., & Jiang, R. (2016). A Shh-Foxf-Fgf18-Shh Molecular Circuit Regulating Palate Development. *PLoS Genet, 12*(1), e1005769. doi:10.1371/journal.pgen.1005769

Xu, X., Han, J., Ito, Y., Bringas, P., Jr., Deng, C., & Chai, Y. (2008). Ectodermal Smad4 and p38 MAPK are functionally redundant in mediating TGF-beta/BMP signaling during tooth and palate development. *Dev Cell, 15*(2), 322-329. doi:10.1016/j.devcel.2008.06.004

Xu, X., Han, J., Ito, Y., Bringas, P., Jr., Urata, M. M., & Chai, Y. (2006). Cell autonomous requirement for Tgfbr2 in the disappearance of medial edge epithelium during palatal fusion. *Dev Biol, 297*(1), 238-248. doi:10.1016/j.ydbio.2006.05.014

Xue, G., & Hemmings, B. A. (2013). PKB/Akt-dependent regulation of cell motility. *J Natl Cancer Inst, 105*(6), 393-404. doi:10.1093/jnci/djs648

Yamada, T., Mishima, K., Fujiwara, K., Imura, H., & Sugahara, T. (2006). Cleft lip and palate in mice treated with 2,3,7,8-tetrachlorodibenzo-p-dioxin: a morphological in vivo study. *Congenit Anom (Kyoto), 46*(1), 21-25. doi:10.1111/j.1741-4520.2006.00097.x

Yanai, H., Negishi, H., & Taniguchi, T. (2012). The IRF family of transcription factors: Inception, impact and implications in oncogenesis. *Oncoimmunology, 1*(8), 1376-1386. doi:10.4161/onci.22475

Yang, L. T., & Kaartinen, V. (2007). Tgfb1 expressed in the Tgfb3 locus partially rescues the cleft palate phenotype of Tgfb3 null mutants. *Dev Biol, 312*(1), 384-395. doi:10.1016/j.ydbio.2007.09.034

Yu, K., & Ornitz, D. M. (2011). Histomorphological study of palatal shelf elevation during murine secondary palate formation. *Dev Dyn, 240*(7), 1737-1744. doi:10.1002/dvdy.22670

Yu, L., Gu, S., Alappat, S., Song, Y., Yan, M., Zhang, X., . . . Chen, Y. (2005). Shox2-deficient mice exhibit a rare type of incomplete clefting of the secondary palate. *Development, 132*(19), 4397-4406. doi:10.1242/dev.02013

Zhang, J., Yue, J., & Wu, X. (2017). Spectraplakin family proteins - cytoskeletal crosslinkers with versatile roles. *J Cell Sci, 130*(15), 2447-2457. doi:10.1242/jcs.196154

Zhang, Z., Song, Y., Zhao, X., Zhang, X., Fermin, C., & Chen, Y. (2002). Rescue of cleft palate in Msx1-deficient mice by transgenic Bmp4 reveals a network of BMP and Shh signaling in the regulation of mammalian palatogenesis. *Development, 129*(17), 4135-4146.

Zhao, G. N., Jiang, D. S., & Li, H. (2015). Interferon regulatory factors: at the crossroads of immunity, metabolism, and disease. *Biochim Biophys Acta, 1852*(2), 365-378. doi:10.1016/j.bbadis.2014.04.030

Zhou, J., Gao, Y., Lan, Y., Jia, S., & Jiang, R. (2013). Pax9 regulates a molecular network involving Bmp4, Fgf10, Shh signaling and the Osr2 transcription factor to control palate morphogenesis. *Development, 140*(23), 4709-4718. doi:10.1242/dev.099028

Zhou, J., Gao, Y., Zhang, Z., Zhang, Y., Maltby, K. M., Liu, Z., . . . Jiang, R. (2011). Osr2 acts downstream of Pax9 and interacts with both Msx1 and Pax9 to pattern the tooth developmental field. *Dev Biol, 353*(2), 344-353. doi:10.1016/j.ydbio.2011.03.012

Zucchero, T. M., Cooper, M. E., Maher, B. S., Daack-Hirsch, S., Nepomuceno, B., Ribeiro, L., . . . Murray, J. C. (2004). Interferon regulatory factor 6 (IRF6) gene variants and the risk of isolated cleft lip or palate. *N Engl J Med, 351*(8), 769-780. doi:10.1056/NEJMoa032909

APPENDIX:

GENERATION OF *SPECC1L*^{cGT} GENE TRAP ALLELE

Construction of 5' and 3' homology arm and gene trap Entry plasmids

This strategy for generating a multifunctional gene trap targeting construct for use in targeted trapping in embryonic stem (ES) cells has been described previously [Strassman, 2017]. In brief, 5' and 3' genomic homology regions (HR) from the second intron of *Specc1l* were PCR-amplified from genomic DNA isolated from EDJ#22 (ATCC SCRC-1021) mouse 129S5/SvEvTac embryonic stem cells using the DNeasy Blood & Tissue Kit (Qiagen). PCR amplification was carried out using the HiFi PCR Kit (Kapa Biosystems) with oligonucleotide primers that contain specific GATEWAY *att* sites at their 5' ends (5' HR, oBB1686 -*attB4* and oBB1687-*attB1*; 3' HR, oBB1688-*attB2* and oBB1689-*attB3*) **(Table 2.2)**. Recombination of these amplified HRs into pDONR-P4-P1R and pDONR-P2R-P3, respectively, to generate pENTR-5'HR and pENTR-3'HR Entry clones was carried out via *in vitro BP Clonase* reactions. Reactions were transformed into chemically-competent *Stbl3* cells (Invitrogen-Life Technologies) and grown on LB agar plates supplemented with Kanamycin. The prsFlipROSA*βgeo**-TT0-ENTR11 Entry plasmid (TT+0 refers to Targeted Trap +0 nt reading frame) was used to contribute an *attL1-attL2*-flanked gene trap cassette that maintains the Specc1l reading frame to the final targeted trapping construct [Strassman, 2017].

Construction of conditional gene trap targeted trapping vector

The three Entry clones, pENTR-5'HR, pENTR-3'HR, and prsFlipROSA*βgeo** TT0-ENTR11, and the pPNT-DEST-R4-R3 Destination vector described previously [Strassman, 2017] were combined to create the final targeted trapping vector via the *in vitro* Multisite GATEWAY recombination system using LR Recombinase II Plus enzyme following manufacturer's protocols (Thermo Fisher Scientific). The reaction was transformed into chemically-competent *Stbl3 E. coli*

cells after Proteinase K digestion and plated on LB agar plates supplemented with Ampicillin. Primers spanning 3 of 4 recombination junction sites were used to screen transformants (pUC_F/oBB 1712, oBB 1713/965 and oBB 1717/hsvtk_R) **(Table 2.2)**, and positive clones were verified using restriction mapping after plasmid DNA was isolated using the QIAprep Spin Miniprep Kit (Qiagen).

Gene trap insertion into mouse ES cells

Plasmid DNA for the final ~20 kb targeted trapping vector, prsFlipROSA*βgeo**-*Specc1l*in2, was isolated using the Endo-free MaxiPrep Kit (Qiagen) and linearized via AscI digestion prior to electroporation into EDJ#22 ES cells. Neomycin-resistant ES cell colonies were grown in the G418 (250 μg/ml) for 10 days. G418-resistant colonies were picked and split into replicate plates for 1) frozen storage in 10% DMSO/DMEM; 2) genomic DNA isolation and 3) total RNA isolation. Genomic DNA was isolated using standard Proteinase K digestion protocols [Nagy, 2003] Total RNA was isolated using Trizol Reagent following manufacturer's protocols (Invitrogen – Life Technologies). The promotorless gene trap depends upon endogenous *Specc1l* expression in ES cells to confer G418 resistance, so titrations of G418 concentrations were tested to determine optimal levels. For our experiment, 250 μg/ml G418 was sufficient to allow correctly targeted ES cells to survive, while still killing most incorrectly targeted ES cells.

To identify correctly targeted ES cell colonies, total RNA was extracted using Trizol Reagent and used as template in One-Step Reverse transcriptase (RT)-PCR assays using primers oBB 1754 and oBB 1125 to amplify a predicted 250 bp product and identify the desired *Specc1l-βgeo** fusion gene trap transcript (Invitrogen - Life Technologies). Of the 48 ES cell lines resistant

to 125µg/µl G418, 24 were RT-PCR-positive. Genomic DNAs exacted from RT-PCR-positive ES clones were screened for desired recombination events using primers (oBB 1112/1753) designed near the 3' end of the gene trap cassette and outside the 3' homology arm sequence to generate a 4.2 kb PCR product in correctly targeted clones **(Gel image; Lane 2)**. Correct 5' targeting was verified only in ES clones that were positive by RT-PCR and the 3' targeting event. These primers (oBB 1752/1115) were designed near the 5' end of the gene trap cassette and outside the 5' genomic homology arm sequence and yielded an ~6 kb product **(Gel image; Lane 1)**.

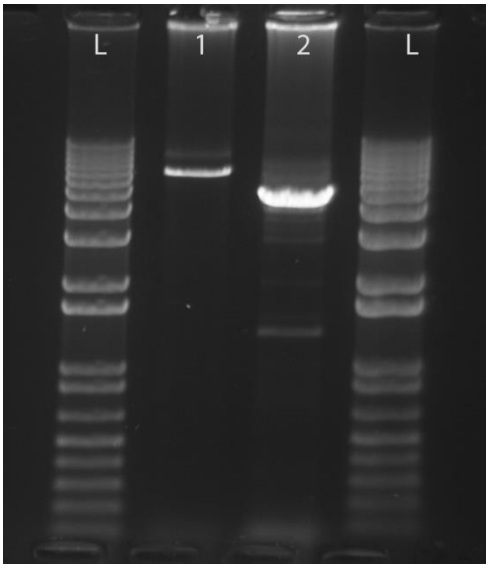

Embryo Generation, Harvest, and Processing

Correctly targeted ES cells containing the cGT cassette insertion into *Specc1l* intron 2 were microinjected into C57BL6/J blastocysts (KUMC Transgenic and Gene-Targeting Institutional Facility, Kansas City, KS). Chimeras were obtained and crossed to C57BL6/J mice to monitor germline transmission. Heterozygous progeny from the C57BL6/J outcross was confirmed by PCR genotyping to identify the *Specc1l*^{cGT} allele. All animals were housed in accordance with University of Kansas Medical Center Laboratory Animal Resources facility regulations, and all

studies were performed consistent with protocols approved by the KUMC Institutional Animal Care and Use Committees.